

Inaugural dissertation
for
obtaining the doctoral degree
of the
Combined Faculty of Mathematics, Engineering and Natural Sciences of the
Ruprecht - Karls - University
Heidelberg

Presented by
M.Biochem Ju Yeon Han
Born in: Cheongju, South Korea.
Oral examination: 25.11.2022

To what extent is digit patterning a Turing system?

Referees:

Prof. Dr. Joachim Wittbrodt

Dr. Miki Ebisuya

Acknowledgements	7
Summary	9
1. Introduction	13
1.1 Turing / Reaction-Diffusion in pattern formation	13
1.2 Limb Development and digit patterning	14
1.3 Classic models explaining digit patterning	15
1.4 Plasticity of the digit patterning	17
1.4.1 Turing stripe model (BSW model) vs Turing spot model (Hiscock model)	17
1.4.2 Plasticity can be only assessed through perturbation	18
1.5 Cell movements and density changes in digit patterning	20
1.5.1 Mechanochemical model, Pure mechanical model and Pure reaction-diffusion model	21
1.5.2 The relative timing of molecular digit patterning versus cellular movements	21
1.6 Known and unknown roles of Wnt signalling in digit patterning	23
1.6.1. Known roles of Wnt signalling in digit patterning	24
1.6.2. Gaps in our knowledge of Wnt signalling	26
1.7 Unbiased screening to address unknown roles of Wnt signalling	28
1.8 Other pathways that modulate digit patterning	30
2. Aims of the study	33
3. Results Part I : For how long is the digit patterning a dynamic self-organisation process?	35
3.1 On Day 11 digit patterning behaves as a very dynamic and plastic Reaction-Diffusion system	35
3.2 Image quantification reveals that patterning plasticity decreases gradually over time	38
3.3 A simple mathematical model of plasticity decrease can capture the dynamical patterning of digits	40
3.4 Optimised data fit model recapitulates gradual plasticity decrease over time	43
3.5 Transcriptional dynamics of stemness/pluripotency/reprogramming factors closely matches the gradual decrease in experimental plasticity	45
3.6 Sox9 digit patterning precedes cell density changes	47
3.7 Part I Summary	53
4. Results Part II : Unbiased screening of digit patterning pathways	55
4.1 Classification of outcome types from micromass assay	59
4.2 Classification of outcome types from limb bud culture	62
4.3 Comparison of results from micromass and limb culture	63
4.4 Wnt production process and Wnt canonical pathways are accountable for digit patterning	71
4.5 All micromass and limb culture phenotypes can be recapitulated using the Turing stripe (BSW) model	74
4.6 Webbing, Distal digit widening, and Peripheral digit loss could be variations of a global digit merging model	78

4.8 Retinoic acid and Notch pathway modulates digit patterning	83
4.9 Part II Summary	87
5. Discussion	89
5.1 For how long is the digit patterning a dynamic self-organisation process?	89
5.1.1 Novel and quantitative analytic method of tissue plasticity	89
5.1.2 Why does tissue plasticity in embryonic limbs decrease in a gradual manner?	91
5.1.3 How can cell density change following molecular patterning?	92
5.2 Unbiased screening of digit patterning pathways	94
5.2.1 How does Wnt mediated Sox9 expression work with the rest of the BSW model	95
5.2.2 Limitations of the study	96
5.2.2.1 Addressing conflicting results	96
5.2.2.2. Validation of experimental results	97
5.2.3 How is ectodermal signal transduced to mesenchyme?	100
6. Outlook	101
7. Materials and Methods	103
Animals	103
Limb Bud Cultures	103
Bead Implantations	103
Digit patterning quantification	103
Wild type digit patterning simulation	104
Simulation of bead insertion experiments	105
Changing plasticity	106
Turing spot model simulation	107
“Data fit” model simulation	107
“Optimised Data fit” model simulation	107
“Steeper” model simulation	108
Micromass culture	108
Immunohistochemistry	109
Micromass / immunohistochemistry Image acquisition	109
Simulating Wild Type micromass	109
Simulating Wnt activation/ inhibition in micromass	110
Simulating distal digit widening phenotype	112
Simulating webbing phenotype	114
Simulating peripheral digit loss phenotype	115
Simulating digit sharpening phenotype	117
Simulating period change phenotype	118
8. Appendix	121
Bibliography	133

Acknowledgements

Thanks to everyone who helped me grow as a scientist and a person for the last four years. Without those four years in Barcelona, I wouldn't be the same person. And in this journey special thanks to James for introducing me into the world of computational developmental biology, and being the most understanding and supportive supervisor. And to the Sharpe lab for the inspiring discussions, coffee chats, infinite drinks, and for all the help. I have scientifically learned so much just by talking to you - Words cannot express how thankful I am! A huge thanks to Chao for always being there for me. Finally to my parents, who let me start this amazing journey of life.

Summary

Building precise, robust patterns and structures from an initially homogeneous state is fundamental to developmental biology. Digit patterning is a representative example of a periodic pattern in development. Previous studies have shown that a reaction–diffusion (Turing) system, in which diffusible activators and inhibitors interact, is the most likely explanation of how the spatial pattern of the digits is formed. Although self-organisation mechanisms such as the Turing system successfully recapitulate many aspects of digit patterning, critical questions remain regarding its timing and behaviour.

First I addressed the question of timing, or how long reaction-diffusion plays a role in the developing digits. I perturbed the digit patterning process of embryonic limbs by inserting beads that contain morphogens involved in the reaction-diffusion mechanism. Then I quantified the degree of pattern change, or plasticity of the patterning, from limbs harvested at different developmental timing throughout the digit patterning stage. For quantification, I developed a custom image analytic pipeline that extracts relevant topology and represents the difference between perturbed and unperturbed patterns. Modelling the plasticity profile over the digit patterning process, through extensive interplay of experiments and modelling, revealed that plasticity during digit patterning decreases in a sigmoidal manner. Transcriptomics analysis that matches with the sigmoidal decrease observed in expression patterns further identified gene candidates that could be critical to the digit patterning. Further, the timing of reaction-diffusion is discussed in the context of the tissue movements, revealing that Sox9 digit patterning happens significantly earlier than cell density changes.

The second part aims at improving our understanding about which pathways and components of the pathways are involved in the digit forming Turing network. Previously identified digit patterning Turing network, such as BSW model, abstracts the entire Wnt and Bmp signalling pathways' activities into each node. Thus there is insufficient knowledge on the mechanistic role of Wnt signalling mediated Sox9 repression. To further clarify detailed mechanisms of the Turing network, I used an unbiased screening approach to systematically perturb digit patterning using small molecule inhibitors, ligands, and peptides at different doses in systems such as limb culture and micromass. Out of multiple steps critical to Wnt signalling, including Wnt production, Wnt receptor interaction, Wnt canonical pathway cytosolic interactions, and Wnt canonical pathway transcriptional interactions, I identified that inhibition of Wnt production and Wnt transcriptional component inhibition category most effectively disrupt digit patterning. I also identified candidate ligands such as sFRP1 and Dkk1 as potential extracellular Wnt inhibitors that effectively change digit patterning upon application.

These results provide the first quantitative insight into the duration of the reaction-diffusion based mechanism in a biological system, and how a screening approach complemented with data driven modelling can complement and clarify workings of a reaction diffusion based system. Further work in improving our knowledge on the Turing system with tissue growth, cell movements, and ectodermal-mesenchymal interaction will eventually allow generation of a complete organogenesis simulation model.

Zusammenfassung

Zu verstehen wie präzise, robuste Muster und Strukturen aus einem homogenen Ausgangszustand entstehen, ist für die Entwicklungsbiologie von grundlegender Bedeutung. Die Musterbildung der Finger ist ein repräsentatives Beispiel für ein periodisches Muster in der Embryonalentwicklung. Frühere Studien haben gezeigt, dass ein Reaktionsdiffusions-System (Turing-System), in dem diffundierende Aktivator und Inhibitoren zusammenwirken, die wahrscheinlichste Erklärung dafür ist, wie das räumliche Muster der Finger gebildet wird. Obwohl Selbstorganisations-Mechanismen wie das Turing-System viele Aspekte der Fingermusterung erfolgreich rekapitulieren, bleiben kritische Fragen bezüglich der zeitlichen Koordinierung und des Systemverhaltens offen.

Zunächst habe ich mich mit der Frage der zeitlichen Koordinierung befasst, d. h. wie lange Reaktionsdiffusion bei der Entwicklung der Finger eine Rolle spielt. Dazu habe ich Kügelchen, die mit Morphogenen des Reaktionsdiffusions-Mechanismus geladen waren, in embryonalen Gliedmaßen platziert, um den Prozess der Musterung zu stören. Anschließend habe ich das Ausmaß der Musterungsveränderung bzw. der Plastizität der Musterung an Gliedmaßen analysiert, die zu unterschiedlichen Zeitpunkten der Fingerentwicklung entnommen wurden. Dazu habe ich eine Bildanalyse-Pipeline entwickelt, die die relevante Topologie extrahiert und den Unterschied zwischen gestörten und ungestörten Musterung quantifiziert. Das gemodelte Plastizitätsprofil der Fingermusterung auf der Basis von Experimenten und mathematischer Modellierung ergab, dass die Plastizität während der Fingermusterung sigmoidal abnimmt. Eine Transkriptomik-Analyse, die mit der sigmoidalen Abnahme der Expressionsmuster übereinstimmt, identifizierte weitere Genkandidaten, die für die Fingermusterung entscheidend sein könnten. Darüber hinaus wird der Zeitpunkt der Reaktionsdiffusion im Zusammenhang mit den Gewebewebungen erörtert, wobei sich herausstellte, dass die Sox9-Fingermusterung deutlich früher erfolgt als Veränderungen in der Zelldichte.

Der zweite Teil meiner Arbeit zielt darauf ab, unser Verständnis darüber welche Signalwege und Signalweg-Komponenten am Turing-Netzwerk der Ziffernbildung beteiligt sind, zu erweitern. Bei den bisher identifizierten Turing-Netzwerken für die Fingerbildung, wie z. B. dem BSW-Modell, werden die gesamten Aktivitäten der Wnt- und Bmp-Signalwege in jedem Knotenpunkt abstrahiert. Daher ist unser Wissen über die mechanistische Rolle der durch Wnt-Signale vermittelten Sox9-Unterdrückung limitiert. Um die detaillierten Mechanismen des Turing-Netzwerks weiter aufzuklären, habe ich einen datengesteuerten Ansatz verwendet, um die Fingermusterung systematisch zu stören. Dazu habe ich Hemmstoffe, Liganden und Peptide in verschiedenen Dosierungen in Systemen wie limb culture und micromass culture, verwendet. Von den verschiedenen Schritten, die für die Wnt-Signalübertragung entscheidend sind, darunter die Wnt-Produktion, die Interaktion mit dem Wnt-Rezeptor, die zytosolischen Interaktionen des kanonischen Wnt-Signalwegs und die transkriptionellen Interaktionen des kanonischen Wnt-Signalwegs, habe ich die Inhibierung der Wnt-Produktion und die Inhibierung der transkriptionellen Wnt-Komponenten als am Wirksamsten identifiziert, um die Entwicklung der Fingermusterung zu beeinträchtigen. Außerdem identifizierte ich Ligandenkandidaten wie sFRP1 und Dkk1, die die Fingermusterung effektiv verändern, als potenzielle extrazelluläre Wnt-Inhibitoren.

Diese Ergebnisse bieten den ersten quantitativen Einblick in die Wirkungsdauer eines Reaktionsdiffusion-Mechanismus in einem biologischen System und zeigen, wie ein datengesteuerter Ansatz unser Verständnis für die Funktionsweise eines Reaktionsdiffusion-Systems verbessern kann. Weitere Arbeiten zur Verbesserung unseres Wissens über das Turing-System in Zusammenarbeit mit Gewebewachstum, Zellbewegungen und ektodermal-mesenchymaler Interaktion, werden in der Zukunft die Entwicklung eines vollständigen Simulationsmodells der Organogenese ermöglichen.

1. Introduction

Self organisation is defined as a process whereby complexity of form and pattern emerges from interactions of unordered components[1]. The complex structures -form or pattern- are emergent properties that cannot be directly predicted from the individual properties of the elements. During this process of self organisation, statistical rules characterising the system generate feedback, and local interactions arise, which embody information[2]. Throughout physics to chemistry to biology, self-organisation is a common fundamental pillar, observed in phase transition[3], liquid crystals[4], and flocking[5] behaviour of birds.

In the context of developmental biology, many phenomena are shown to be compatible with the principles underlying reaction-diffusion mechanism. Initial symmetry breaking in early mammalian embryos to morphogenesis of various organs[6] are some examples.

1.1 Turing / Reaction-Diffusion in pattern formation

The mechanism behind the development of well-organised patterns and structures from a homogenous state is a central question in developmental biology. There have been multiple theories proposed to characterise strongly coordinated pattern formation processes involving chemical signals, gene expression, mechanical cell movements, and growth[7]. Due to their complexity and nonlinearity, biological systems are far too intricate to be explained by intuition or assumption which would be directly accounted for by experiments[8]. Mathematical theories and modelling are advantageous in that multiple inputs can be incorporated and initial hypotheses can be improved. Further, it is possible to design multiple theories to explain a phenomenon, motivating experimental approaches to tell them apart.

Two distinct categories of molecular patterning mechanism explain spatial organisation of different cell fates: (1) Positional Information and (2) self-organised reaction-diffusion. Positional Information is based on the idea that information can be transmitted from one part of an embryo to the other side[9]. The information is presented in a scalar form, for instance as a gradient of chemicals, or the time elapsed since cells were exposed to a signal[10]. The information is distributed monotonically throughout a tissue, enabling each cell to make position-based decisions about their fates[1]. The concept of the information gradient is something that distinguishes Positional Information from earlier ideas proposing that patterning arises from a single organising centre[11]. The discovery of a bicoid gradient solidified the idea that an information-carrying entity specifies the level of information at each point in the space[12]. In the *Drosophila* embryo, the level of bicoid turns on a different set of genes at each level, meaning that the gradient is interpreted by individual cells[13]. Although defining the identity of the information gradient and how they work in other systems is a challenge, positional information was widely accepted due to its intuitive nature and its ability to explain certain early case studies[14].

On the other hand, reaction-diffusion systems (RD) can explain simpler periodic patterns. A Turing system is different from Positional Information because the gradient is self-organising through the dynamics of an activator-inhibitor pair, instead of requiring

spatially-localised production. Alan Turing proposed the simplest mathematical system of interacting morphogens that establishes the pattern through pure self-organisation by the local interactions of reacting and diffusing proteins, without requiring any predefined pattern[7]. The local interactions can be specified as locally self-strengthening components coupled with lateral inhibition. Turing also suggested that appropriate reaction constraints are required for pattern formation: that both components need to diffuse through the space, and that the inhibitor has a longer working range than the activators[15]. The self-activating property of the activator, combined with faster diffusion of the inhibitor, eventually generates periodic distribution of concentrations, which comes up as spots or stripes in 2D. It was Alan Turing in 1952 who created the term “morphogen” to name the reacting and diffusing biochemical components [7]. Initially, searching for the identity of morphogens relevant to biological pattern formation was a challenge because the technology of that era was not able to identify the relevant molecules. Recent investigations show that the identity of the morphogens does not necessarily have to be a chemical - for instance, zebrafish stripes are shown to arise from two types of cells that are respectively activators and inhibitors. The stripe pattern is generated in the skin by cell to cell interactions between pigment cells[16]. So for the mechanism to work, the cells must have contact with one another. Many other 1D or 2D biological systems, such as regularly spaced mammalian palette ridges [17] and hair follicles in mice [18] can be explained by the Turing-type reaction–diffusion(RD) self-organising mechanism.

1.2 Limb Development and digit patterning

Vertebrate Limb development is a classical system to study patterning and morphogenesis[19]. Mouse limb development begins with the protrusion of undifferentiated, mesenchymal cells, covered with an ectodermal layer, from the lateral plate mesoderm of the embryo. The limb bud in the mouse embryo appears around 9.5 days post fertilisation.

The Mouse limb skeleton consists of three parts: stylopod, the most proximal element, the zeugopod, and the autopod that contains the wrist and digits[20] (Figure 1). Limb skeletons are identified in a proximal to distal manner as the limb grows[21] : the stylopod is specified first, then the zeugopod and finally the autopod.

Throughout this thesis, all experimental developmental timepoints specified are measured using the morphometric staging system eMOSS[22] (Figure 2). Previous determination of mouse embryonic age provided a rather low temporal resolution of 12 hours, and eMOSS resolved this problem by enabling both accurate and objective identification of the mouse embryonic age, which is necessary for identifying timepoints in digit patterning. Developmental timepoints in this study are indicated with the embryonic day followed by hour - for instance, E11:13 means 11th day and 13hr of gestation.

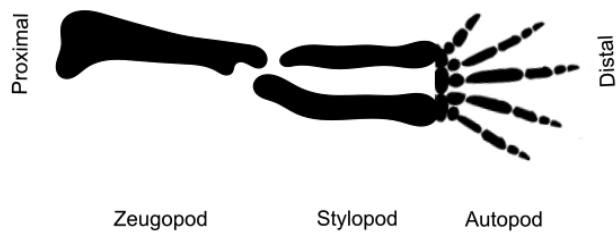


Figure 1. Adopted from Zeller et al [20], reproduced under the terms of the Creative Commons attribution licence (CC-BY 4.0). Stylopod with one element(humerus), zeugopod with two elements(ulnar, radius) and an autopod with five digits.

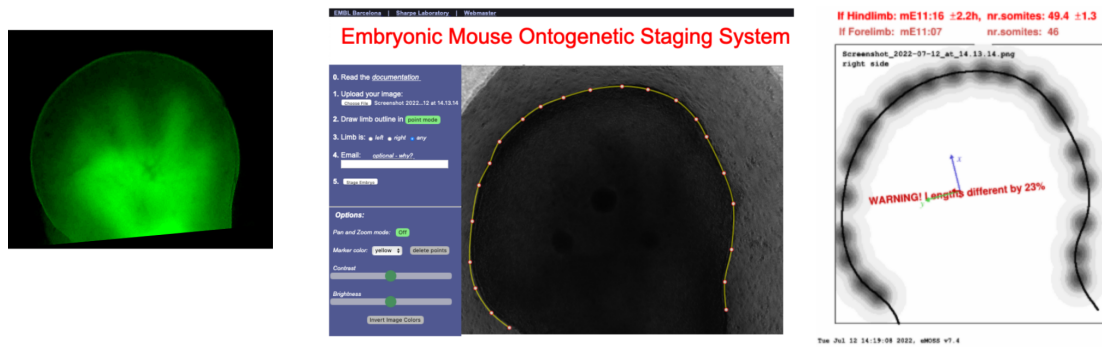


Figure 2. Brightfield channel of the Sox9-GFP image is taken into eMOSS staging system [22] for accurate determination of limb embryonic stage.

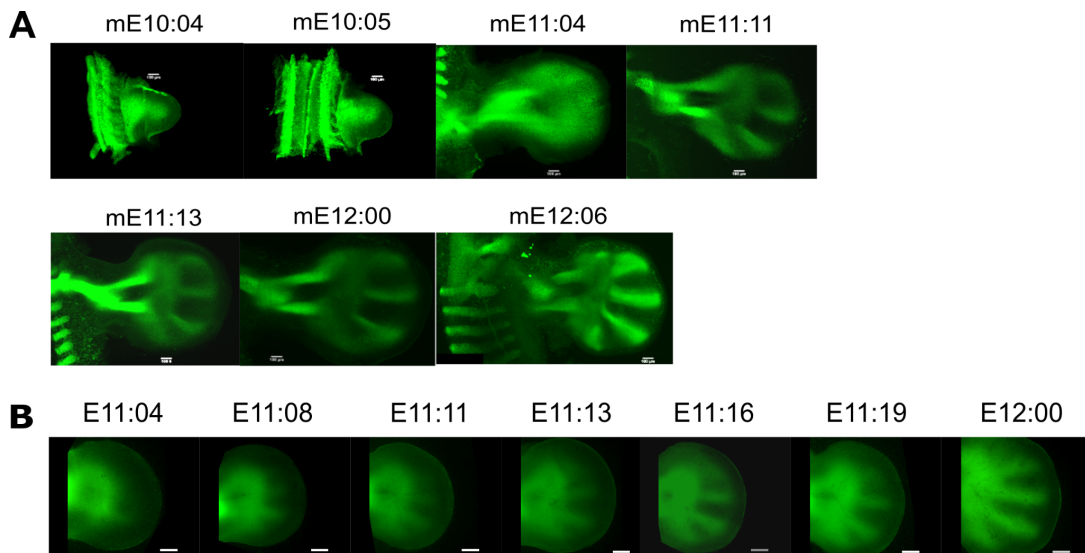


Figure 3. A) Selective Plane Illumination Microscopy (SPIM) images of fixed mouse embryonic limbs. Images from Heura Cardona. B) Time-course of Sox9 expression showing wild type dynamics of digit patterning, using Sox9-GFP mouse line. Scale bars represent 200µm.

The anterior-posterior axis is defined along digits 1 to 5 : starting from the most anterior thumb as digit 1 and the little finger digit 5. Digit patterning involves the mesenchymal cell decision-making process of choosing either the digital or the interdigital fate - in which initially identical mesenchymal cells lose symmetry.

Digit patterning is defined as a process of establishing a periodic pattern of future digital cells(pre-chondrogenic cells) over mouse autopod. Before any digits arise, SRY-Box Transcription Factor 9 (Sox9) is expressed in the central area of the early bud from when the bud is formed around E9.5 (Figure 3A). Sox9 is a well known marker of the skeleton that precedes the cartilage appearance. Silencing Sox9 in the limb results in loss patterning and chondrogenic differentiation [23], and Sox9 overexpression promotes polydactyly [24], suggesting that Sox9 plays a central role in both processes. The first digit, which is always digit 4 - the fourth finger from the anterior part of the limb - emerges around E11:04. Digit 3 follows, then digit 2, and lastly digits 1 and 5. All five digits are usually established by E11:12. At this embryonic stage, there is an emergence of a molecular periodic pattern (Figure 3B), consisting of a repetitive set of stripes expressing the (Sox9), a transcription factor necessary for cartilage condensation, or chondrogenesis [23]. The peaks of the Sox9 positive area specifies where a digit will subsequently emerge.

1.3 Classic models explaining digit patterning

The classic anterior-posterior limb patterning model involves the Zone of Polarizing Activity (ZPA) [25], a region of cells in the posterior part of the limb that produces Sonic HedgeHog (SHH) [14] (Figure 4). When a portion of the posterior mesenchyme in the ZPA region was grafted in the anterior part of the limb, a mirror-image duplication of the digit was induced, generating 6 digits instead of three [25]. It was also proposed that Shh acts as a diffusing morphogen across the anterior-posterior axis whose concentration is the highest in the ZPA. While initially considered as a strong evidence for positional information, recent studies revealed that Shh cannot be a limb morphogen because it acts at only short-range, unable to diffuse further across the limb tissue [26].

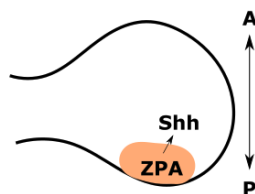


Figure 4. Schematics of the limb bud with anterior-posterior axis, ZPA and Shh highlighted.

On the other hand, reaction-diffusion/Turing-type mechanism clearly explains digit patterning (Figure 5). One prediction of the Turing mechanism is that diffusible molecules involved in the mechanism have periodic patterns that are spatially in-phase or out-of-phase with each other[27]. Raspopovic *et al.*[28] have previously found evidence, both experimental and theoretical, that a Turing-type mechanism may explain the first periodic pattern of the digit patterning.

Sox9, a skeletal precursor marker and a critical component of a self-organising network, demonstrates periodic expression across the digits. In search of other morphogens which also demonstrate periodic patterns across digits and interdigits, microarray analysis was performed, identifying the Bmp and Wnt signalling pathways as components of the network. Immunostaining results further confirm that Bmp and Wnt are respectively in-phase and out-of-phase of the Sox9 pattern. This network responsible for the self-organisation of digit patterning was named BSW model.

Then, the rate of change of Sox9, Bmp and Wnt are expressed in a set of differential equations. Linear Stability Analysis followed by eigenvalue analysis generated the Turing-pattern generating network with minimal topology. Overall, modelling a Bmp-Sox9-Wnt (BSW) network successfully recapitulates the dynamics of Sox9 patterning from initial homogeneous expression, through symmetry breaking and into the final five-digit form.

The proposed BSW model has, in fact, the simplest topology out of nine networks that generate the correct digit pattern (Figure 5). The model consists of two key interactions, Bmp upregulation of Sox9 (k_2) and Wnt downregulation of Sox9 (k_3), which are respectively supported by molecular evidences [29] [30]. Other interactions, such as Sox9 mediated Bmp repression (k_4), Self Bmp downregulation (k_5), Sox9 mediated Wnt repression (k_7), and self Wnt downregulation (k_9) are not conserved components of potential BSW models with a variety of topology. This version of the model is proposed because it is the simplest and the most robust Turing network that produces a periodic pattern.

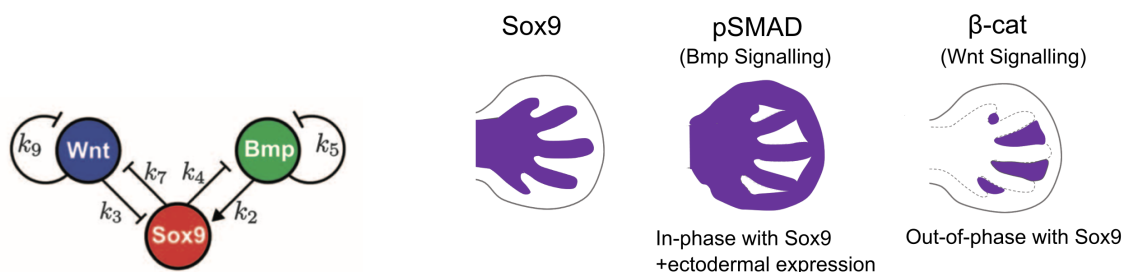


Figure 5. Bmp-Sox9-Wnt model is a Turing-type network responsible for digit patterning. Adapted figures from experimental results of Raspopovic *et al.*, [28]. Figures reproduced under the terms of the Creative Commons attribution licence (CC-BY 4.0). (A) BSW model is a three-component version of a Turing model, with Bmp as a substrate, which promotes the activator Sox9. The inhibition from Sox9 to Bmp over time leads to out-of-phase patterns of Bmp and Sox9. (B) Expression patterns of each protein highlighted with colour.

1.4 Plasticity of the digit patterning

1.4.1 Turing stripe model (BSW model) vs Turing spot model (Hiscock model)

Despite the BSW model accurately recapitulating many aspects of digit patterning, important questions remain regarding its timing and behaviour. Turing-like systems are generally believed to be responsible for the first signs of periodicity [31], but differing theories exist about what happens after the initial Sox9 patterning.

It was originally suggested by Raspopovic et al [28] that the dynamic self-organised reaction-diffusion behaviour persists long enough for the stripes of Sox9 expression to appear. Therefore the BSW model is referred to as the 'Turing Stripe Model'. The degree of reaction-diffusion throughout digit patterning is not compromised in the Turing Stripe Model (Figure 6, right).

As an alternative, the Turing Spot Model proposes that Turing patterning occurs only at an early stage of the digit patterning - resulting only in a collection of Sox9 spots [32], though an examination of wildtype Sox9 time-courses does not reveal any clear spots (Figure 6). After this brief period of patterning, the Turing Spot Model proposes that Turing patterning does not continue to shape the Sox9 stripes, but instead the elongation of spots into stripes is achieved primarily by growth and morphogenesis. The initial Sox9 spots in this model are referred to as digit organising centres (DOCs), and as they move radially outward, they leave behind a trail of condensing Sox9+ mesenchyme (Figure 6). It has been suggested that DOCs are related to the previously described phalanx-forming regions (PFRs) [32]). The Turing Spot Model proposes that the dynamic reaction-diffusion behaviour of the mesenchymal cells terminates before it can contribute to the subsequent stripe shape of Sox9 domains (Figure 6). The Sox9 spot is then elongated through proliferation and incorporation of distal cells. It thus predicts that the reaction-diffusion plasticity of the mesenchymal cells decreases rapidly after the initial spots have formed.

Therefore, investigating how long Turing patterning lasts in digit patterning, or obtaining a profile of 'Turingness' over time will differentiate between the Turing stripe and spot model.

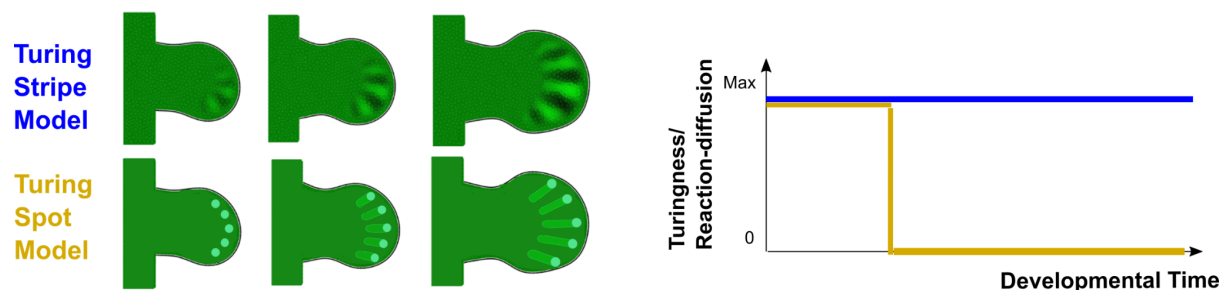


Figure 6. Previously published Turing Stripe model (BSW model) assumed that the degree of reaction-diffusion is constantly high throughout the digit patterning process and afterwards. In contrast, the Turing Spot model proposes that the dynamic reaction-diffusion phase is brief, and the Turingness phase shuts off. The schematics on the right is an illustration of change in degree of Turingness over time.

1.4.2 Plasticity can be only assessed through perturbation

In developmental biology, plasticity was originally defined as the ability to activate and silence genes [33], but is increasingly understood as the ability of cells and tissues to change their fate [34]. A traditional view of plasticity in developmental biology focused on fate decision between individual cell types. The initial exploration into the idea of plasticity started from a question whether a differentiated state of a cell is irreversible, and investigated into capacity for altered gene expression in the fully differentiated muscle cell [33]. From transdifferentiation [35] experiments to induced pluripotent stem (iPS) cell

generation [36], plasticity research has focused on inducing changes in cell type. Organogenesis, differentiation, growth and coordination of these processes, including self-organising digit patterning, all depend on plasticity because cell fate changes are involved in all of these processes.

Importantly, Turing patterning itself depends on plasticity. Since Turing patterning is intrinsically a highly dynamic process, guiding cells in their fate making decisions, it thus depends on the cells capacity to change their fate choices. For instance, the Turing Spot Model proposes that the dynamic reaction-diffusion behaviour of the mesenchymal cells terminates before it can contribute to the stripe formation - meaning that cells have turned off their capacity to establish digits at this timepoint.

At the cellular level, plasticity would be the degree to which the cell adapts its fate according to the signals present in the local tissue (Figure 7). In this sense, plasticity can be understood as the extent to which a change occurs in response to local changes in signals and cues - whether they come from endogenous environments or from an experimental perturbation. In a broader context, in multiple cells or tissue, plasticity could be defined as the degree to which a local perturbation may propagate through the field of cells and alter the states of distant cells.

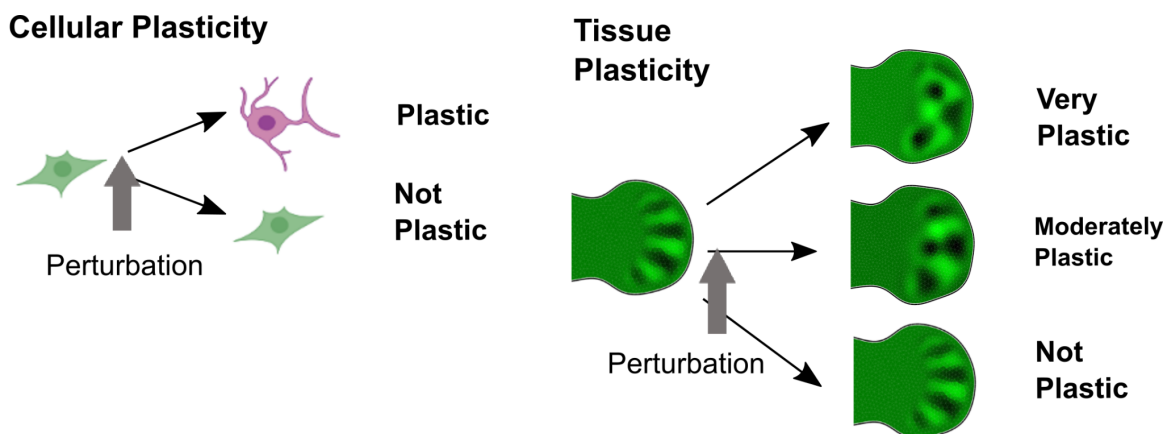


Figure 7. Plasticity can be considered at different scales. Cellular plasticity is broadly defined as an ability of the cell to change its states. Here I explore a broader definition, which addresses the degree to which a field of cells can coordinately change their spatial arrangements of states.

Plasticity, by definition, cannot be measured from wildtype development. It is defined by the response to an external perturbation: a deviation from its predicted developmental trajectory. The plasticity of gene expression would reflect how much it may have changed from what it would have been if no perturbation had taken place.

Tissue perturbations can be chemical, mechanical, or cellular - for example, a perturbation can involve removing a cell from its normal context and grafting it into other tissue regions [37]. These perturbations can in turn address the spatial context of an embryo. Transplantation of a cell or small tissue into a complex embryo environment allowed the researchers to focus on the fate response of the transplanted cell. For instance, *Drosophila* imaginal disc transplantation experiments revealed that explanted cells from the genital area to the head or wings changed their fate in accordance with their new

environment [38]. Further, a series of transplantation experiments led to the curation of drosophila disc fate map, which provided information about the disc organisation [38]. There were also efforts to investigate embryonic limb plasticity along the mouse limb P-D axis by transplantation experiments [39]. A few mesenchymal cells were transplanted from distal to proximal region, and plasticity was measured by the cells ability to change Hox gene expression.

It is important to note that while all of the literature so far addresses spatial context in an embryo, they all investigate plasticity along a 1D single axis.

1.5 Cell movements and density changes in digit patterning

While the previous discussion focused on the molecular aspects of digit patterning, it is worth emphasising the importance of cellular movements and tissue density changes, and expand the discussion to probe whether these tissue changes are completely independent processes that follow digit patterning.

In the early dynamics of digit patterning, identical mesenchymal cells choose between the digit/interdigit fate and start condensation. This process is referred to as the “symmetry breaking point” [40], because cell fates from mesenchymal limb tissue are not identical anymore. Condensation involves cells moving towards the digital region, while cells moving out of the interdigital areas, which progressively lose their density. The digital region thus transforms from initially homogeneously distributed mesenchymal cells into a periodic pattern of cell density, and the condensations then transform into cartilage. However, very early dynamics of cell movements have not been documented, despite a general belief that condensation is followed by digit patterning [41]. However, whether condensation/cell movement happens at the early “symmetry breaking point” of digit patterning, is not known. Could it be involved in molecular digit patterning while reaction-diffusion is being established, or is it a downstream process happening after molecular digit patterning?

1.5.1 Mechanochemical model, Pure mechanical model and Pure reaction-diffusion model

Indeed, the intertwined nature of cellular signalling and tissue movements makes it difficult to navigate this question. Classical mechanochemical models suggested that a two-way feedback between cell movements and molecular patterning could be required for a pattern formation. Oster, Murray and Harris [42] suggested that cell traction forces on the extracellular matrix drive local cell motion, which in turn leads to chemical response of guidance cue secretion from a deformed ExtraCellular Matrix(ECM). For instance, ECM digesting proteins from the cells, or diffusible extracellular proteins/lipid factor can guide cell-cell contacts. In the context of digit patterning, chondrocytes are already aligned in multiple ‘rod’ patterns following initial digit patterning. Chondrocytes secrete hyaluronic acid, which is an osmotic agent, swelling the matrix and creating tissue stress along their border, creating circumferential ‘hoop’ stresses, which would help the cells to migrate towards the centre of the rods [42]. This way, the mechanochemical model proposes that the initial presence of cell traction forces, which then triggers chemical cues, can lay out coordinated movements of tissue further promoting subsequent cell movements.

Mechanochemical control of mesenchymal condensation has also been demonstrated in different systems such as tooth formation [43]. Early epithelial signals such

as FGF8 and SEMA3F respectively attract and repulse mesenchymal cells, leading to condensation of the cells. This compaction process in turn brings cell shape changes, which then activates odontogenic transcription factors such as PAX9.

On the other hand, pure mechanical models propose that cell density change can occur solely from mechanical processes, such as local compressive stress, rather than dynamic molecular reaction-diffusion [44] (Figure 8). For instance, a tissue that is growing in a constrained manner can lead to tissue compression, resulting in surface buckling, or wavy patterns on the surface [44]. Although it has not been found how pure mechanical forces inside limb mesenchymal tissue can drive condensation, it is a theoretically possible scenario.

The alternative extreme is a model in which digit patterning is driven by pure reaction-diffusion (Figure 8). In this case, the digit patterning process happens prior to condensation and cell movements are interpreted as a downstream result of molecular patterning (instead of having molecular patterning and condensation heavily coupled).

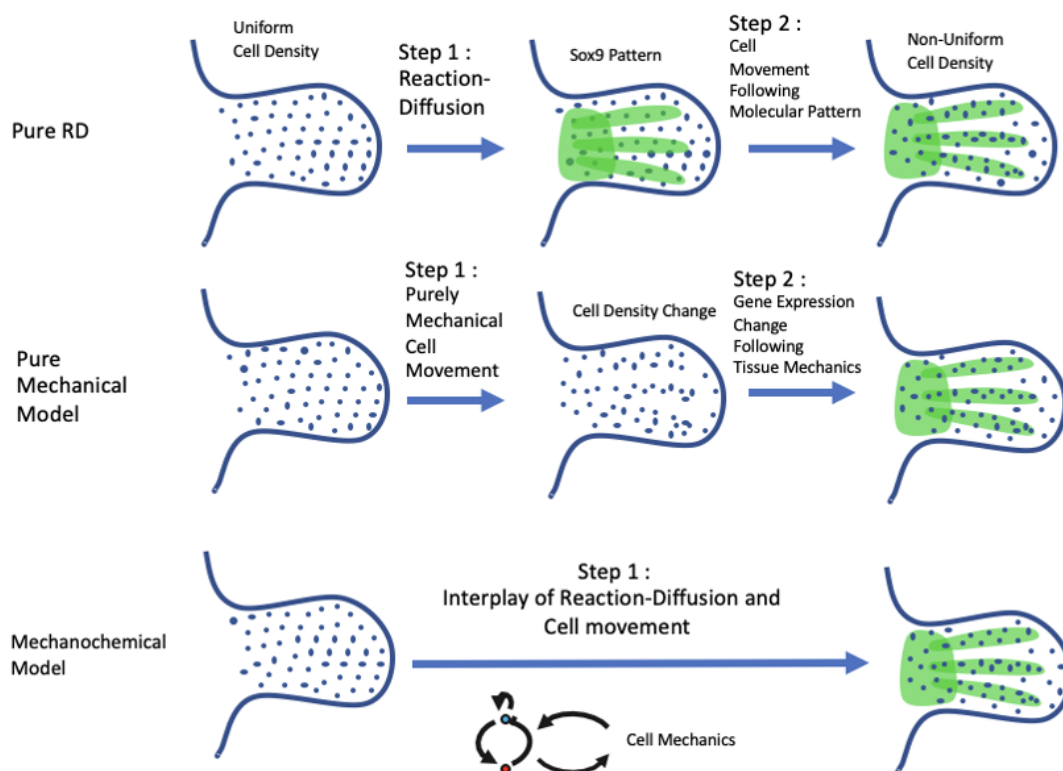


Figure 8. Different scenarios of digit patterning. Cellular movements could be interpreted as a downstream result of molecular patterning (Top). Pure mechanical model proposes that cell density change can occur solely from local compressive stress(Middle). Alternatively, the mechanochemical model suggests that a two-way feedback between cell movements and molecular patterning is required (Bottom).

1.5.2 The relative timing of molecular digit patterning versus cellular movements

A previous study distinguished Sox9 intensity from cell density in mouse embryonic limb zeugopod [45] at E11:06(Figure 9). The experiment revealed that despite the apparent

Sox9 expression in zeugopod, the cell density between Sox9+ and Sox9- regions are not different. The cell density was quantified by counting the number of nuclei in a unit area. The study showed that at E11:06, Sox9 expression change is detected but mesenchymal condensations are not observed..

The technique applied in this study [45] can be further extended to broader developmental time to reveal the relative timing of digit patterning against cell density changes. Doing so would unravel the intertwined nature of cellular signalling and tissue movements, and would indeed examine whether molecular Sox9 patterning in the digit and cell movements are distinguishable processes. To investigate the temporal order of Sox9 patterning and cell movements during the digit patterning process, the experiment should be performed on embryonic limb autopods.

Knowing the temporal order of Sox9 expression and cell density change would reveal whether the underlying mechanism of digit patterning is the Mechanochemical model, Pure mechanical model and Pure reaction-diffusion model. If cell density change occurs before Sox9 pattern arises, the result would support a pure mechanical model, in which that cell movements prime the molecular pattern change. If Sox9 patterning happens before the cell density starts to change, then cell density change/ digit condensation is a downstream event of molecular patterning, possibly mediated by consequences of signalling pathways that are relevant to digit patterning.

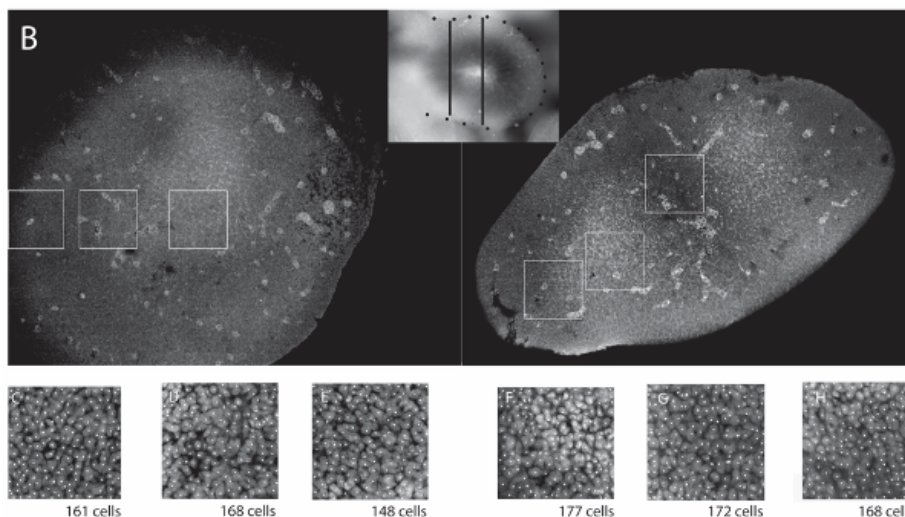


Figure 9. Sagittal cryosections of a limb bud at E11:06, across different points of PD axis. Both sections are fluorescently stained for Sox9 expression and for the nucleus. Two sections were imaged. And square sections each representing digit, interdigit, and border region are selected. Figure from Boehm et al[45].

1.6 Known and unknown roles of Wnt signalling in digit patterning

1.6.1. Known roles of Wnt signalling in digit patterning

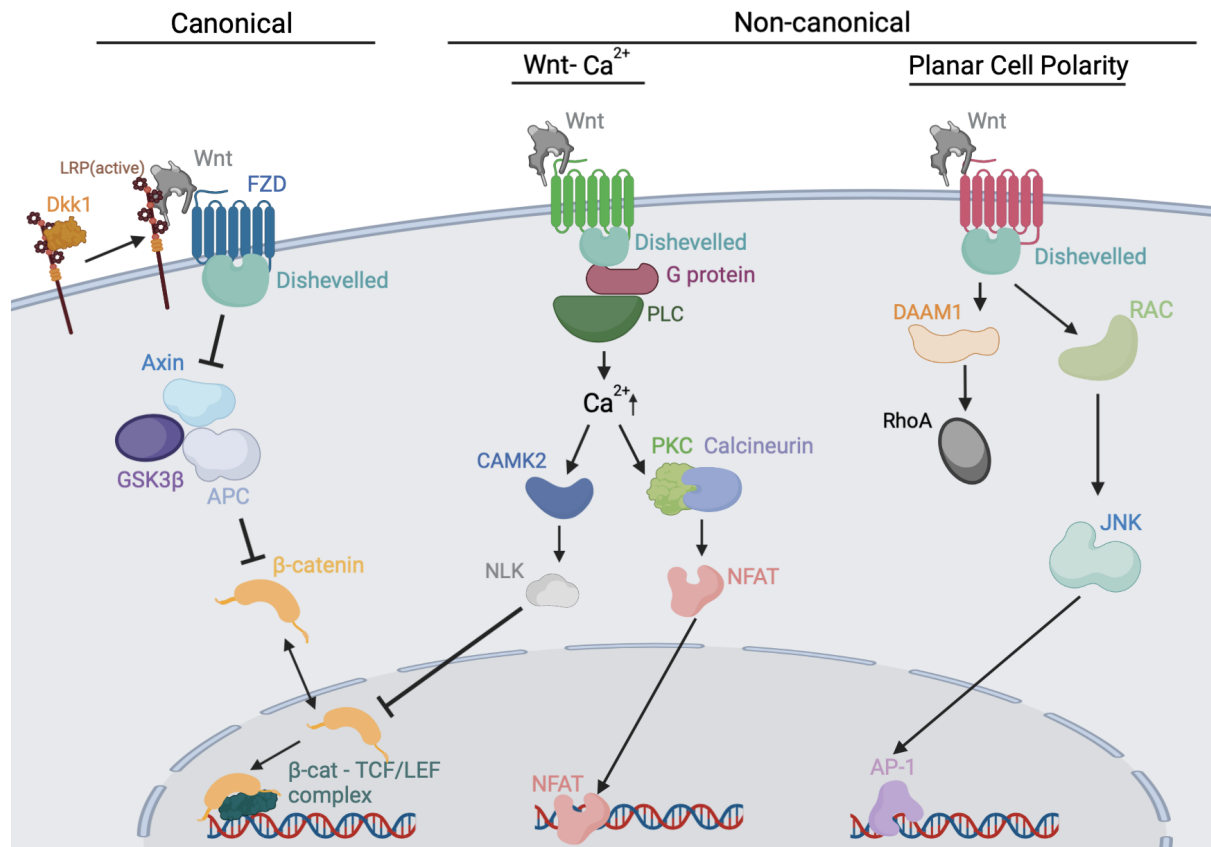


Figure 10. Schematics of canonical and non-canonical Wnt pathways.

The Wnt signalling pathway plays major roles in embryonic development by governing differentiation processes, a critical step towards formation of a multicellular organism. Wnt signalling is required for building major body structures, such as vertebrate body axis[46], central nervous system [15] and somites [48]. Wnt signalling plays pervasive roles in most aspects of embryonic development[49], including dorsoventral and anteroposterior body axes in multiple animal species [50].

Wnt proteins are secreted from the endoplasmic reticulum, through the Golgi body to the extracellular environment (Figure 10). Wnt proteins need to be palmitoylated by the action of Porcupine in the endoplasmic reticulum prior to secretion [51]. Palmitoylation is critical for the Wnt protein's ability to bind to its cell surface Frizzled (FZD) receptors [52]. Wnt proteins also require Wntless, which is a seven-pass transmembrane protein cargo receptor, in order to be brought outside of the cell [53].

In mice, secreted Wnt ligands can be regulated by Wnt-binding antagonists such as the secreted Frizzled-related protein (sFRP) family. sFRP binding to WNT is mediated by N-terminal cysteine-rich-domain homologous to those of FZD receptors [54]. One example of

Wnt ligand binding to sFRP family is WNT3A - it is shown to bind to sFRP1, 2, 3 and 4 by surface plasmon resonance. However, only SFRP1 and 2 were shown to inhibit WNT3a-dependent signalling in mouse embryonic stem cells [55]. In developing chick neural tubes, both SFRP1 and SFRP2 can inhibit WNT3a activity while SFRP3 cannot [56]. sFRPs bind directly to FZD proteins by the cysteine-rich domain as well. sFRP-FZD binding prevents the interaction with WNT and thereby inhibits Wnt signalling [57].

Wnt signalling pathways are conventionally divided into canonical β -catenin mediated pathways, and non-canonical pathways characterised by β -catenin-independent actions [58].

In the Wnt canonical pathway, Wnt proteins bind FZD proteins - seven-pass transmembrane receptors with an extracellular N-terminal cysteine-rich domain which enables Wnt interaction [59]. Then Lipoprotein Receptor-related Proteins (LRP) family co-receptors further bind with the WNT-FZD complex to fully activate the signalling downstream [60]. LRP binding is a critical regulatory point by a variety of extracellular antagonists, some of which such as the Dkk family alter the Wnt receptor activity. Active Wnt signalling has LRP5/6 forming a complex with Wnt ligand and FZD to activate downstream cytosolic components such as dishevelled [61]. On the other hand, Dickkopf (Dkk) proteins inhibit Wnt signalling by direct binding to LRP5/6, internalising and inactivating of LRP5/6 [62]. Dkk family proteins, like sFRP family, use cysteine-rich domains that mediate protein-protein interactions to bind onto LRP6 co-receptor and inhibits beta-catenin-dependent Wnt signalling [62].

In the absence of Wnt signalling, β -catenin is phosphorylated by GSK-3 in the "destruction complex" brought together by Axin and APC. Phosphorylated β -catenin was then recognized by the ubiquitination machinery and sent to degradation in the proteasome. On the other hand, when active Wnt-Fzd-Lrp5/6 complex is formed outside the cell, Dishevelled is activated, which leads to disassembly of the β -catenin "destruction complex" such that β -catenin phosphorylation is reduced and stabilised. The stabilised β -catenin then translocates to the nucleus where it regulates downstream gene expression by binding to Lef/Tcf factors.

The non-canonical Wnt- Ca^{2+} pathway signals through regulating intracellular calcium mobilisation [63]. The planar cell polarity (PCP) pathway controls tissue polarity and cell movement through the activation of RHOA, c-Jun N-terminal kinase (JNK), and nemo-like kinase (NLK) signalling cascades [64]. In vertebrates, Wnt5a is considered a default non-canonical wnt ligand, and is the most investigated [65].

There have been suggestions of a network of integrated Wnt signalling pathways instead of the binary classification, because of the significant degree of intertwined canonical and non-canonical pathways [66]. For instance, the non-canonical pathway can inhibit the canonical pathway at multiple levels. Wnt- Ca^{2+} pathway can inhibit β -catenin signalling through NLK, or through NFAT transcription [64].

Understanding wnt signalling is challenged by the number of molecular components with roughly 20 secreted Wnt proteins, which may interact with 10 different Frizzled (Fzd) receptors on the cell surface [59]. Further, the promiscuity of Wnt-Fzd protein interaction in which a single Wnt can bind multiple Frizzled proteins, and the presence of co-receptors to activate the signalling on the cell surface adds onto the complexity of Wnt signalling.

The variety of receptors and co-receptors not limited to FZD makes the pathway activation complicated. Some examples of these co-receptors include receptor tyrosine kinase (Ryk), tyrosine-protein kinase transmembrane receptor 1/2 (Ror1/2) and collagen triple helix repeat containing protein 1 (CTHRC1)[65]. Unique combinations of these receptor/co-receptor/ligand complexes, as well as the type of cells that express these signalling components, determine whether the pathway is activated or not [67].

In the context of mouse embryonic limb buds, Wnt signalling is active in the interdigital Sox9⁻ area, whereas it is inactive in the interdigital Sox9⁺ area [28]. Wnt signalling components, such as active β -catenin are selectively expressed at interdigital (Sox9⁻) tissue, demonstrating active canonical wnt signalling upregulated in out-of-phase manner with Sox9 patterns. Such observation satisfies the condition of the Turing network, which requires its components to have periodic patterns that are either in-phase or out-of-phase, respectively. It has already been previously known that canonical Wnt signalling mediated by β -catenin inhibits Sox9 expression and chondrogenesis [30]. Genetic studies also have shown that conditional β -catenin knockout in the limb results in the expansion of Sox9 toward the ectoderm[68], and β -catenin limb gain-of-function mutation results in Sox9 downregulation [69].

Microarray analysis between Fluorescence-Activated Cell Sorted(FACS) Sox9⁺ and Sox9⁻ cells identified various diffusible Wnt inhibitors *Dkk1*, *Dkk3*, *Sfrp2*, *Sfrp1*, *Shisa2* and *Sulf1* to be upregulated in Sox9⁺ cells. Some of them - *Sfrp2*, *Shisa2* and *Sulf1* - have *in situ* digital expression in mouse embryonic limb (Figure 11). sFRP family is a diffusible Wnt inhibitor that directly targets Wnt proteins using its cysteine-rich domain [70], unlike Dkk antagonists that alter Wnt receptor/co-receptor activities as previously explained. sFRP Knockout mutants usually have mild brachy-syndactyly and polydactyly[71]. Not only Wnt regulators, but also Wnt target genes (such as Axin2 and Twist1, see Figure 11) are upregulated in the interdigital regions [28].

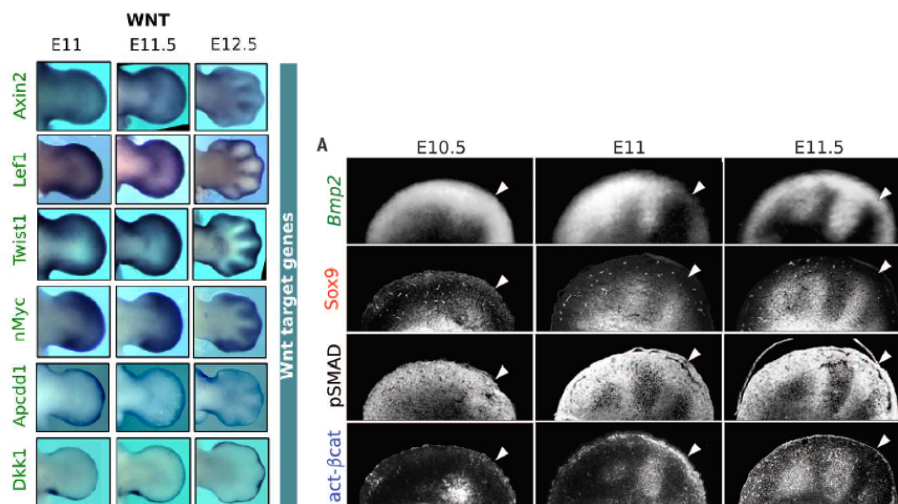


Figure 11. In situ and immunostaining images of Wnt target genes and active- β -catenin. Adopted from Raspopovic *et al* [28].

Perturbation studies show that activation of the canonical Wnt pathway, specifically by Wnt3a, downregulates Sox9 [28]. In a local manner, insertion of Wnt3a-soaked beads in the limb culture prevents Sox9 expression in the surrounding area (Figure 12). Global Sox9

patterns are also prevented upon application of Wnt3a in micromass (high-density cell cultures of dissociated limb bud mesenchymal cells). Global application of Wnt inhibitor IWP2 on limb culture only leaves Sox9+ cells, abolishing periodic digit patterning [28].

Micromass is a useful tool in investigating limb pattern because Sox9 expression in micromass forms a spot or stripe pattern. Because micromass seeds high-density cultures, it forms three-dimensional, multilayered mesenchymal cells, which move, change gene expression during the patterning, and even differentiate [72]. The culture system also includes pericellular and extracellular matrix molecules (ECM) [73].

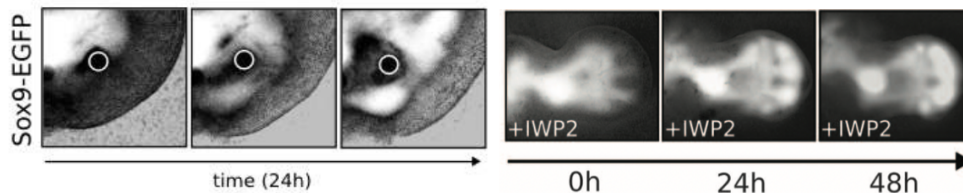


Figure 12. Left) Insertion of a bead in limb culture. Sox9-EGFP expression in white, and bead outline in circle. Right) Application of IWP2 on limb culture. Figure from Raspopovic *et al* [28].

1.6.2. Gaps in our knowledge of Wnt signalling

The most important remaining question is to uncover the mechanism through which Wnt acts on repressing Sox9. Although the BSW model consists of a set of interactions that explain periodic digit pattern emergence, there is not much known about how Wnt repression on Sox9 (via parameter k_3) works in the context of individual molecular interactions (parameters k_2 - k_9) to generate the digit pattern. In fact, the topology of the BSW model presented in Figure 13 is the simplest topology out of nine networks that generate the correct digit pattern, meaning that there could be different combinations of k_2 - k_9 . In all versions, Wnt repression on Sox9 (k_3) is conserved, meaning k_3 is an indispensable interaction in the BSW model.

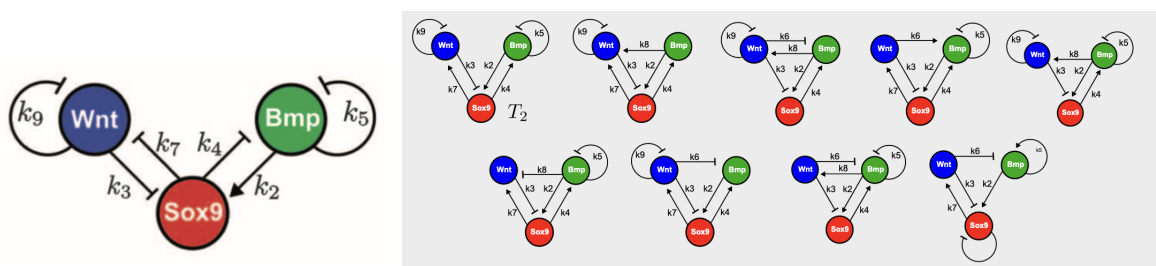


Figure 13. Left) The simplest network topology of the BSW model. Right) All possible topologies of the BSW model that can generate in-phase pattern between Sox9 and Bmp, and out-of-phase pattern between Sox9 and Wnt signalling. Figure from Raspopovic *et al* [28]

As previously mentioned, there is ample biochemical evidence from limb culture (Figure 12) [28], genetics [68] and bead interruption (Figure 12) [28] that Wnt does indeed interrupt the digit patterning and disrupt Sox9 patterning.

However, the specifics of molecular mechanism, including which type of Wnt pathway is involved (canonical/non-canonical), which components of Wnt pathways are involved (Wnt ligands/Wnt receptors/cytosolic components/transcription factors), which specific Wnt ligands are involved (Wnt3a, Wnt5a etc), and which Wnt antagonists are involved (Dkk1,

Sfrp1, etc) have not been investigated, especially in a systematic, data driven way. Putting together these details would highlight the possible mechanisms through which Wnt represses Sox9, and how it cooperates with the rest of the interactions in the BSW model.

The current BSW model with the simplest topology requires a negative feedback from Sox9 to Wnt (via parameter k_7), in order to generate complete five digits [28]. Since Sox9 is a transcription factor and can only act inside the cell [74], the simplest interpretation is that Sox9 promotes a Wnt inhibitor or antagonist that inhibits Wnt signalling in the extracellular manner. However, the identity of the Wnt inhibitor is unknown, as well as to which component of the Wnt pathway is the inhibitor targeting. For instance, WIF can bind directly to Wnt proteins, while others like the Dkk family alter the Wnt receptor activity [70]. sFRP family is able to bind directly to Wnts and FZD receptors [75]. Still, previous microarray analysis [28] identified that some diffusible Wnt inhibitors such as Sfrp2 and Shisa2 are differentially expressed in Sox9+ and Sox9- cells, meaning that these could potentially direct Wnt signalling in digit patterning.

Some Wnt production inhibitors, such as IWP2 are known to cause digit merging [28] (Figure 14), but it is unverified if all categories of Wnt inhibitors will lead to digit merging. There is also a possibility that different Wnt inhibitors will bring about different spatial and temporal dynamics of digit merging, or a completely different type of digit phenotype. So it is important to identify the digit phenotype that arises upon application of these different categories of inhibitors.

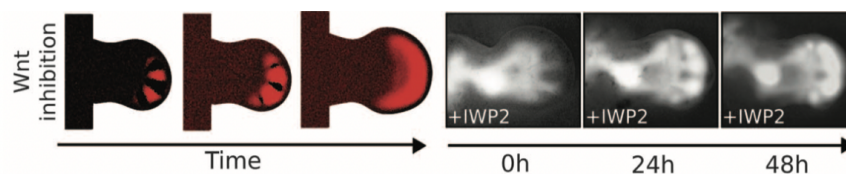


Figure 14. Left) Modelling result of Wnt production inhibitor (IWP2). Right) mouse embryonic limb incubated with IWP2 for 48 hours. Figure from Raspopovic *et al*[28].

Understanding which Wnt components/pathways are involved in digit patterning, and repression of Sox9, would reconcile some puzzling results. For instance, even though IWP2 - an inhibitor of Wnt secretion - has digit merging effects in limb culture, its application does not have any impact on 2D micromass culture (Raspopovic *et al*, unpublished). Application of multiple ligands that has similar effect to IWP2, or targets different components will give insight to such contradictory results.

As previously shown in Figure 12, the perturbation experiments identify Wnt3a as a candidate ligand responsible for digit patterning[28]. However, Wnt3a expression is exclusive to the ectoderm, meaning that its signal is transduced to full mesenchyme tissues. In contrast, basic conditions of a Turing model indicate that the diffusible molecules should be expressed throughout the tissue, and these diffusible molecules of the Turing network should form periodic patterns.

Further, it is not known how ectodermal specific signals generate an activating cue of Wnt signalling in the limb mesenchyme. There is a hypothesis suggesting that the central Sox9 expression pattern at the mouse embryonic limb initiation stage (Figure 3A) is due to ectodermal Wnt signalling towards the mesenchyme, and proposes that the working range of the ectodermal Wnt signal is about 100 μm , which is the distance between the ectoderm and Sox9 expressing cells [30]. However, it is apparent that in later digit patterning stages, the tips of the Sox9 pattern are adjacent to the ectoderm - less than 100 μm . More importantly,

numerous canonical Wnt signalling target genes (*Axin2*, *Lef1*, *Twist1*, *Mycn*) are expressed throughout the mesenchyme before the start of digit patterning (Figure 11) [28]. The molecular mechanism of ectodermal Wnt3a activating mesenchymal Wnt signalling is still missing.

If instead we look for WNTs that are known to be expressed throughout the mesenchyme, one clear candidate is Wnt5a (Figure 15) - however so far, experiments have not found it playing a role in digit patterning [76]. Wnt5a bead insertion experiment in the mouse embryonic limb has not previously shown any pattern change [28]. Without changing the number and wavelength of the digits, Wnt5a limb specific conditional knockout generates short, stumpy digits [77]. Still knowing that Wnt5a is the most well studied PCP pathway ligand [64], there is a possibility that the non-involvement of Wnt5a in digit patterning despite its mesenchymal expression is due to its non-canonical specific actions.

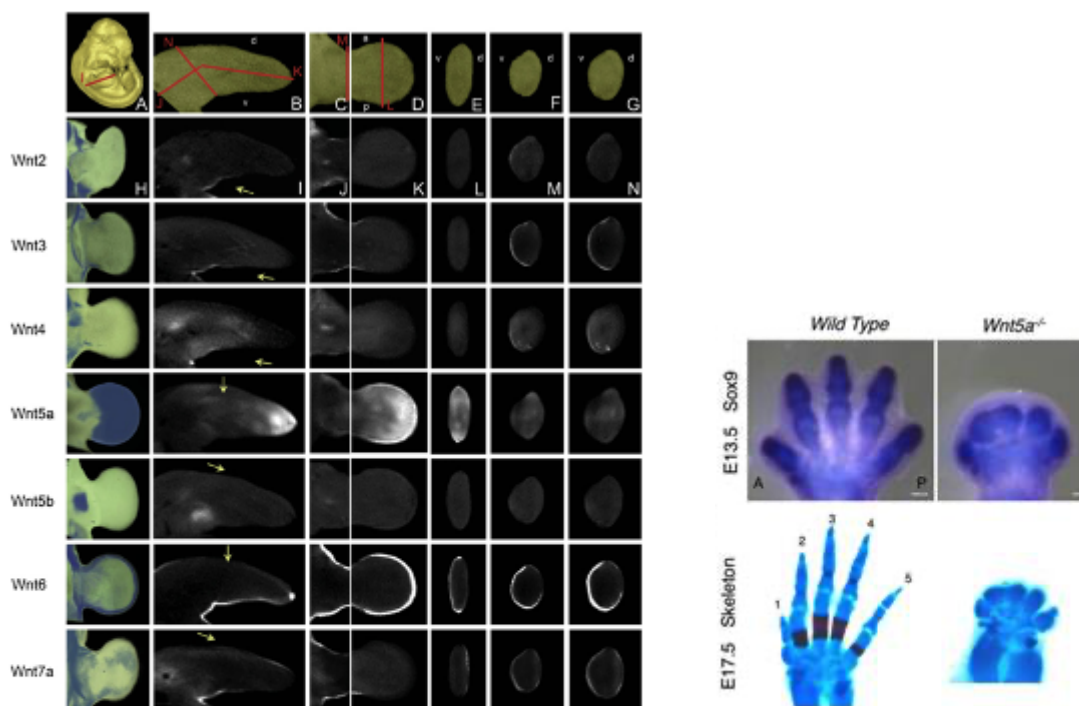


Figure 15. Left) Wnt expression patterns in mouse embryonic limbs at E11:12. Adopted from Summerhust *et al* [76]. Right) Wnt5a conditional knockout generates stumpy digits. Adopted from Gao *et al* [77].

1.7 Unbiased screening to address unknown roles of Wnt signalling

Screening approach refers to the application of a variety of candidates with known function to systematically perturb a system [78]. A vast amount of data is generated from the screening approach - which comes in a variety of forms depending on the initial experiment. Screening approach allows systematic exploration and analysis in a non-hypothesis-driven manner. This less biased approach can lead to discovery of a novel target and pathway to achieve a desired phenotype [79].

Developmental biology has benefited from the use of screening approaches. Early examples include forward genetic screening in zebrafish using either chemicals or insertional mutagenesis [80]. Recently, high-throughput screening and imaging of organoids revealed biological principles [81].

Availability of a variety of experimental systems, such as limb bud culture, micromass and bead insertion, is critical to a screening approach. In the murine limb bud culture system, limb buds are dissected and transferred onto a system that allows media-gas interface, such as membrane inserts with pore. Limb bud culture is a reliable system that allows limb development mimics that of *in vivo*, with approximately 70% growth rate. If left after E14.5, cartilage differentiation can be observed, leading to the formation of proximal and distal structures [82]. On the limb culture, small molecule inhibitors can be applied in the media and its impact on the digit patterning can be assessed globally.

Micromass is a 2.5D mesenchymal high density cell culture that has a few layers of mesenchymal cells from freshly dissected mouse embryos. Without perturbation, micromass cells undergo symmetry breaking, mesenchymal condensation and generate periodic Sox9 patterns by 15 hours [28], with dynamics resembling a two-dimensional Turing system. Micromass is a convenient system to quantify subtle changes upon small molecule application, because changes in period or intensity of the Sox9+ condensation pattern can be easily quantified. Both naked eye observation and Fourier transform analysis can be used to assess the sensitivity of the system to the given treatment. Another advantage is that micromass experiments allow exposure of small molecule inhibitors directly onto mesenchymal cells, without ectodermal protection.

Bead insertion is a useful technique to deliver specific small molecules in a bead, directly into the mesenchymal cells of the tissue, overcoming the ectodermal barrier. A variety of beads from affigel to heparin beads can be used [83]. In mouse embryonic limb, change in the expression of endogenous marker genes, such as Sox9 from Sox9-EGFP transgenic mouse can be observed.

One advantage of the screening approach is that it allows easy targeting of the application time window. Another advantage is that the use of results from multiple perturbation methods / systems could complement one another.

Screening approach combined with data driven modelling will help to understand limb development as a complex system, by providing multiple lines of experimental evidence to construct a model. For instance, to identify the main feedbacks involved in digit patterning, Raspopovic *et al* [28] performed microarrays, *in situ* of signalling pathway components, and used these findings to build a three-node model using linear stability analysis. Based on the experimental result, the models with periodic patterns in which Sox9 is in phase with Bmp expression and out of phase with Wnt signalling activity were selected. In a different study, Uzkudun *et al* [84], *in situ* gene expression patterns on mouse embryonic limbs were used to predict the regulatory mechanisms that underlie mouse limb bud proximodistal patterning. In this study, spatial expressions of proximal distal markers *Meis1*, *Hoxa11* and *Hoxa13* are identified. Once candidate gene regulatory networks are generated, they are reverse engineered to interpret the opposing gradients of FGF and retinoic acid (RA) along the PD axis.

Similarly, LimbNET, a Sharpe lab-built mesh-based simulation of molecular patterning in limb development, can be used to reconcile perturbation results from different experiments in various systems. LimbNET can already model gene expression dynamics and can

recapitulate wild type Sox9 digit patterning using BSW model. LimbNET allows recapitulation and assessment of experimental results from screening approach, allows to build and develop new models, and to test hypotheses generated from screening approach.

1.8 Other pathways that modulate digit patterning

Although it has been suggested in the BSW model that Wnt pathway is one of the main feedback loops involved in digit patterning, it is necessary to confirm whether the Wnt pathway has primary importance over other pathways. Previous microarray analysis, which searched for differentially expressed genes between Sox9+ and Sox9- cells, looked at a few signalling pathways including Wnt, Bmp, TGF, and FGF. However, other significant pathways, such as the Retinoic acid pathway or Notch signalling pathway traditionally known to be involved in limb patterning processes or patterning of other organs, have not been systematically assessed for their relative importance against the Wnt pathway.

Like the Wnt pathway, Retinoic acid(RA) pathway is involved in both limb patterning, and has been long suggested as a modulator of chondrogenesis[85]. RA forms a gradient along the proximal-distal axis[86], higher in the proximal end. RA concentration in the distal end is low due to the expression of *Cyp26b1*, an enzyme that degrades RA to inactive forms[87]. RA treated chick limbs exhibit anteroposterior duplications[88] involved in establishing the proximodistal axis of the limb, while applying retinoic acid itself has anti-chondrogenic effect, subsequently generating stunted limbs[89].

RA is able to make downstream transcriptional changes through Retinoic acid receptors(RARs). RARs are nuclear receptors that have RA bound onto specific RA response elements (RAREs), and once activated by RA, they form heterodimers with members of the retinoid X receptor (RXR) subfamily. RARs also activate kinase signalling pathways, which can possibly modulate RA target gene transcriptional level. Out of many different types of RAR, RARs α and γ are expressed in overlapping regions during fore limb development from E9.5 to E11.5[90].

Genetic studies, *in vivo* injection studies, and some small molecule applications already suggest that applying RA inhibits chondrogenesis[91] and leads to a variety of digit phenotype changes including digit merging[89], digit loss[92], and period change[93]. Kochnar *et al*[89] showed that RA injection into a pregnant mouse at a concentration of 80mg/kg once at E12:10 disrupts spatial patterning of mesenchymal cells(Table 1). Interestingly, injection 24hrs later was less impactful to the digit patterning, meaning that RA impact is sensitive during digit patterning stage. Other more constitutive RA upregulation, such as *Cyp26b1* limb conditional knockout shows digit loss[94]. RAR mediated activated RA pathways, such as constitutive activation of RAR α 1 exhibited a spectrum of defects that included poly/syndactyly, and carpal fusions[92]. Apart from genetic modulations, a small molecule application study by Galdones and Hales [93] allowed time-specific RAR activation. However, in their experiment, RAR activator BMS961 was administered from E12:12 onwards. Later administration of the RA pathway inhibitor already gives digit loss/period change phenotype - therefore it is important to try similar inhibitors during the digit patterning stage, from E11:06-E11:13.

Micromass also shows clear and correlated pattern change - RA pathway activation interrupts condensation of Sox9+ cells, leading to interrupted and lost pattern[91] [95], while

RA pathway inhibition through RAR inactivation leads to stronger condensation[91]. Still, the micromass and imaging protocol are inconsistent across different literatures. For instance, the seeded quantity of the cells(10 μ l [91] Vs 20 μ l [95]), days of culture(4 days [91] Vs 7 days [95]), and magnification(5x [91] Vs 40x [95]) are different. Therefore, it is critical to validate the published results under the consistent condition using a variety of small molecules/ligands at different doses.

Overall, non-severe limb phenotypes in constitutive knockouts, such as syndactyly, suggests that RA pathway is likely to be modulating digit patterning rather than being a critical part of the digit patterning network. Again, it is critical to validate this hypothesis with unbiased screening and by targeting the inventions specific to the digit patterning stage.

Another pathway that is important in many different developmental processes is Notch signalling. It plays a critical role in cellular differentiation pathways and morphogenesis during embryogenesis. The Notch signal is activated by interaction of the Notch receptor with other epidermal growth factor (EGF)-repeat-containing transmembrane ligands, such as Delta and Jagged. Ligand binding to Notch triggers proteolytic cleavage of the intracellular domain of Notch. Subsequently, the intracellular part is translocated into nuclei and activates target genes such as those of the Hes and Herp families.

The Notch-delta pathway is also a candidate that is likely to indirectly modulate digit patterning, because Notch signalling perturbation generates even less subtle phenotypes than RA pathway interventions. For instance, DAPT, a pharmacological inhibitor of Notch signalling, leads to irregular digit fusion *in ovo* [96] (Table 1). Other genetic interventions, such as constitutive activation of Notch intracellular domain, only results in slightly diffuse Sox9 pattern at E12.5 [97] (Supplementary Table 1). Deletion in the DSL domain of Notch receptor Jag2 shows mild syndactyly in neonatal mice [98].

Micromass treatment by DAPT increased alcian blue positive area and the number of the nodules, after 7 days[99]. After 7 days, *Id1*, a downstream target of canonical BMP signalling, was also considerably increased by the DAPT treatment. It would be critical to repeat the experiment and validate the micromass patterns during the symmetry breaking stage (15hr-24hr from seeding), because at later stages Notch signalling can be inhibited by developed characteristics of the nodules. At day 7 micromass culture, a large amount of matrix is produced by maturing chondrocytes, and these matrix proteins separate each cell from direct contact with its neighbours. This physical separation may interrupt Notch signalling from the neighbouring cells.

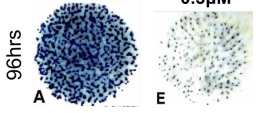
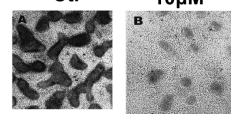
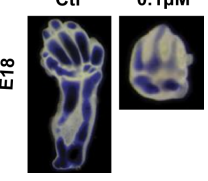
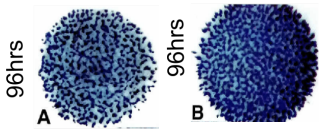
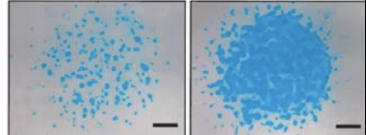
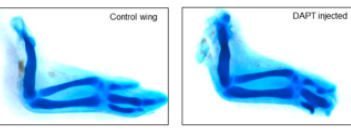
	Mechanism	Micromass - Literature	Period Change	Limb Culture- Literature	Limb Pattern change
RA activation	Retinoic acid application	<p>RA application [91]</p> <p>Ctl 0.3μM</p> <p>96hrs</p> 	Longer	<p>80mg/kg injection into pregnant mouse [89]</p> 	Digit merging
	Cyp26b1 inhibition	<p>Liarozole application [95]</p> <p>Ctl 10μM</p> 	Longer	<p>Cyp26b1 conditional knockout [94]</p> <p>Ctl cyp26b1^{-/-}</p> 	Digit loss
	RAR activation	Could not find	-	<p>Small molecule activation of RARγ by BMS961 [93]</p> <p>Ctl 0.1μM</p> <p>E18</p> 	Syndactyly, digit merging /period change
RA inhibition	RAR inhibition	<p>RARβ antisense RNA application [91]</p> <p>Ctl 6μM</p> <p>96hrs</p> 	shorter	Could not find	-
Notch inhibition	Gamam secretase inhibition	<p>DAPT applied micromass day7[99], 100nM</p> <p>Control DAPT</p> 	Shorter	<p>DAPT injected chicken limb Image from Bhat R <i>et al</i> [96]</p> 	Digit curving

Table 1. Literature search of RA and Notch pathway modulations in micromass and limb.

2. Aims of the study

The overall aim of this project is to study an emergent biological process - digit patterning - as a dynamical system, finding out what model can explain the system through interplay of modelling and experiments. Based on previous studies, digit patterning has already been described as a self-organising system, but I further study detailed dynamics of the system, and reexamine molecular pathways/components involved in the network, by asking the question “To what extent is digit patterning a Turing system?”

To answer the first part of the thesis, “For how long is digit patterning a dynamic reaction-diffusion system”, characterising and quantifying the plasticity of the emerging digit pattern is necessary. The goal for this part is to devise a method to quantify plasticity, and to apply the quantified values into the modelling platform, with the aim of verifying whether the measured plasticity dynamics can account for digit patterning mechanism.

Then the second part, unbiased screening of molecular pathways, attempts to experimentally extract more details about Wnt signalling during the digit patterning. I ask the following questions : How strong is the evidence for WNT being a major player? Can I pin-down whether this is canonical versus non-canonical signalling? What are the different impacts on patterning caused by different types of Wnt perturbation?

To fill the gap in knowledge, such as finding out the molecular mechanism of Wnt signalling, a variety of perturbation approaches are adopted. The aim of this section is to analyse and make sense of a volume of data generated from the screening approach, using the LimbNET modelling platform. I hope to provide new insights into the digit patterning mechanism and identify future questions to be answered.

3. Results Part I : For how long is the digit patterning a dynamic self-organisation process?

Although the BSW model successfully recapitulated many aspects of digit patterning, important questions remain about the details of its timing and behaviour. Most accounts agree that a Turing-like system is responsible for the first signs of periodicity [31], [32], but different proposals exist about what happens after the initial Sox9 pattern is formed.

3.1 On Day 11 digit patterning behaves as a very dynamic and plastic Reaction-Diffusion system

The first step of plasticity measurement in digit patterning would be to explore to what extent the self organising behaviour of the system can be disrupted or manipulated. Since two of the BSW components - Bmp and Wnt - are signalling molecules, I explored in more detail the extent to which the insertion of beads containing these diffusible ligands could disrupt the digit pattern. Beads containing Bmp2 or Wnt3a - the proposed morphogen components of the reaction-diffusion based model - were inserted into the limbs, and I assessed the response of the system by reading out 2D Sox9 pattern changes. According to the BSW model and prior literature [30], Wnt inhibits Sox9, and Bmp upregulates Sox9, so demonstrating this result in the limb confirmed that mouse limb mesenchymal tissue is a dynamic system that responds to RD perturbation. Any changes in the Sox9 pattern would reveal not only about the RD dynamics of the system, but also about molecular plasticity and cell fate plasticity since Sox9 is a pre-chondrogenic marker.

Upon bead insertion on Day 11, digit patterns are significantly altered (Figure 16A, Figure 16B), indicating high level of plasticity in the system. Control beads (soaked in PBS 1x, without any ligands) are used to monitor the impact of the experiments - normal stripes of Sox9 continue to develop, despite the physical intrusion of the bead (top panels in Figure 16A,B). By contrast, Wnt beads cause an interesting reorganisation of the Sox9 pattern - typically causing the stripes to become curved “around” the bead. Notably, the curved shape of the Sox9 stripe indicated that at a distance beyond the direct influence of the inhibitor, Sox9 levels have actually been increased - despite the experimental perturbation being a Sox9 inhibitor (Figure 16A). This supports the idea of patterning being a reaction-diffusion system, in which longer-distance “indirect” effects can cause the opposite expression changes (up-regulation) compared to the local direct effects (down-regulation), due to a chain of cell-cell signalling events.

To push the system further, and to explore to what extent the entire autopod pattern could be reorganised, I next inserted combinations of Wnt and Bmp beads simultaneously at E11 mouse embryonic limbs. These experiments showed that the whole autopod region is still very malleable at this stage (Figure 16B). The combination of Sox9 expression “peaks” (from Bmp beads) and “valleys” (from Wnt beads) allowed arbitrary patterns to be created, depending on the location of the beads. In summary, the limb bud is still very plastic in its response to new spatial distributions of natural ligands which are expressed at this stage during normal development.

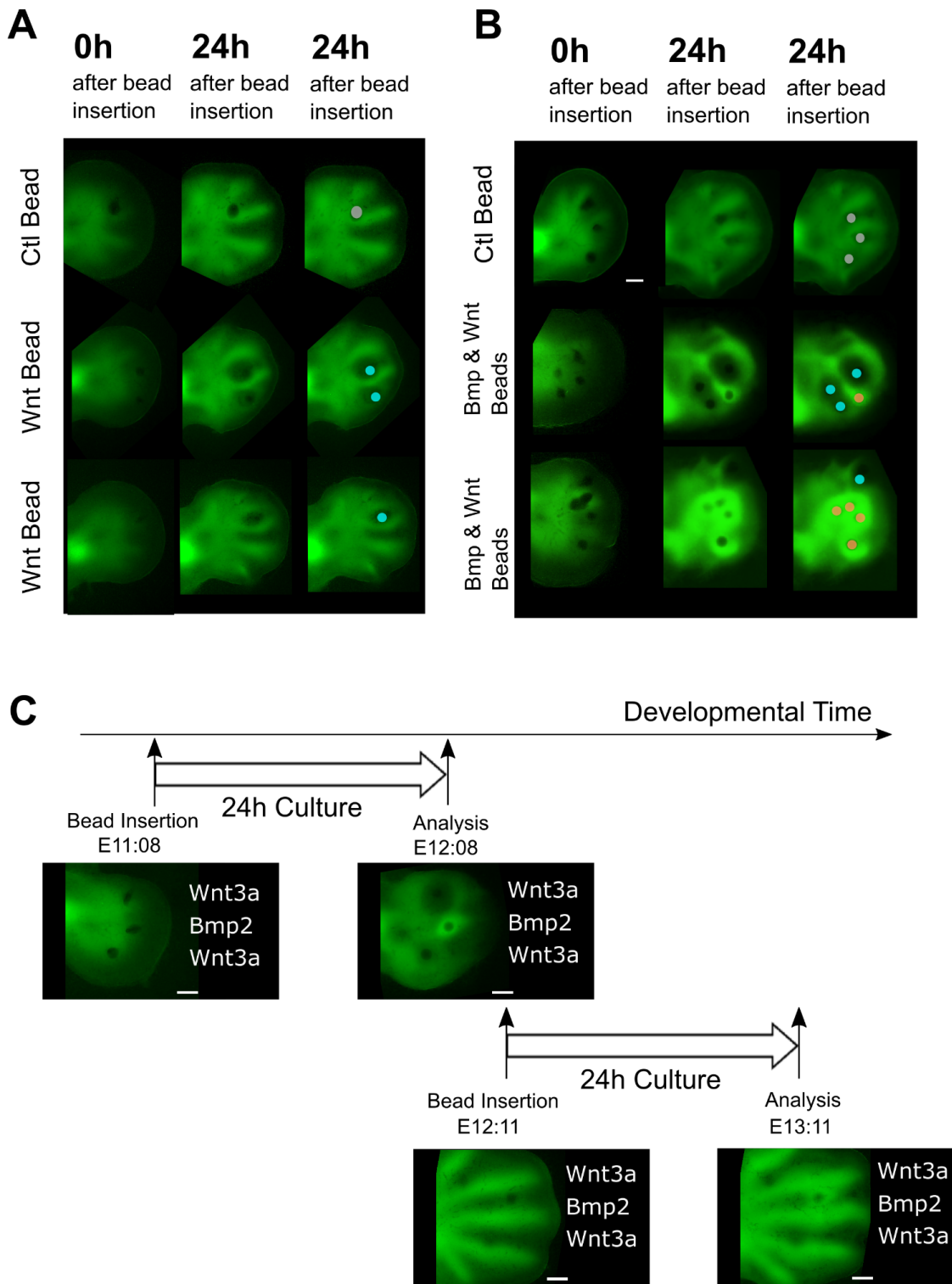


Figure 16. Sox9 reorganisation experiments. (A) At early Day 11 control beads do not alter the Sox9 digit pattern, whereas Wnt beads cause the normally straight Sox9 stripes to become curved. The third column is a duplicate 24h post bead insertion result to indicate the precise locations of the beads. Control beads are depicted in grey, and Wnt beads in blue. (B) Simultaneous insertion of both Wnt beads and Bmp beads leads to complex rearrangements of the Sox9 pattern, revealing very high plasticity at this stage. In the third column, Bmp beads are depicted in orange. (C) Experimental schematics for bead insertion experiments. Following Wnt or Bmp containing bead insertion, mouse embryonic limbs are cultured for 24 hrs, and the resulting pattern is analysed. Comparison of bead

insertion experiments on Day 11, versus Day 12, shows that the degree of patterning plasticity decreases over time.

Applying multi-bead into E12 mouse embryonic limbs revealed a very different result. By this time point, Bmp and Wnt beads showed a small impact on Sox9 expression (Figure 16C). Even the residual Bmp impact caused no rearrangement beyond the immediate local up-regulation. In other words, the tissue no longer displayed any reaction-diffusion-like behaviour in which longer-distance effects propagate through cell-cell interactions.

For standard experiments, I chose to insert 3 beads in a linear sequence along the AP axis: 2 Wnt beads, with 1 Bmp bead in between (as shown in Figure 16C). This provides both positive and negative influences on Sox9, can allow for strong rearrangements, but also allows enough self-organisation to be interpretable. Use of 3 beads is advantageous over using too few beads, which would not push the system sufficiently, and using too many beads which can force the system into a completely externally-driven pattern that can no longer display its self-organising properties.

3.2 Image quantification reveals that patterning plasticity decreases gradually over time

Although the change in pattern plasticity from Day 11 to Day 12 is easy to observe by eye, to characterise the decrease in plasticity over time more precisely, a quantitative metric is developed. As mentioned above, plasticity can only be observed through the response of a system to perturbation, and therefore it is necessary to compare each experimental result with the equivalent unperturbed controls. Furthermore, the read-out of these experiments is the spatial pattern of Sox9 - not simply the expression levels of the gene *per se*. There is a need for a method to extract the relevant aspect of the spatial patterns, and to quantify the difference between perturbed and unperturbed patterns. I thus chose to use the topology of the Sox9 pattern as the basis for this comparison.

A major challenge in extracting the topology is the wide range of relevant Sox9 intensity-levels. This is not just a challenge between different images, but more specifically within a single image. For example, the topological features of digit 2 may be visible at very different intensity levels than the features of digit 4. The philosophy of the technique was thus to extract useful topological features at multiple different intensity values, and then to combine this information in such a way to retain the most valuable information for the whole image.

The first step was to binarise both control and experimental microscopy images at different GFP intensity thresholds, to highlight different 2D digit shapes within the limb (Figure 17). The binarised images were then skeletonised at these respective thresholds, revealing the digit topology at each different threshold. To compose the most representative topology of the Sox9-GFP pattern, I chose to overlay, gaussian blur, and integrate all of the skeletonised versions of the images. Re-skeletonising the merged overlay created a single canonical Sox9 Topology for each image which was then converted into a graph formalism

(using the optimal edit path method from Networkx) for the subsequent comparison step (Figure 17).

To compare each experimental Sox9 graph with its equivalent control, I used minimum cost calculation. The minimum cost metric is defined as the number of operations -individual modifications to a network's nodes and/or edges- required to transform one graph to the other. In this context the algorithm was used to convert the graph from control image to the perturbation experiment. The minimum cost is a proxy of the plasticity value, or a deviation of a perturbed limb pattern from the control, at a given developmental timepoint.

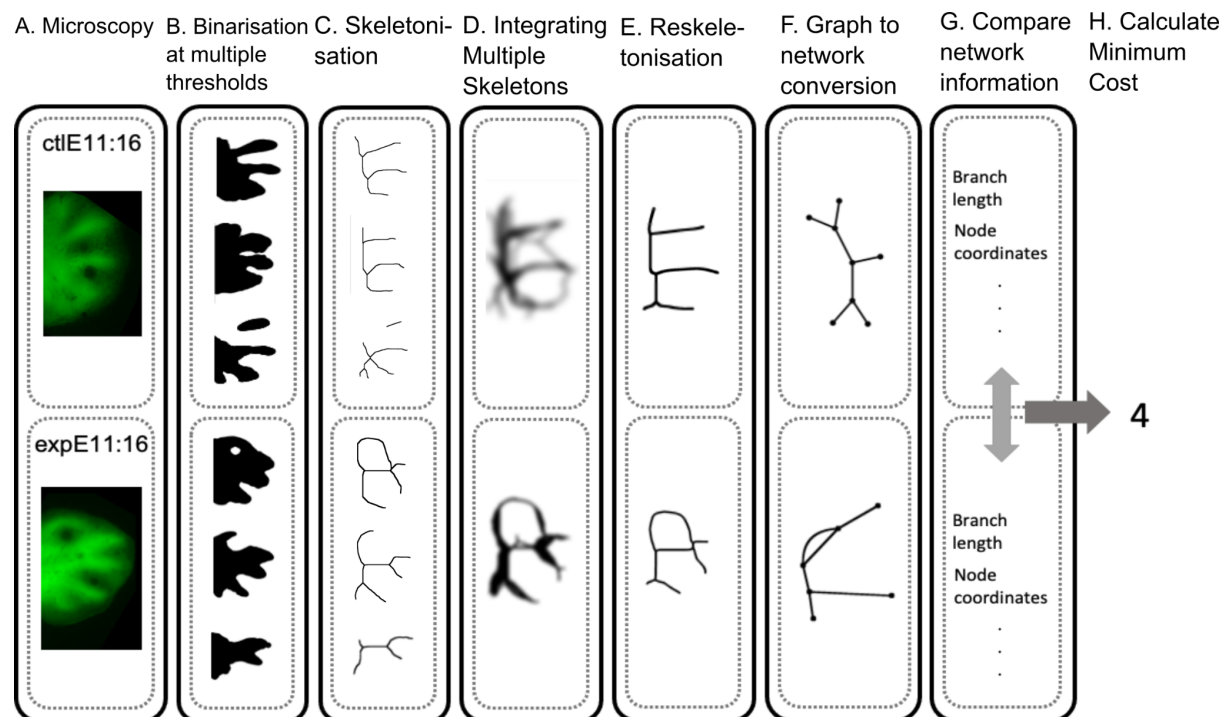


Figure 17. Tissue plasticity/dynamicity quantification pipeline. (A) Following bead insertion, control and experimental images after 24hrs are collected. (B) Images are then binarised at around 100 different GFP intensity thresholds to capture the variety of topology arising from a single image. (C) Then each of the binarised images are skeletonised using Fiji Skeletonise(2D/3D) plugin. (D) Integrating Multiple Skeletons step allows the best representation of skeletonised limb, as erroneous branches of the skeleton are eliminated. (E) (F) Blurred images are reskeletonised and the skeletons converted into graphs using the python package Networkx. (G) Network information and statistics extracted. (H) Minimum cost, signifying the difference between two images, calculated using the Networkx package.

Using the minimum cost calculation tool, I was able to plot tissue plasticity levels over a 48 hour time window (Figure 18). Minimum cost values between the control and experiments were calculated at 14 timepoints ranging from E10:22 to E12:20. The quantitative plot agrees with the intuitive conclusion from examining the raw images by eye: namely, a gradual decrease in the ability of the digit pattern to respond to external perturbations. The most significant part of this smooth decrease occurs during the 24 hours from early Day 11 to early Day 12. It is notable that this gradual decrease appears to reflect a situation which is intermediate to the two models discussed above: It is neither a constant high plasticity as modelled in the previous Turing Stripe Model, nor is it a brief moment of

plasticity as required by the Turing Spot Model. RD plasticity clearly extends into the phase when stripes are elongating.

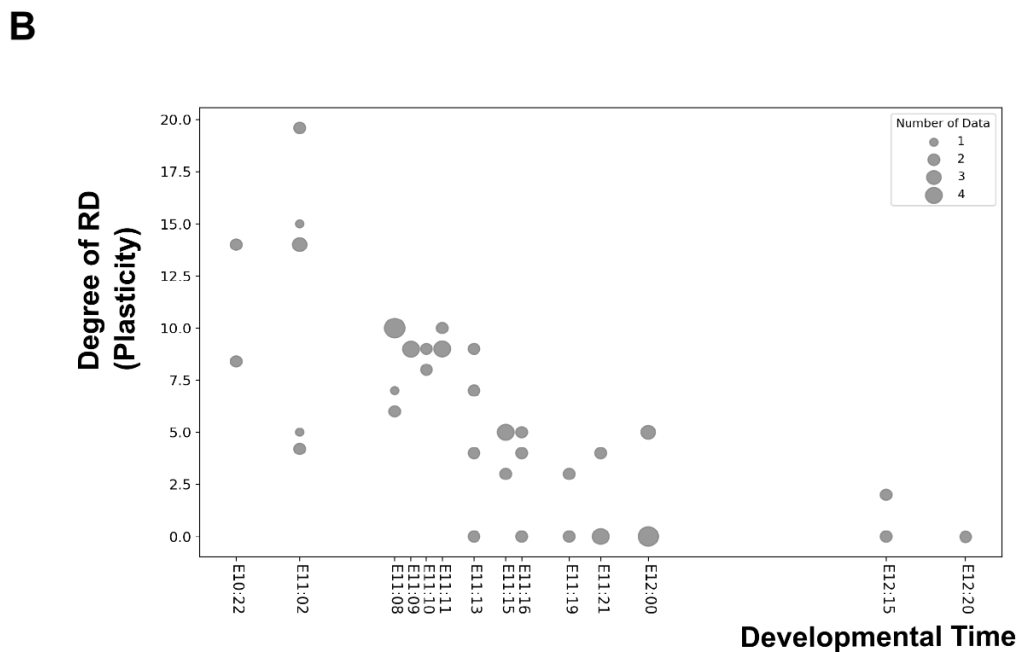
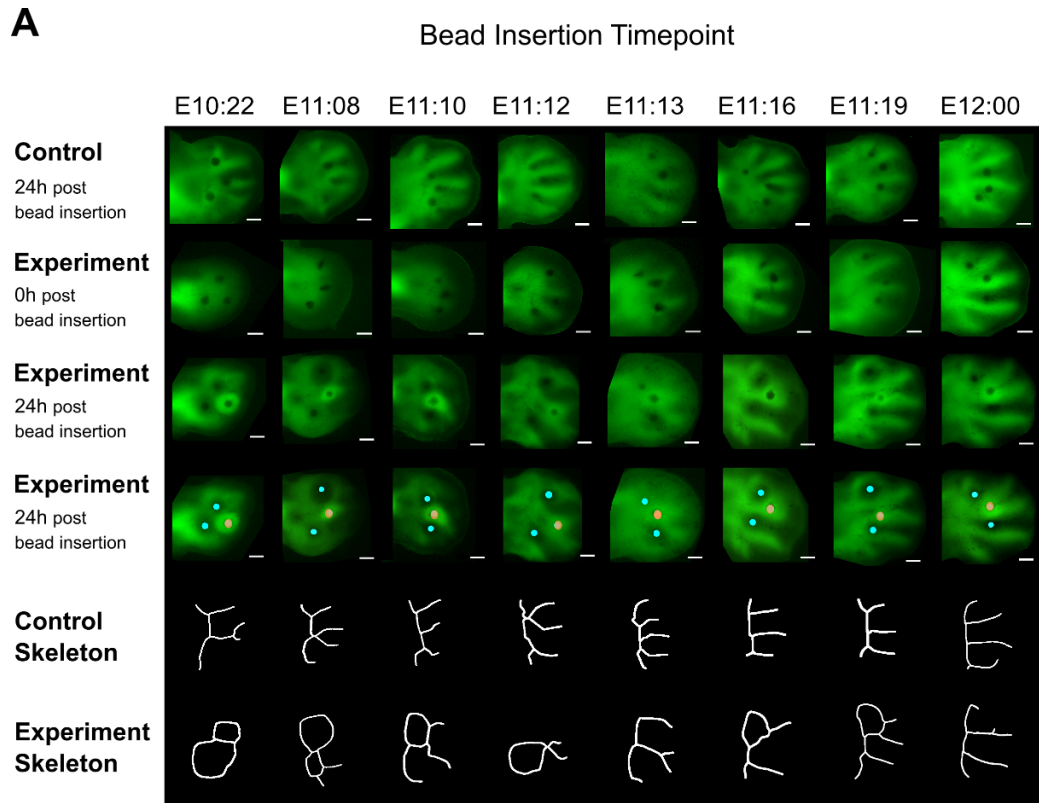


Figure 18. Plasticity in mouse digit patterning gradually decreases over time. (A) Representative experimental results over eight different bead insertion timepoints. Over developmental time, experiments demonstrate ‘straighter’ digits, losing their round skeleton coming from reorganisation. The control limbs with beads only containing PBS are shown in the first row, followed by experimental limbs, with Bmp or Wnt containing beads, are shown in the second and third row. The fourth row indicates the identity of the inserted beads - Bmp bead in orange, and Wnt beads in blue. (B) Plotted

degree of RD/Plasticity over developmental time. Marker point size denotes the number of experiments with a given RD degree at a given time point.

3.3 A simple mathematical model of plasticity decrease can capture the dynamical patterning of digits

Sharpe Lab has previously created mesh-based simulations of molecular patterning in limb development[84]. These simulations use a data-driven description of tissue movements and integrate predefined, *in situ* data of certain genes as an input, along with preset diffusion, noise, and initial value of the variable. Partial differential equations were solved in each of the predefined meshes representing the limb, illustrating local gene expression at a certain embryonic time. LimbNET is a recently built new version of these simulations (manuscript in preparation), which I employed to explore different *in silico* models of plasticity dynamics, to see which model would fit best with the data from the bead experiments (Figure 19A).

A single and simple mechanistic basis for plasticity is not known and not expected. As explained, plasticity is defined purely by the response of genes or cells to perturbations. Any feature of a cell that could increase or decrease its ability to respond will contribute to plasticity, and thus it is not likely to reside at just one level of control. Changes in chromatin state[100], in dynamic gene circuits, metabolism of the cell[101], physical mechanics[102] or even cellular geometry[103] could all influence the plasticity of a cell. Since I measure plasticity by response to perturbations, rather than any of the possible underlying mechanisms, I chose to capture plasticity in the computer model by clearly defining it. I sought to add a plasticity variable, *plas*, which would adjust the ability of genes to change their expression levels. For Sox9 in particular, this would also represent cell fate plasticity, as Sox9 reflects the digital fate.

We aim to modulate and incorporate different plasticity time courses into the simulations. Like the *in vivo* experiments, for each model the virtual beads are introduced into simulated limbs at different time-points ranging from E10:08 to E12:00. (Figure 19B).

Modulating plasticity in the model requires *plas* to control the degree to which any molecular component can change. For example, if Sox9 levels cannot change, this is equivalent to saying that Sox9 plasticity has been reduced to zero. Therefore, I use the *plas* variable as a coefficient for differential equations describing any molecular variable in the model. When *plas* equals 0.0, the differential equation is “frozen”, the molecular concentration cannot change, and there is no plasticity at all. Alternatively, when the variable value is 1.0, the molecular concentration is fully regulable, and plasticity reaches its maximum. The *plas* variable is dynamic, and can therefore be defined to maintain its value over time, or to decrease fast or gradually. This way, we are able to recapitulate multiple theoretical models - continuous high plasticity for the Turing Stripe Model, and an early rapid drop in plasticity for the Turing Spot Model (Figure 19C).

The results demonstrate that the Turing Stripe Model does not accurately reflect experimental digit patterns once the bead is inserted at later developmental stages (E11:13-E12:00). Compared to the experiments, simulation results of the Turing Stripe Model

are far more dynamically rearranged, characterised with loss of straight digits and notably bigger local and global impacts from the beads (Figure 19D).

The Turing spot model does not represent real digit dynamics either. The beads inserted after the simulated plasticity drop are not able to impact the digit patterning. On the other hand, mouse mesenchymal limb cells have a certain level of plasticity(Figure 19D), as shown by experiments around E12:00 that changes the digit pattern.

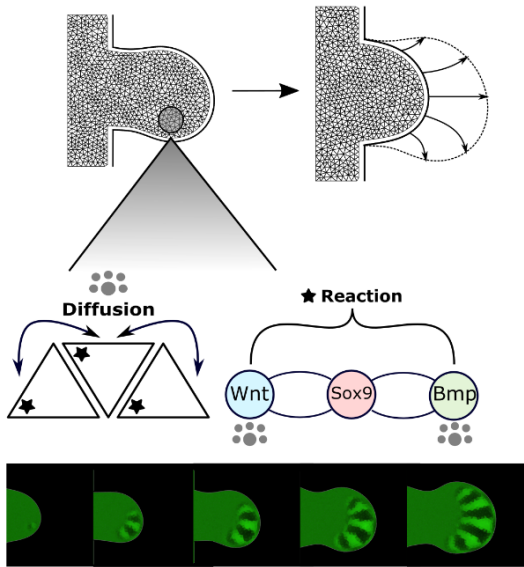
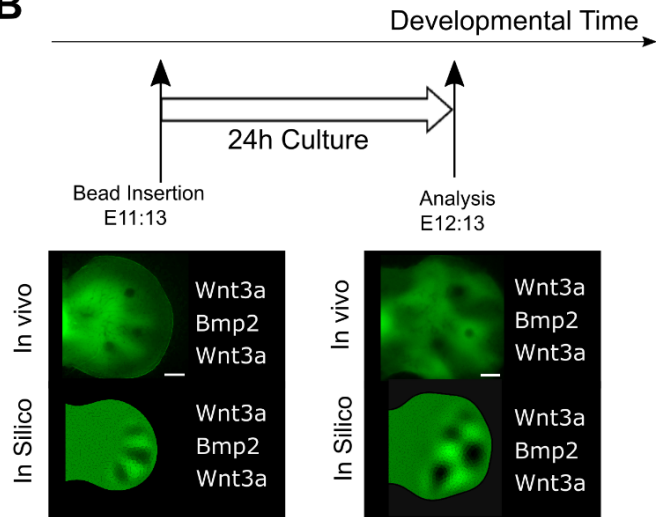
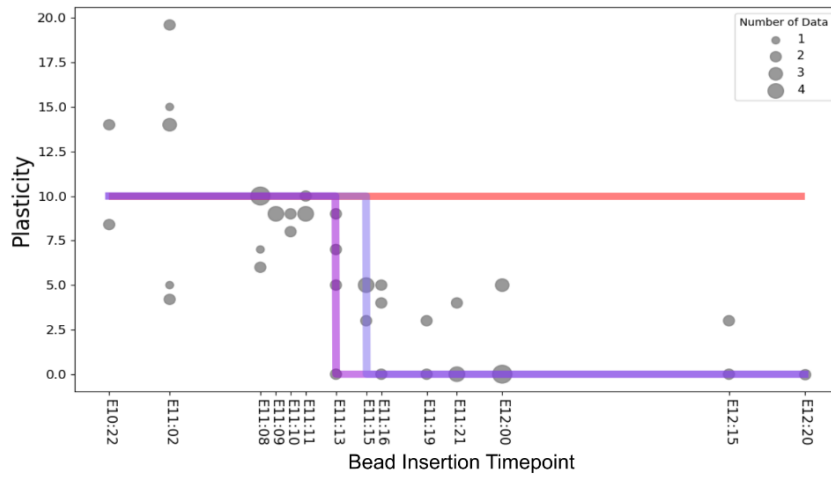
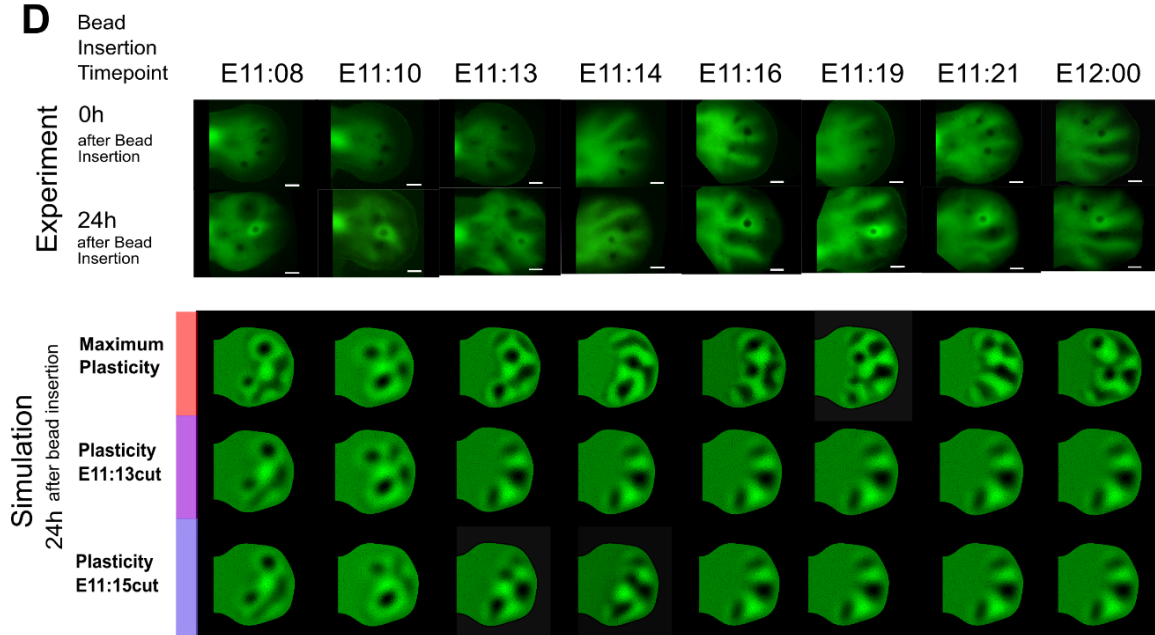
A**B****C****D**

Figure 19. Mathematical modelling of various dynamics of plasticity decrease. (A) LimbNET recapitulates growth and gene expression dynamics in limb development through mesh-based simulations. Once reaction-diffusion is put into place, LimbNET can recapitulate wild type digit patterning using the BSW model. (B) Schematics of modelling bead experiments. The beads can be inserted at the desired developmental timepoint, and the resulting pattern can be obtained following 24hrs of simulation. (C) Plasticity schematics for three different models: Maximum plasticity model (red), Plasticity cut model-E11:13 (violet), and Plasticity cut model-E11:15 (slate purple). (D) Neither maximum plasticity model nor plasticity cut models represent real digit dynamics.

3.4 Optimised data fit model recapitulates gradual plasticity decrease over time

The next step is to find out if plasticity decay profile identical to that of the experiments can genuinely represent experimental data. To achieve this, I first fitted experimental data into a sigmoidal Hill function, generating a 'data fit' model (Figure 20A). Sox9 dynamics are simulated from the 'data fit' model. The 'data fit' model captures early (E11:08-E11:16) dynamics - however, at later developmental timepoints (E11:19-E12:00), simulated Sox9 patterns are globally reorganised, characterised by curviness of digit patterns that are distant from the beads (Figure 20B, first row). Therefore, the dynamicity of the 'data fit' model at later digit patterning timepoints needs to be modulated in order to more accurately recapitulate experimental observations.

To improve the 'data fit' model, I created another model in which plasticity has similar dynamics up to $t = plas_{0.5}$ (the time when the plasticity is equal to half of the original value), and decays faster after $t = plas_{0.5}$ (Figure 20A). $t = plas_{0.5}$ from the data fit model is E11:12:50. The 'optimised data fit' model decays faster and has lower values of plasticity after E11:12:50. The optimised data fit model is designed to have only a marginal amount (3.0×10^{-3}) of RD/plasticity at E12:00, which is above 0 but still somewhat lower than in the 'data fit' model. This feature of the optimised model is based on the experimental results, which show local Sox9 expression changes at E12:00. For comparison, the 'steeper data fit' model with a higher Hill coefficient (steeper change in plasticity over time) is also simulated. This model has the highest rates of decay around E11:12:50, so the plasticity is still high in early stages, but in later stages plasticity decays faster and reaches 0 around E11:19.

I conclude that 'optimised data fit model' best recapitulates the experimental data (Figure 20B). During E11:19-E12:00, the optimised data fit model demonstrates straighter digits that are only locally interrupted by bead insertion. This is in contrast to the original data fit model in which curved digits and globally interrupted altered Sox9 expression arise after bead interventions. The optimised model also represents experimental data better than the 'steeper data fit' model, because the optimised model retains RD/Plasticity until E12:00 and therefore demonstrates some degree of local Sox9 changes at E11:19 and E11:21, in agreement with experimental observations. On the other hand, the steeper model does not account at all for effects of a bead insertion later than E11:19.

It is clear through modelling that experimentally measured tissue plasticity gradually decays in a sigmoidal manner. Once all five digits have emerged, around E11:12-E11:13, the tissue plasticity decreases to half of its original value. The 'optimised data fit' model with

residual marginal plasticity at E12:00 successfully reproduces local Sox9 changes. I conclude that there is indeed a sustained - albeit varying - level of plasticity in the system throughout the developmental timecourse.

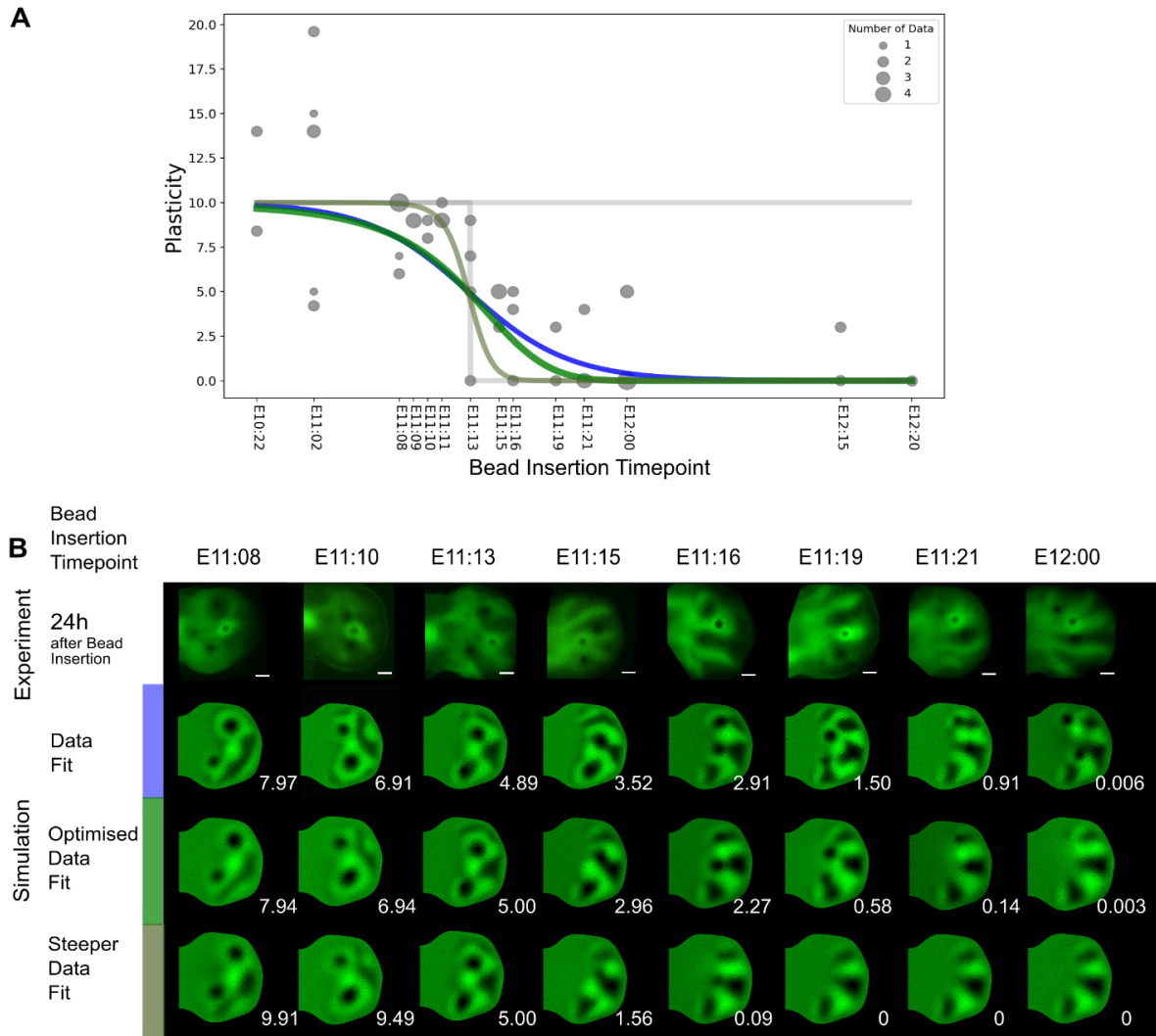


Figure 20. Optimised “data fit” model recapitulates experimental plasticity. (A) Schematics of “Data fit” model in Blue, ‘optimised data fit’ model in green, and ‘steeper data fit’ model in khaki. (B) Simulations of all three types of models, with respective plasticity values. Towards later developmental timepoints, a marginal amount of plasticity difference leads to huge differences in digit patterns.

3.5 Transcriptional dynamics of stemness/pluripotency/reprogramming factors closely matches the gradual decrease in experimental plasticity

Tissue plasticity is a complex phenomenon involving thousands of factors. However, it is possible to gain biological insights by identifying groups of genes that follow the gradually decreasing tissue plasticity trend. To do so, consensus clustering analysis was performed on transcriptomics data of limb autopod at 6 stages between E11:02 and E12:07, to identify the genes that closely match and potentially in charge of the experimentally measured plasticity decrease (Data collection by Lucia Russo, analysis by Xavier Diego). To identify clusters of genes that follow the experimental plasticity decay, the equation for 'data fit' model was normalised against the maximum count of each gene. Transcription factors were the focus of analysis, as in early development they may be the main effectors of the plasticity change. A list of transcription factors in the mouse genome was obtained by the Gidford lab from a recent study of human transcription factors[104]. The consensus clustering solution was constructed by integrating the clusters obtained with Affinity Propagation, K-Means and Hierarchical Clustering.

Amongst the genes that cluster with the plasticity measurement, a subset of genes consistently clusters with the plasticity measure (Figure 21), independent of the clustering method employed or the parameters used. Some genes in the cluster include: *Lin28*, *Lin28b*, *Sall1*, *Sall4*, *Trim71*, *Gbx2*, *Tcf15*, *Arid3b*, *Cebpz*.

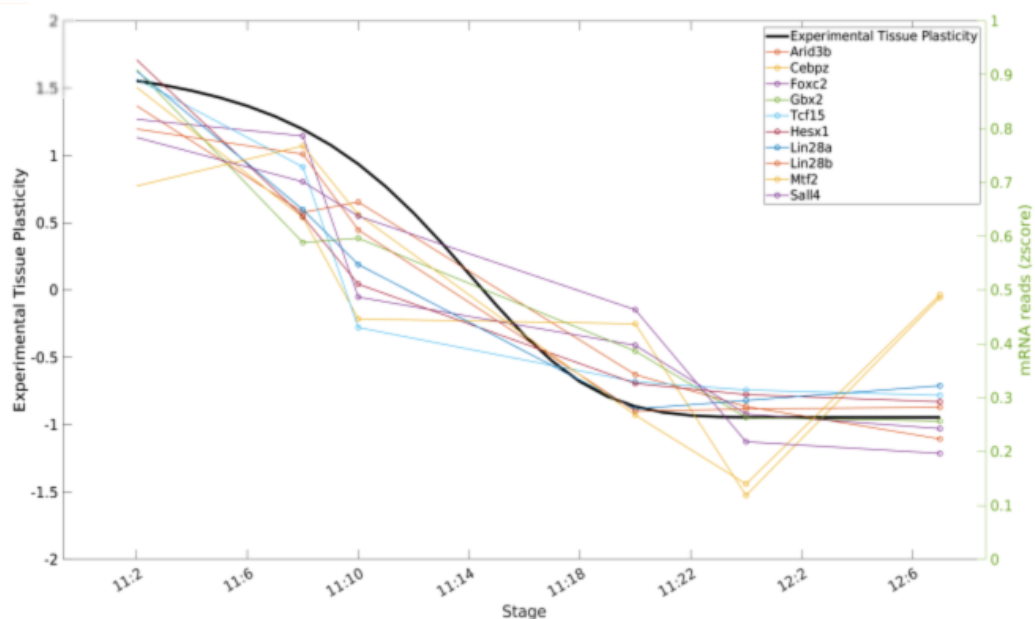


Figure 21. Black line indicates the measured tissue plasticity values. Subset of the “plasticity cluster” genes and their normalised expression levels are shown. Figure generated by Xavier Diego.

All of these genes have been previously documented to be stemness, pluripotency, or regeneration associated in the limb context. Of particular interest is *Lin28*, which is a pluripotency regulator[105], and is already known to be downregulated throughout the limb development process[106]. *Lin28b* is also a pluripotency associated gene[107], *Lin28* and *Sall4* have also recently been suggested as limb specific reprogramming factors, meaning that these genes are capable of imparting limb progenitor like properties to non-limb

fibroblasts[108]. *Sall4* is also known to be essential for the limb outgrowth before anterior-proximal skeletal element development[109]. *Sall1* is a multi-zinc finger transcription factor that functions redundantly with *Sall4* [77]. *Trim71* maintains cells in a limb progenitor-like state[108]. *Gbx2* is a reprogramming factor that promotes retention of the pluripotent ground state[111].

The clustering result is consistent with a previous study[112], which used hierarchical clustering on distal mouse embryonic limb cells from four different timepoints (E9.5, E10.5, E11.5 and E12.5). Out of seven clusters, there were two main clusters with downward trends, an early and late decaying cluster that contained *Lin28a* and *Lin28b*, respectively. The existence of these clusters was interpreted as reflecting a progressive loss of stemness state in distal limb progenitors. Other genes such as *Sall4* have also been found in the identical cluster with *Lin28*.

The most significant GO terms of the clustered genes are: miRNA catabolic process, pre-miRNA processing, positive regulation of miRNA-mediated gene silencing, and stem cell population maintenance. The results suggest a potential mechanism to control tissue plasticity through the regulation of miRNAs involved in mRNA degradation and translational repression of genes required for differentiation. miRNAs have been known to regulate the balance between the self-renewing and differentiated cell states found during development [113].

Strikingly, previous publications suggest a potential mechanism in which *Lin28*, *Lin28b*, *Sall4*, and *Trim71* can coordinate to maintain plasticity through a miRNA mediated mechanism [108]. In this mechanism, *Lin28* and *Lin28b* are thought to block the production of the *let-7* microRNA, which is critical for repressing multiple pluripotency factors [81]. Over developmental time, corresponding to *Lin28* decrease, *let-7* expression level in limb buds is increased as limb outgrowth proceeds [115]. Both *Sall4* and *Trim71* are targets of *let-7* and are therefore degraded upon increased *let-7* expression. *Trim71* in particular promotes stemness by antagonising translation of *Egr1*, a pro-differentiation factor for limb progenitors. Series of experiments show that combinatorial overexpression of *Lin28a* and other factors induces limb progenitor marker expression in non-limb fibroblasts, as well as adding *Trim71* onto non-limb fibroblasts accelerates proliferation of limb progenitor states[108].

Another study highlights the 'stemness' cluster of genes in a developing mouse embryonic limb, and identifies *Lin28* and *Gbx2*, which are also found to cluster with our measurement of tissue plasticity[116]. In the study, heterochronic grafts of distal limb cells from an older to a younger limb were made. Following the grafting, transcriptomic dynamics was analysed from 0 to 24h, revealing a cluster of genes that can be reset by the host signalling environment. The cluster also contains *Zbtb16*, which we also find to decrease closely with the plasticity measurement but only in *Sox9+* cells. The presence of the stemness cluster might suggest the existence of a regulatory network operating during early limb development to maintain the multipotency of mesenchyme cells.

3.6 Sox9 digit patterning precedes cell density changes

To investigate the relative timing of molecular digit patterning (Sox9 patterning) and cell density changes, I investigated the detailed time-course of cell density change in relation to digit patterning dynamics, starting at E10:20 and continuing onto E12:10. To identify cell density I generated cryosection, stained the tissue with DAPI, and counted the number of cells in a unit area. To identify the intensity of Sox9 expression, I performed immunostaining on the cryosection with primary anti-Sox9 antibody followed by secondary GFP antibody. For each timepoint, 3-4 biological replicates are used, and in each sample, Sox9 expression and cell density in multiple selected prospective digital and interdigital areas are counted (Figure 22).

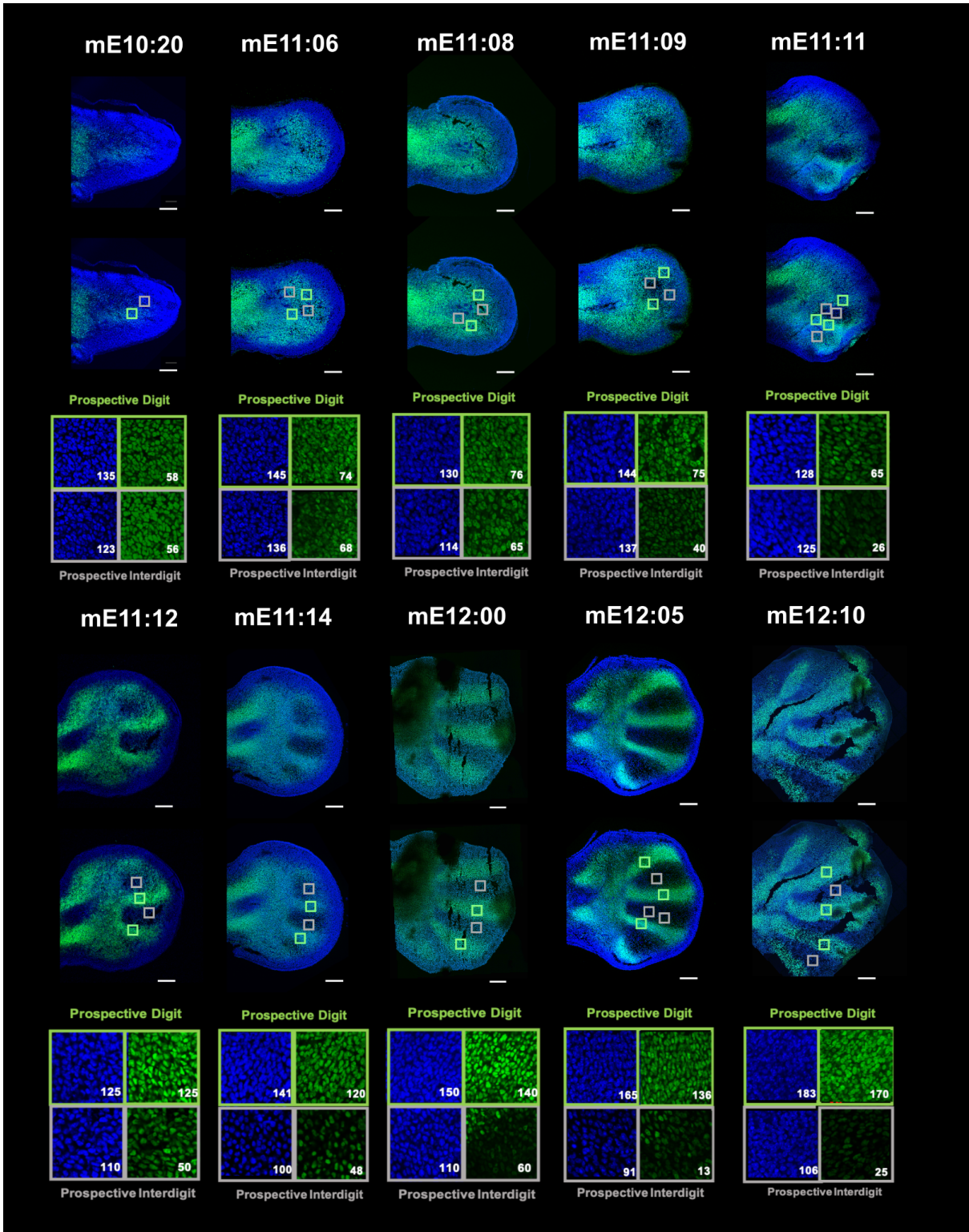


Figure 22. Cell density and Sox9-eGFP immunostaining intensity are counted at selected prospective digital and interdigital regions. High resolution images of one of each prospective digital and interdigital regions per cryosection are demonstrated, with the numbers in each box indicating cell counts or fluorescence intensity. Scale bars represent 200 μ m.

It is clear that molecular digit patterning is established before cell density change happens. E11:06 is the first timepoint with the significant Sox9 expression difference between the digital and interdigital region(Figure 23), in line with the fact that the first digit emergence, in mouse embryonic limb happens in between E11:04-E11:08. On the other hand, the first significant cell count difference between digital and the interdigital region is shown at E11:12, indicating that the symmetry breaking point of molecular Sox9 patterning happens ~6hrs before that of cell density.

The results indicate that Sox9 digit patterning happens significantly earlier(~6hrs) than cell density changes. The observation supports the hypothesis that digit patterning is primarily driven by reaction diffusion, and cellular movements lie downstream of molecular patterning. Despite a variety of mechanochemical hypotheses, in the context of embryonic digit formation molecular patterning and condensation are not found to be coupled, or at least not simultaneous.

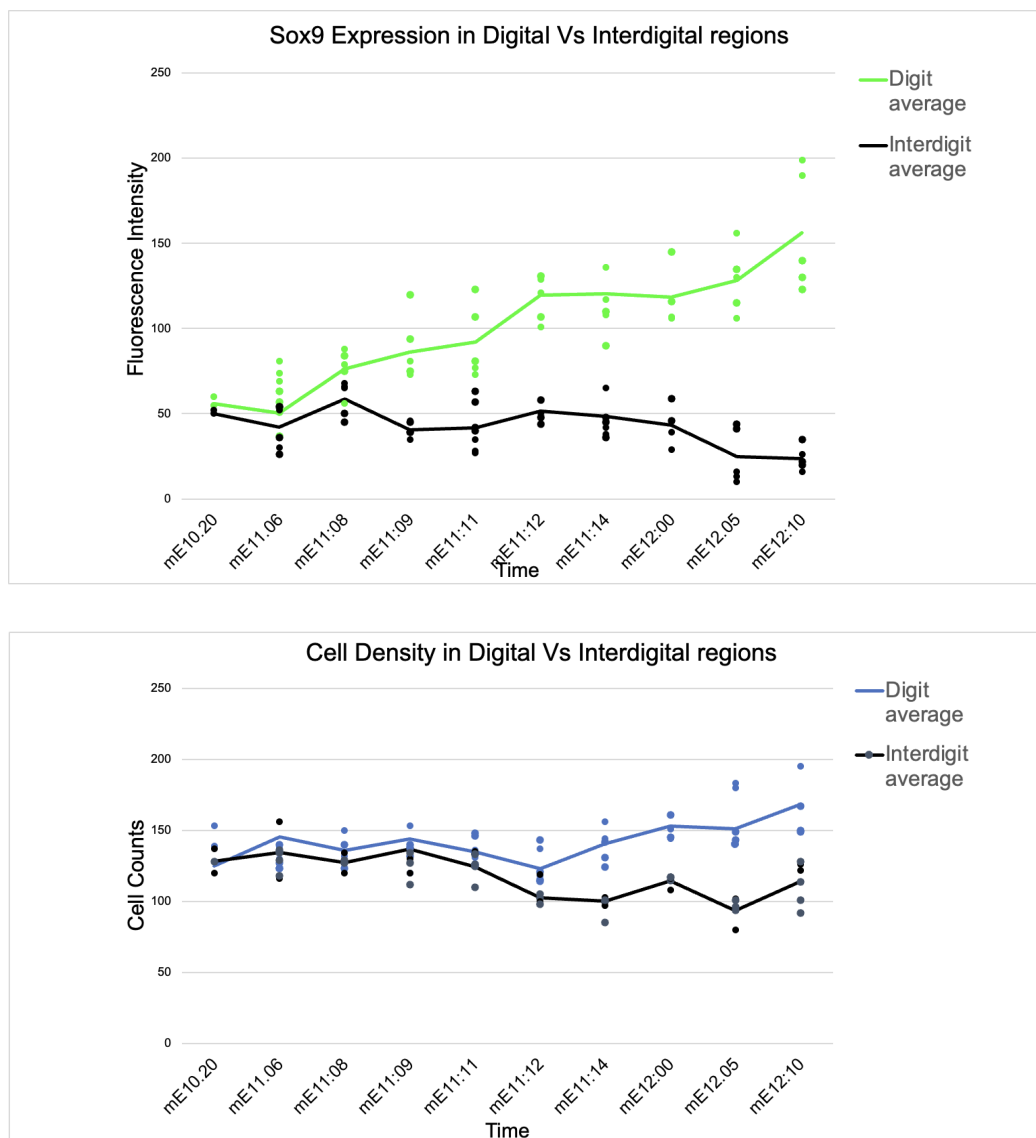


Figure 23. Symmetry breaking point of Sox9 molecular patterning happens ~6hrs before cell density changes.

To confirm that selected areas are indeed representative of prospective digital and interdigital regions, cryosectioned limb tissue is divided into unit areas, then the number of cells, as well as corresponding Sox9 intensity in each unit area are counted. Cell density counts across the whole autopod region of the limb are visualised in a cell density heatmap format(Figure 24). Global cell density heatmap validates that up to E11:11, there is no apparent density difference between each unit area. From E11:11 onwards, the outline of digits and interdigits are visible on the heatmap, agreeing with the previously made observation that the symmetry breaking point of cell density happens around E11:12.

For more quantitative analysis, cell density values and corresponding Sox9 fluorescence values from each unit area of global heatmaps, are made into a scatterplot (Figure 25). From E11:11, there is a positive correlation of Sox9+ intensity and cell density, which continues throughout developmental time. Scatterplot also reveals generation of two distinct clusters(digits and interdigits), which can be shown after E11:12 or E11:14. Digital cluster consists of datapoints with high cell number counts and Sox9 intensity, and interdigital cluster with both low cell counts and Sox9 intensity. Towards later developmental timepoint, the two clusters are better distinguished.

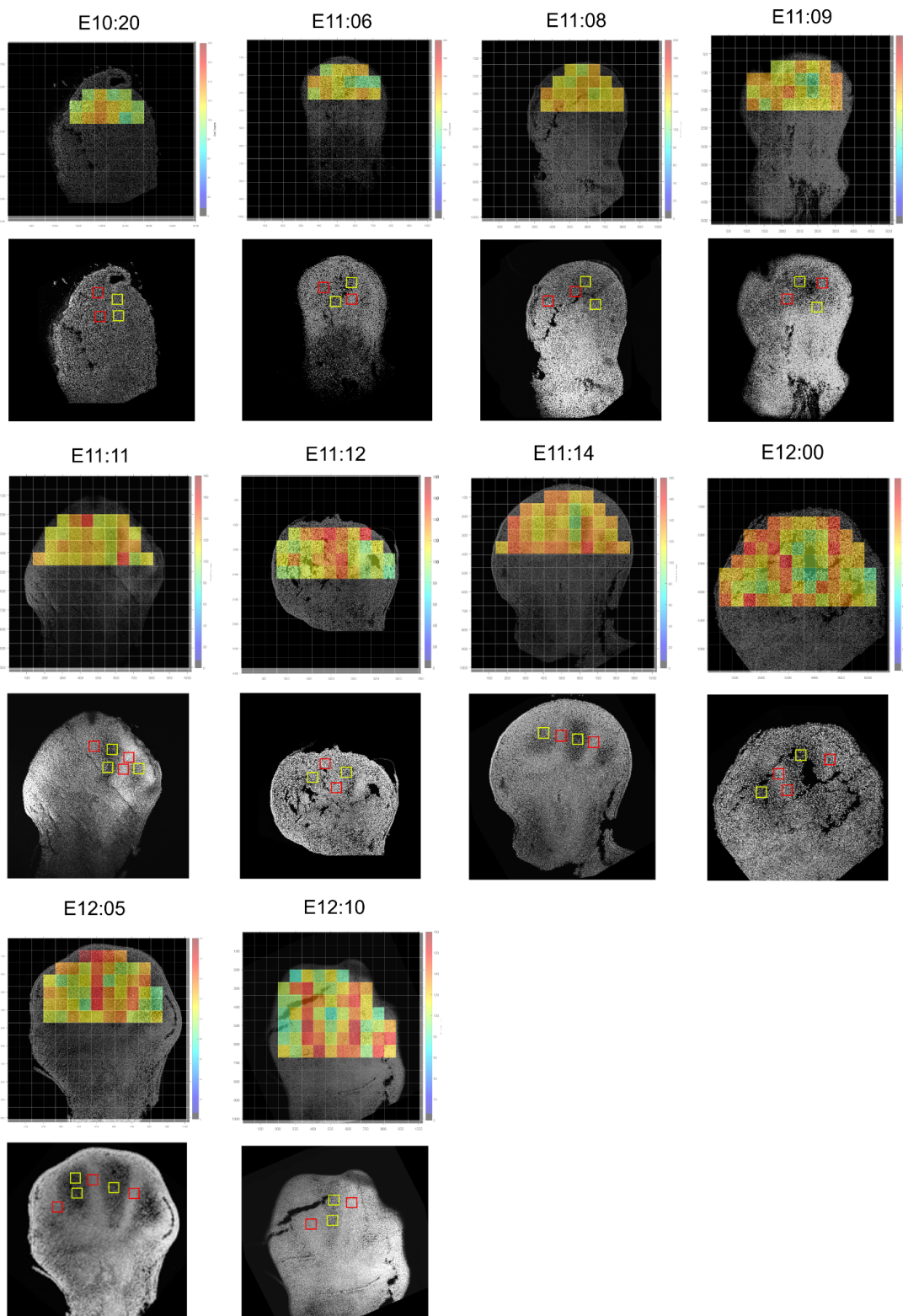
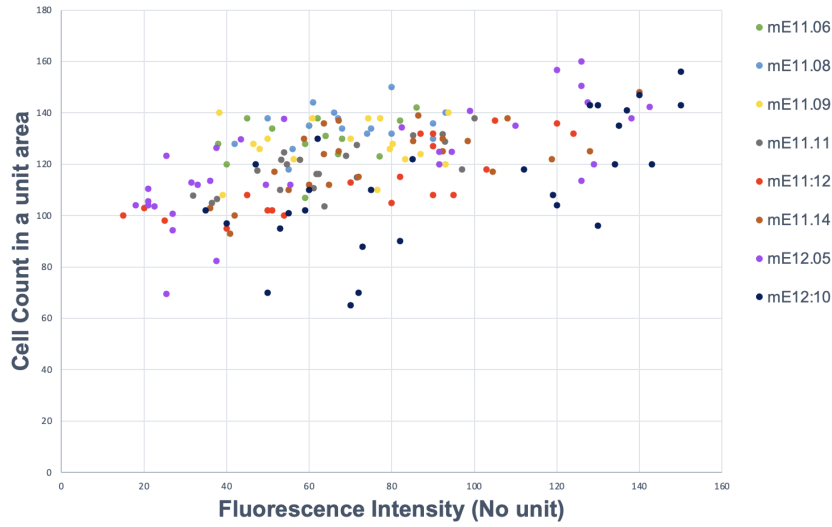
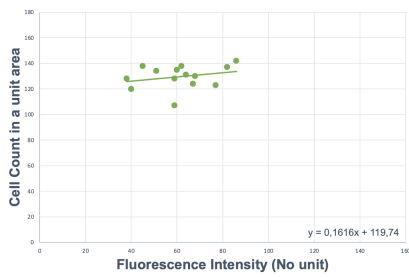


Figure 24. Global cell density count heatmap. Cell count distributions are relatively homogeneous before E11:11, whereas there are significant differences along digit/interdigit borders from E11:12 onwards.

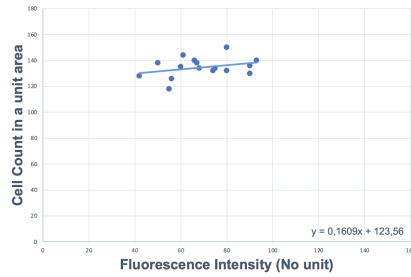
Cell Density Vs Sox9 intensity



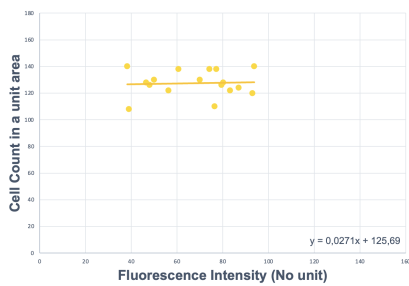
E11:06 Cell Density Vs Sox9 intensity



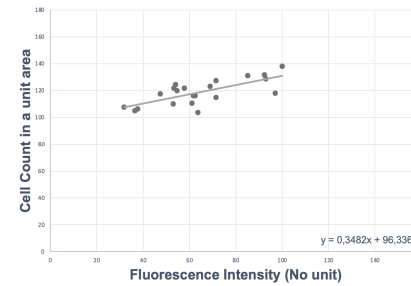
E11:08 Cell Density Vs Sox9 intensity



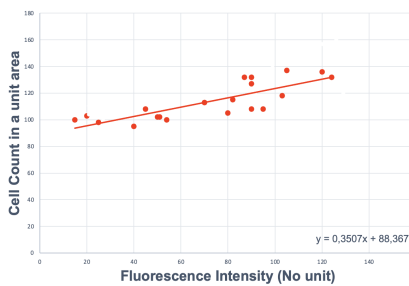
E11:09 Cell Density Vs Sox9 intensity



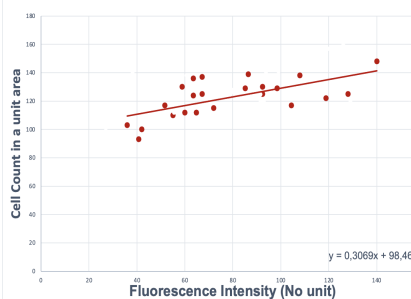
E11:11 Cell Density Vs Sox9 intensity



E11:12 Cell Density Vs Sox9 intensity



E11:14 Cell Density Vs Sox9 intensity



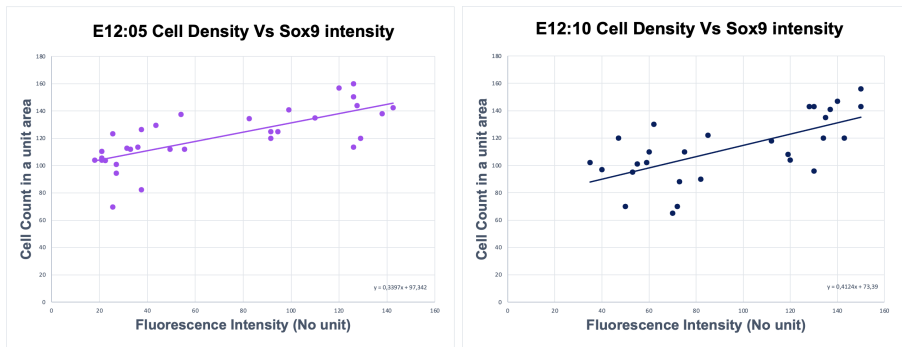


Figure 25. Scatterplots of cell density Vs Sox9 intensity. Each datapoint is from a unit area of the heatmap. based on global cell density counts and Sox9 fluorescence intensity counts.

3.7 Part I Summary

In this section, I revealed the detailed dynamics of digit patterning by relating Sox9 pattern variations with information about the reaction-diffusion in the system. I also related the degree of reaction-diffusion in the system to plasticity - ability of the cells and tissues to change their fate. I found that the plasticity in mouse embryonic limb decreases in a gradual, sigmoidal manner, and with other members of the Sharpe Lab, highlighted candidate genes from the transcriptomics data that follows the measured plasticity profile. The identified stemness cluster can potentially regulate plasticity through miRNA mediated mechanisms. While the plasticity dynamics in digit patterning adopts gradual decrease of 24hr period, In the broader context of tissue growth, molecular digit patterning is clearly established before the onset of cell density change.

4. Results Part II : Unbiased screening of digit patterning pathways

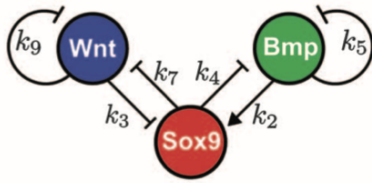


Figure 26. Proposed BSW model network. Figure from Raspopovic *et al.*, [28] reproduced under the terms of the Creative Commons attribution licence (CC-BY 4.0).

It is well-documented in the literature that Wnt signalling from the ectoderm can repress Sox9 during limb development [30]. However, that is a simple “linear” repression - not a self-organising feedback. The BSW model proposes that this repressive interaction forms part of the Turing feedback to pattern digits, but how much evidence exists for this? As described in the introduction, we have evidence that (a) various members of the WNT signalling pathway are expressed in-phase or out-of-phase with Sox9, (b) beads of Wnt3a can disrupt digit patterning, and (c) application of the Wnt repressor IWP2 can also disrupt digit patterning. However, these earlier findings singular evidence helped conceptualising and building the BSW model, so therefore there is a need to investigate further consolidating evidences that systematic Wnt interruption impacts BSW network and changes digit patterning.

To confirm whether Wnt signalling is the major responsible pathway for digit patterning, and to find out the molecular mechanism of Wnt signalling, a variety of perturbation approaches can be adopted. Perturbation means an interruption in a biological system by external or internal means such as environmental stimuli, drug inhibition, and gene knockdown [117]. Upon systematic perturbation, and by recording the responses of the system, a model or gene regulatory network can be fine tuned, clearly depicting the relationships between genes.

It is important to note that only a subset of methods in the Table 2 is applied in a screening manner - Small molecule inhibitor/ligand application in limb bud culture, micromass, and bead insertion. While ectoderm removal and conditional knockouts can be used for screening, that is not the case of this study.

Ectoderm removal is an interesting perturbation method which is a mechanical, non-genetic intervention. This is an alternative approach that would collectively analyse the impact of multiple Wnt ligands that are expressed in the ectoderm, and especially investigate the question of how ectodermal Wnt signalling is brought into mesenchyme. This will also shed light to the conundrum why ectodermal ligands such as Wnt3a are more relevant to changing digit patterning compared to pan-mesenchymally expressed ligands such as Wnt5a.

	Types of experiment	Role
Perturbation	Small molecule inhibitor/ligand application - Limb bud culture	illustrates the global impacts of the inhibitor on digit pattern
	Small molecule inhibitor/ligand application- Micromass	quantification of period or intensity changes upon small molecule application
	Small molecule inhibitor/ligand application- Bead insertion	tells local upregulation/downregulation of Sox9 in <i>in vivo</i> limb culture
	Ectoderm removal	Spatiotemporal specific removal of Wnt components that are specifically expressed in the ectoderm
	Conditional knockout	Inactivation of a target gene in a desired tissue/organ. Can observe tissue/patterning outcome while bypassing the limits that are usually observed with constitutive knockout (lethality etc).
Modelling	LimbNET	<i>In silico</i> perturbation. To test hypotheses and generate predictions for further experiments.

Table 2. Types of perturbation experiments and its roles.

For systematic perturbation of the Wnt signalling pathway, 11 small molecules, 1 peptide, and 6 Wnt signalling ligands were tested on micromass and limb bud culture systems. The full list of Wnt modulators, and their targets are available in Table 3. Most of the inhibitors are specific to components of Wnt pathways (Wnt ligands/ Wnt receptors/cytosolic components/transcription factors) and types of pathways, discriminating on a specific molecular target (Figure 27). Names of each small molecule/peptides/ligands and their molecular targets are outlined. In summary there are: 2 inhibitors that interfere with Wnt production; 7 ligands and one small molecule that modulate Wnt-receptor interaction; and 9 small molecules that specifically target Wnt canonical pathways, 3 of which are cytosolic, 3 inhibiting nuclear translocation, and the other 3 directly inhibiting β -cat interaction with its transcriptional partners. Information about target pathways/molecules, and impact on the pathways upon application is summarised in the Table 3.

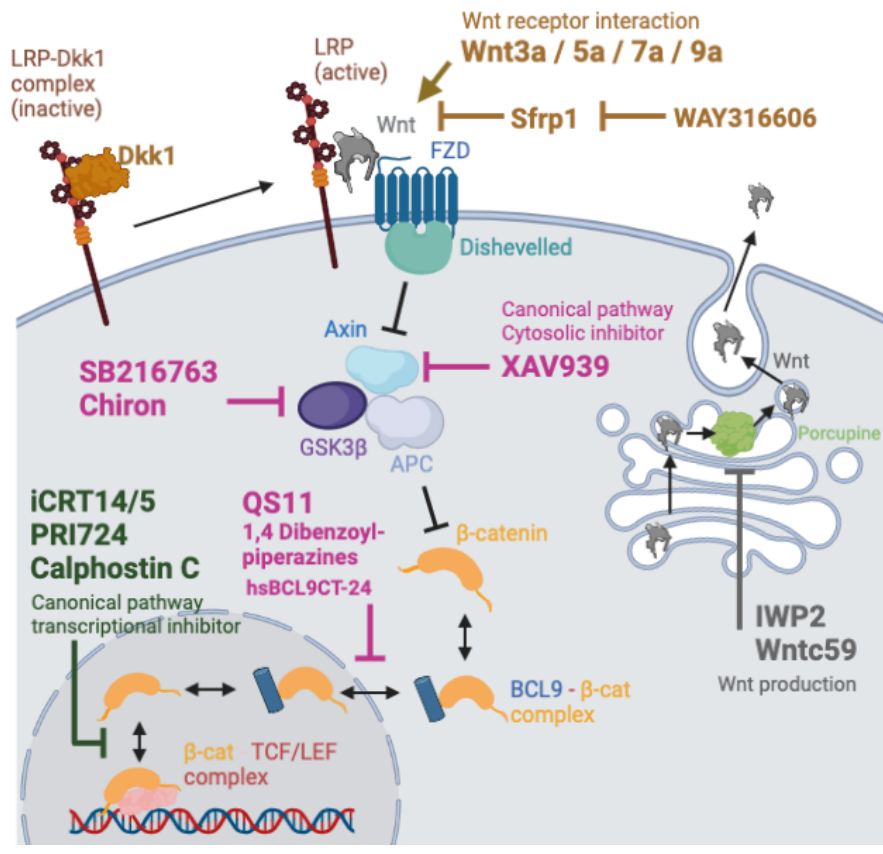


Figure 27. Names of small molecule/ligand/peptides used in this study and their target Wnt pathway parts.

On both micromass and limb bud culture, small molecules/ligands/peptides were applied in multiple different doses(3-10) (Supplementary Figure 1,2). The concentration to be applied was determined based on literature, mostly IC50/ED50 values of Wnt pathway activation in cell culture(Table 3). In micromass, the minimum dose applied was aimed to be around or above the IC50/ED50 concentration if available, and in limb culture, much higher.

Method of modulation	Name	Canonical / non canonical	Impact on the pathway	Mechanism	Target Molecule	Concentration from the literature
Small Molecule inhibitor	IWP2	All Wnt pathways	↓	Wnt production inhibition	Porcupine inhibitor	10µM, digit patterning change [28]
	Wntc59					IC50 = 74 pM against porcupine (Tocris)
Ligands	Wnt3a	Canonical	↑	Wnt Receptor interaction	FZD2/4/5, LRP6 etc	Zebrafish embryo, caudal forebrain organiser disruption, 0.5mM [118]
	Wnt5a	Non-canonical	↑		FZD1/2/4	Mouse embryo blastocyst perturbation, 200 ng/mL [119]
	Wnt7a	canonical	↑		FZD9, FZD5-LRP6	IC50 = 1.2µM in ovarian cancer cells [120]

	Wnt9a	Un known	↑		Fzd4, 7 and 9, WIF-1	ED50=8-40 ng/mL, Wnt TCF reporter activity in HEK293 (Tocris)	
	Sfrp1	All Wnt pathways	↓		Competes with Wnt on Fzd receptors	-	
	Dkk1		↓		Inactivating LRP6 co-receptor on the cell surface	100 ng/ml, reduce mouse blastocyst development [121]	
Small molecule inhibitor	WAY316606		↑		Sfrp1 inhibitor	IC ₅₀ = 0.65 μM against Sfrp1[75].	
	SB216763	Canonical	↑	Wnt canonical pathway cytosolic component inhibitor	Inhibits GSK and stabilises β-catenin	-	
	CHIR99021						5-10mg/ml in ovo injection, chick embryo, induce feather follicles [122]
	QS11		↑			ARFGAP1. Upregulates β-cat nuclear translocation	HEK293 cells, Wnt activation EC ₅₀ = 0.5 μM[123]
	XAV939		↓			Axin Tankyrase inhibitor, activate axin	Human lymphoblasts tankyrase elevation, 1.0 μM[124]
	1,4 Dibenzo piperazines		↓			Bcl9- β-cat inhibitor. prevents shuttling of β-cat in and out of the nucleus	HCT116 cells, Wnt/β-cat inhibition IC ₅₀ = 191 nM [125]
Peptide	hsBCL9CT-24						<i>in vivo</i> mouse, 30 mg/kg over 7 days [126]
Small molecule inhibitor	iCRT14		↓	Wnt canonical pathway transcriptional component inhibitor	TCF4-β-cat binding inhibitor	IC ₅₀ = 40.3nM HEK293 cells (Tocris)	
	PRI724		↓		CBP-β-cat binding inhibitor	IC ₅₀ = 5μM NTERA-2 cells(Germ cell tumour cell line)[127]	
	Calphostin C		↓		TCF-β-cat binding inhibitor	Exposure of HEK293 cells at 1 μM for 30 min leads to β-cat accumulation [128]	

Table 3. References to concentration from literature, tissue/cell type used in the literature annotated.

4.1 Classification of outcome types form micromass assay

Before dissecting which molecular wnt targets result in Sox9 pattern changes, this section outlines the types of outcome from the screening approaches. and whether results from micromass and limb culture agree.

Out of 18 Wnt ligands, small molecules, and peptides, 15(83%) showed Sox9 pattern changes in either micromass or in limb culture. In the micromass, 11(61%) resulted in pattern loss, 2(11%) resulted in stronger pattern, and 5(27%) did not change any pattern. In the limb culture, 9 changed patterns, and 9 did not. Comprehensive results with representative micromass and limb bud culture results are attached in Table 4.

The main outcome of Wnt interventions in micromass culture is change in periodicity of the condensation patterns(Table 4). From an initially homogeneous distribution of Sox9+ and Sox9- cells, micromass culture establishes spot shaped Turing-like patterns around the 15th hour. All micromass data presented are taken after 48hrs of culture. Depending on the type of small molecule applied, the pattern can be interrupted and lost or, conversely, show a higher degree of condensation. Pattern change in each data was quantified with reverse Fourier transform analysis, which decomposes an image into its sine and cosine components [129]. The output of the Fourier transform is a graph that represents the dominant frequencies present within the periodic condensation pattern. Fourier transform image analysis script is written by Xavier Diego. The x-value of the peak of each graph indicates the most representative period between the adjacent condensations(Table 4). The y-value of the graph indicates the power, proportional to the amount of pixels in the image demonstrating the periodic pattern. When the pattern is lost, for instance upon Calphostin C application, the periodicity peak is less notable with multiple noisy, low-power peaks(Table 4, left). Stronger periodicity is demonstrated with more salient peak structure, which corresponds to the higher number of condensations in the image, or stronger condensations that demonstrate connecting ridges between the spots.

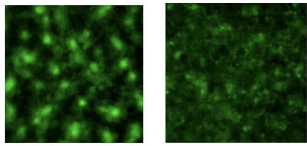
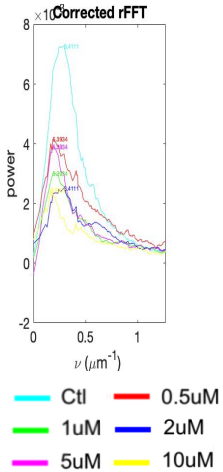
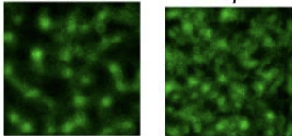
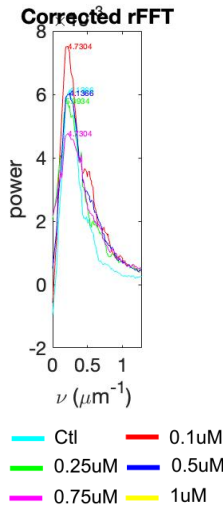
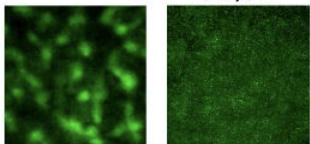
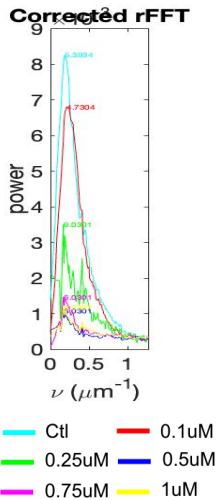
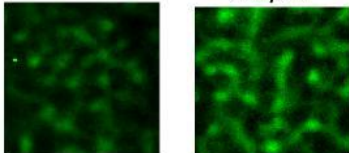
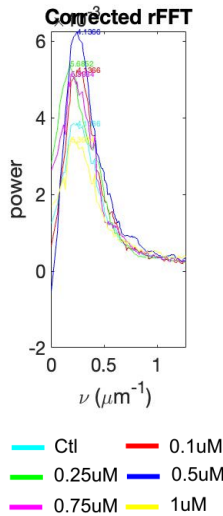
Types of change	Data	Types of change	Data
Periodicity lost	<p>Wnt3a</p> <p>Ctl 0.15 μM</p>  <p>Corrected rFFT</p>  <p>power</p> <p>ν (μm^{-1})</p> <p> — Ctl — 0.5uM — 1uM — 2uM — 5uM — 10uM </p>	Periodicity Stronger	<p>Sfrp1</p> <p>Ctl 0.25 μM</p>  <p>Corrected rFFT</p>  <p>power</p> <p>ν (μm^{-1})</p> <p> — Ctl — 0.1uM — 0.25uM — 0.5uM — 0.75uM — 1uM </p>
	<p>Calphostin C</p> <p>Ctl 0.5 μM</p>  <p>Corrected rFFT</p>  <p>power</p> <p>ν (μm^{-1})</p> <p> — Ctl — 0.1uM — 0.25uM — 0.5uM — 0.75uM — 1uM </p>		<p>Dkk1</p> <p>Ctl 0.5 μM</p>  <p>Corrected rFFT</p>  <p>power</p> <p>ν (μm^{-1})</p> <p> — Ctl — 0.1uM — 0.25uM — 0.5uM — 0.75uM — 1uM </p>

Table 4. Main outcomes of micromass at 48h post seeding : loss of periodicity or stronger periodicity. 10x magnification of micromass images. Plots from rFFT are attached below each micromass experiment. X-axis : period between the adjacent condensations. Y-axis : power.

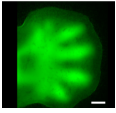
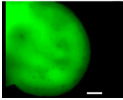
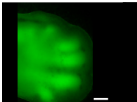
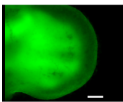
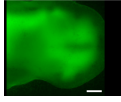
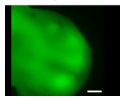
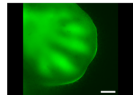
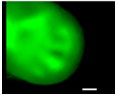
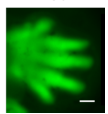
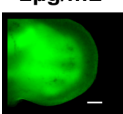
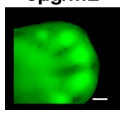
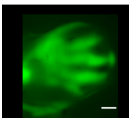
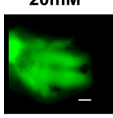
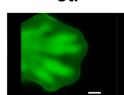
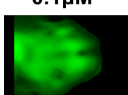
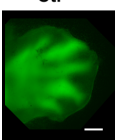
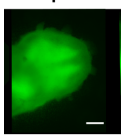
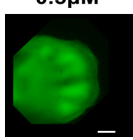
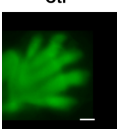
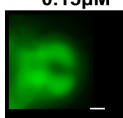
4.2 Classification of outcome types from limb bud culture

Limb culture shows various types of digit shape changes, mostly digit merging. 9 out of 18 small molecule/ligand/peptide application resulted in 4 subtypes of digit merging phenotypes, and one digit sharpening. Webbing, Digit period increase, Peripheral digit loss, and Distal digit widening are four subtypes of the digit merging phenotype (Table 5). The Webbing phenotype has Sox9 expressed between the distal end of digits. Phenotypes comprising Peripheral digit loss and digit period increase are similar in that two digits are left following small molecule application, but peripheral digit loss involves merging of the most anterior digit into the second anterior digits, and the most posterior digits into the next posterior digits. Distance in between the two middle digits does not change, resulting in no period change. On the other hand, digit period increase involves change of the overall digit period, meaning that the two central digits move apart and away from each other. Dynamics (Supplementary Figure 1) show clear period change in the period increase phenotype, compared to the peripheral digit loss phenotype. Distal digit widening involves widening and increase in Sox9 expression of the digital end. In distal digit widening, digit tips are less obviously connected across originally-interdigital spaces, compared to the webbing phenotype.

Out of four digit merging subtypes, peripheral digit loss shows the most variable phenotype, because one or both peripheral digits can be lost. PRI724 shows both peripheral digits having been lost and merged with the central digits, but CHIR99021 and Wnt9a shows only the posterior digit partially merged, and the most anterior digit intact (Table 5).

One peculiar digit phenotype which cannot be categorised as digit merging is digit sharpening, which is demonstrated upon iCRT14 and QS11 application. In the four aforementioned phenotypes, digits widen and/or merge, whereas in the digit sharpening phenotype digits appear to become slightly narrower and more pointed towards their tips.

Out of four different digit merging phenotypes, webbing, peripheral digit loss, and distal digit widening can be co-observed from some Wnt modulators (Table 5). For instance, a low dose of WntC59 application results in webbing, whereas a higher dose gives distal digit widening (Table 5). However, the digit merging phenotype does not necessarily change in response to increasing dosages. 0.65 μ M and 5 μ M CHIR99021 application leads to distal digit widening, whereas an intermediate concentration of 1.5 μ M shows peripheral digit loss phenotype, and 2.5 μ M shows webbing. Another example is PRI724, in which distal digit widening and peripheral digit loss are again observed together. Digit period increase is an exception that is not co-observed with other types of digit merging phenotype.

		Webbing 	Peripheral digit loss 	Distal digit widening 	Digit period increase 	Digit Sharpening 
	Control					
IWP2	Ctl 	25μM 	-	-	-	-
CHIR99021	Ctl 	2.5μM 	0.65μM 	5μM 	-	-
Sfrp1	Ctl 	1.25μg/mL 	-	-	-	-
Wntc59	Ctl 	2μg/mL 	-	5μg/mL 	-	-
XAV939	Ctl 	-	20mM 	-	-	-
Wnt9a	Ctl 	-	0.1μM 	-	-	-
PRI724	Ctl 	-	10μM 	0.5μM 	-	-
Calphostin C	Ctl 	-	-	-	0.15μM 	-

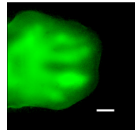
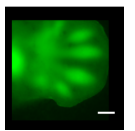
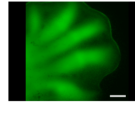
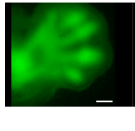
iCRT14	Ctl 	-	-	-	-	5µM 
QS11	Ctl 	-	-	-	-	100µg/ml 

Table 5. Collection of representative digit phenotypes for each inhibitor presented. Biological replicates of these phenotypes, or phenotypes at different concentrations, are in Supplementary Figure 2. Scale bar = 200µm. The number of experimental replicates for each experiment is annotated in Supplementary Figure 2.

4.3 Comparison of results from micromass and limb culture

Out of 18 small molecules/ligands/peptides that modulate the Wnt pathway, 15 resulted in either micromass or limb pattern change, indicating that the majority were effective in eliciting pattern changes, and confirming that Wnt pathway modulation does lead to Sox9 pattern change.

Out of 18 different small molecule/ligand/peptides, the micromass and limb culture experiments are in agreement in 13 cases, meaning that patterns in both experiments have changed or have not changed consistently for a given intervention.

Out of those 13 cases, 9 resulted in change in both micromass and limb culture (Table 6, yellow). There is only one case (IWP2) which does show change in limb culture but not in the micromass. The IWP2 result has been already demonstrated by Raspopovic *et al.*[28] and has been replicated by different groups. Still, overall, all Wnt modulators that are able to elicit limb pattern change response also change micromass patterns, except IWP2.

There are 4 molecules/ligands that did not result in limb pattern nor micromass change: Wnt5a, Wnt7a, Way316606, and 1,4 Dibenzoyl piperazines (Table 6, green). In the Wnt5a limb culture experiment, the maximum concentration tried was 4mM, which is higher than the concentration known to impact developmental changes. For instance, 400ng/mL of Wnt5a can change Inner cell mass to trophectoderm proportion in early bovine embryos[119]. The maximum dose of Way316606 was 100µM, much higher than its IC50 of 0.65µM against Sfrp1[75].

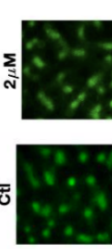
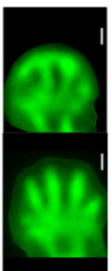
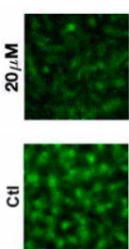
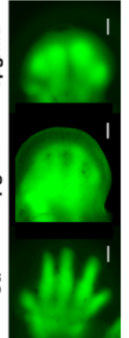
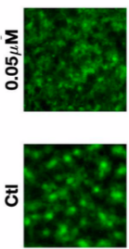
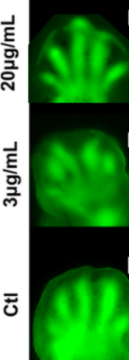
There are 4 small molecules/ligands/peptides (Table 6, blue) in which the micromass pattern has changed but limb pattern has not been impacted. Possible reasons for discrepancy will be explained in the discussion section.

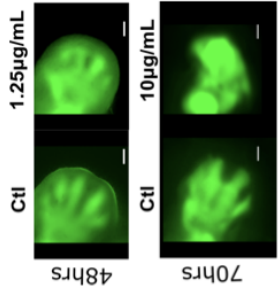
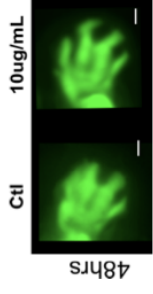
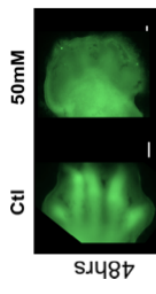
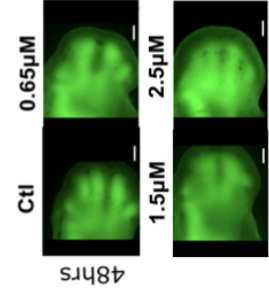
In both micromass and limb culture, it is critical to prevent obtaining false positive results, meaning that each result is from a genuine change in the Sox9 expression pattern, rather than from other causes such as cell death. In both micromass and limb culture, dead cell cultures are easily distinguishable and therefore not taken into account of the result analysis (Supplementary Table 2). In micromass, cell death higher than 40-50% leads to detachment of the culture from the ibidi plate, preventing imaging (Supplementary Table 2).

All micromass cultures that can be imaged have more than 70% of viable cells, which is checked during the micromass seeding stage. In the limb culture, dead limbs are easily distinguishable due to overall blurring of Sox9-EGFP fluorescence and complete loss of patterns.

Name	Target Molecule	Impact on the pathway	Micromass pattern change	Limb pattern change	Agreement between micromass and limb culture
Wntc59	Porcupine	↓	lost	Webbing, Distal digit widening	✓
CHIR99021	Inhibits GSK and stabilises β-cat	↑	lost	Webbing, Distal digit widening, peripheral digit loss	✓
Sfrp1	Competes with Wnt on Fzd receptors	↓	stronger	Webbing, distal digit widening	✓
PRI724	CBP-β-cat binding inhibitor	↓	lost	Distal digit widening, peripheral digit loss	✓
XAV939	Axin Tankyrase inhibitor	↓	lost	peripheral digit loss	✓
Wnt9a	Fzd4, 7 and 9, WIF-1	↑	lost	peripheral digit loss	✓
Calphostin C	TCF-β-cat binding inhibitor	↓	lost	Digit period increase	✓
iCRT14	TCF4-β-cat binding inhibitor	↓	lost	Digit sharpening	✓
QS11	ARFGAP1. Upregulates β-cat nuclear translocation	↑	lost	Digit sharpening	✓
Wnt5a	FZD1/2/4	↑	no change	no change	✓
Way316606	Sfrp1 inhibitor	↑	no change	no change	✓
1,4 Dibenzoyl piperazines	Bcl9- β-cat inhibitor	↓	no change	no change	✓
Wnt7a	FZD9, FZD5-LRP6	↑	no change	no change	✓
Wnt3a	FZD2/4/5, LRP6 etc	↑	lost	no change * but beads do cause a pattern change	some agreement-
IWP2	Porcupine inhibitor	↓	no change	webbing	-
SB216763	Inhibits GSK and stabilises β-cat	↑	lost	no change	-
hsBCL9CT-24	Bcl9- β-cat inhibitor.	↓	lost	no change	-
Dkk1	Inactivating LRP6 co-receptor on the cell surface	↓	stronger	no change	-

Table 6. Result summary table from Table 7. Molecules that elicit both limb culture and micromass changes are listed first.

Pathway	Method of modulation	Name	Canonical/non-canonical	Impact on the pathway	Mechanism	Target Molecule	Micromass (48h of culture)	Limb Culture
Wnt	Small Molecule inhibitor	IWP2	All Wnt pathways	↓	Wnt production inhibition	Porcupine inhibitor	<div style="display: flex; justify-content: space-around;"> <div> <p>Raw experimental Results</p>  </div> <div> <p>Periodicity change</p> <p>-</p> </div> </div>	<div style="display: flex; justify-content: space-around;"> <div> <p>Raw experimental Results</p>  </div> <div> <p>Digit shape change</p> <p>Digit merging : Webbing</p> </div> </div>
		Wntc59					<div style="display: flex; justify-content: space-around;"> <div> <p>Raw experimental Results</p>  </div> <div> <p>Periodicity change</p> <p>lost</p> </div> </div>	<div style="display: flex; justify-content: space-around;"> <div> <p>Raw experimental Results</p>  </div> <div> <p>Digit merging.</p> <p>2 μg/mL : webbing 5 & 10 μg/mL: Distal digit widening</p> </div> </div>
	Ligands	Wnt3a	Canonical	↑	Wnt Receptor interaction	FZD2/4/5, LRP6 etc	<div style="display: flex; justify-content: space-around;"> <div> <p>Raw experimental Results</p>  </div> <div> <p>Periodicity change</p> <p>lost</p> </div> </div>	<div style="display: flex; justify-content: space-around;"> <div> <p>Raw experimental Results</p>  </div> <div> <p>Digit shape change</p> <p>-</p> </div> </div>

Ligand	Sfrp1		↓	Competes with Wnt on Fzd receptors. Wnt3a [55], FZDs target FZDs unknown[57]		Digit merging : 1.25µg/mL - Webbing, 10 µg/mL : Distal digit widening
	Dkk1		↓ [135]	Inactivating LRP6 co-receptor on the cell surface [135]		-
Small molecule inhibitor	SB216763	Cano nical	↑	Inhibits GSK 3β and stabilises β catenin		-
	CHIR99021					Digit merging : 0.65µM, 5µM - Distal Digit Widening, 1.5µM - peripheral digit loss 2.5µM - webbing

4.4 Wnt production process and Wnt canonical pathways are accountable for digit patterning

Small molecules/ligands/peptides are able to target Wnt pathways in four major steps: Wnt production, Wnt receptor interaction, Wnt canonical pathway cytosolic interactions and Wnt canonical pathway transcriptional interactions (Figure 28). Out of 18 Wnt modulators, 15 are known to target β -cat specific canonical pathways. IWP2 and Wnt-C59 are two molecules that globally impact both canonical and non-canonical pathways, as they are involved in Wnt production inhibition. Wnt5a is the most well known and the only non-canonical pathway specific modulator in this study, due to lack of other non-canonical pathway specific modulators.

The Wnt production inhibition, and the Wnt canonical pathway-transcriptional component inhibition categories most effectively yield Sox9 pattern changes, with 3/4 and 6/6 experiments, respectively (Figure 28, Table 8). Still, all categories of modulators show near or higher than 50% response for combined micromass and limb bud culture experiments (Table 8).

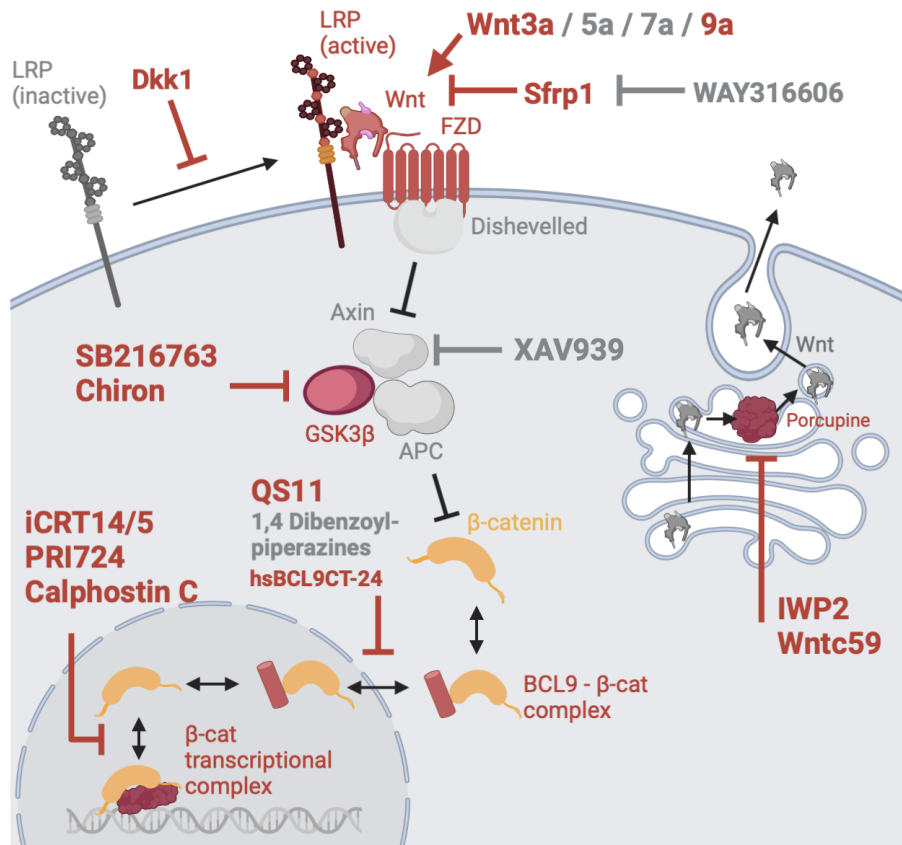


Figure 28. Wnt components, ligands/inhibitors, and inhibitor targets that resulted in pattern change in either micromass or limb culture are highlighted in red.

In the Wnt production step, targeting porcupine and acetylation of Wnt components changes digit patterning. The Receptor-Wnt interaction stage shows a variety of ligands working as digit patterning modulators, and their targets which cooperate in altering the Wnt signalling outcome to change pattern. FZD2/4/5/7/9 which interact with Wnt3a and 9a, and

LRP6 co-receptor which is a target of DKK1, are all relevant Wnt components to digit patterning(Figure 28, Table 8). In the cytosol - cell internal part of the canonical Wnt pathway, CHIR99021 application on GSK3 β generates several digit merging phenotypes(Figure 28, Table 8). Modulating the transcriptional role of β -catenin, by increasing β -catenin nuclear translocation, and inhibiting TCF/CBP - β -catenin binding most effectively changed Sox9 digit patterning, with 5 out of 6 modulators in this category(Table 8).

Mechanism	Canonical or non-canonical	Name	Impact on the pathway	Micromass pattern change	Limb pattern change	Target Wnt components by the ligand(if applicable)	Number of experiments resulted in Sox9 pattern change
Wnt production inhibition	Both	IWP2	↓	-	webbing	-	3/4
		Wntc59		lost	Webbing, Distal digit widening	-	
Wnt Receptor interaction	Non Canonical	Wnt5a	↑	-	-	-	7/13
		Wnt3a	↑	lost	-	FZD2/4/5, LRP6 etc	
		Wnt7a	↑	stronger	-	-	
		Wnt9a	↑	lost	Webbing	Fzd4/7/9, WIF-1	
		Way316606	↑	-	-	-	
		Sfrp1	↓	stronger	Webbing, distal digit widening	Wnt3a, FZDs	
		Dkk1	↓	stronger	-	Lrp6	
Wnt canonical pathway cytosolic component inhibitor	Canonical	SB216763	↑	lost	-	-	8/12
		CHIR99021	↑	lost	Webbing, Distal digit widening, peripheral digit loss	-	
		QS11	↑	lost	Digit sharpening	-	
		XAV939	↓	lost	peripheral digit loss	-	
		1,4 Dibenzoyl piperazines	↓	-	-	-	
		hsBCL9CT-24	↓	lost	-	-	
Wnt canonical pathway transcriptional component inhibitor		iCRT14	↓	lost	Digit sharpening	-	6/6
		PRI724	↓	lost	Distal digit widening, peripheral digit loss	-	
		Calphostin C	↓	lost	Digit period increase	-	

Table 8. Wnt modulators are classified according to its target part of the Wnt pathway. The number on the rightmost column indicates the number of experiments that resulted in pattern change out of the total number of experiments in each category.

4.5 All micromass and limb culture phenotypes can be recapitulated using the Turing stripe (BSW) model

Using LimbNET, the Sharpe Lab's new version of mesh-based simulations of molecular patterning in limb development, the strength of Wnt signalling acting on Sox9 can be modulated. In LimbNET, data-driven descriptions of tissue movements were taken, and predefined, with *in situ* data of certain genes as an input, along with preset diffusion, noise, and initial value of the variables[140]. LimbNET also allows changing the dimension of simulation from limb tissue to micromass, enabling prediction of Wnt signalling changes in micromass.

Previously, simulating Wnt signalling reduction predicted digit merging, in which all digits expand and merge into a continuous domain of Sox9 expression[28]. The expansion happened towards both sub-ectodermal mesenchyme and in between the interdigital regions. The prediction is comparable with some of the IWP2 limb culture application experiments(Figure 12).

Using LimbNET, I have manipulated Wnt signalling in two different ways: a) by adjusting the parameter that controls Wnt influence on Sox9, and b) integrating an additional Wnt inhibitor/activator variable into the partial differential equation that determines the Wnt signalling level in each mesh. The detailed equations for each simulation are in Materials & Methods.

In simulated micromass, integrating an additional Wnt inhibitor/activator into the partial differential equation alone (Materials and Methods) recapitulated the pattern loss and the stronger condensation throughout the culture system(Table 9). In the simulated limbs, digit sharpening could be replicated through the identical method of integrating an additional Wnt activator(Table 9). Webbing and distal digit widening can be replicated by integrating an additional Wnt inhibitor. Webbing and distal digit widening phenotypes are generated from an identical model, and are differentiated from each other by different strengths and application duration of Wnt inhibitor.

Period change in the limb pattern is recapitulated by changing parameter 3 from the original BSW model (Materials and Methods), where k_3 controls the influence of Wnt on Sox9(Figure 26). Recapitulating the peripheral digit loss phenotype requires both changing k_3 and introducing an additional Wnt variable.

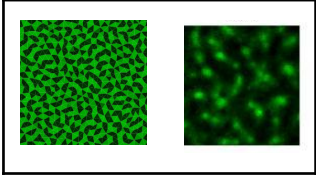
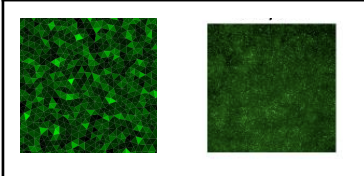
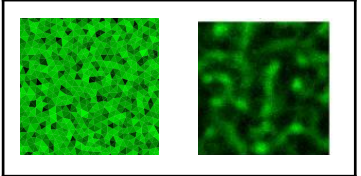
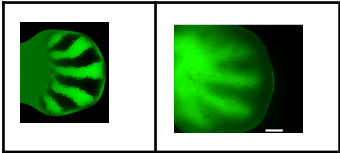
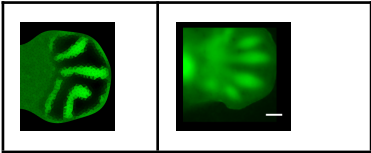
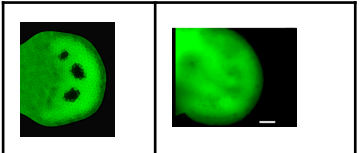
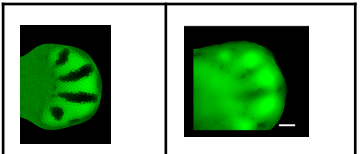
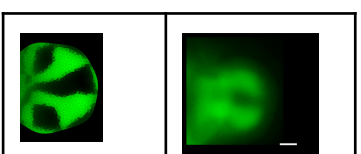
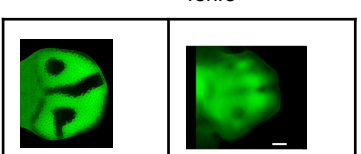
	Unperturbed	Wnt activation	Wnt inhibition
Micro mass	<p>Simulation Experiment Untreated 48hrs</p> 	<p>Pattern Loss, Sox9 ↓</p> <p>Simulation Experiment Calphostin C 48hrs</p> 	<p>Stronger condensation, Sox9 ↑</p> <p>Simulation Experiment Dkk1 48hrs</p> 
Limb culture	<p>Simulation Experiment Untreated 48hrs</p> 	<p>Digit Sharpening</p> <p>Simulation Experiment iCRT14 48hrs</p> 	<p>Webbing</p> <p>Simulation Experiment IWP2 48hrs</p> 
			<p>Distal Digit widening</p> <p>Simulation Experiment wntc59 48hrs</p> 
			<p>Period Change</p> <p>Simulation Experiment Calphostin C 48hrs</p> 
			<p>Peripheral digit loss</p> <p>Simulation Experiment Wnt9a 48hrs</p> 

Table 9. Summary of Wnt activated/inhibited phenotypes in both systems and their simulation.

Next, I examined whether each Wnt activator/inhibitor yields predicted results according to our simulation. For instance, in the Wnt inhibition column of Table 10, Dkk1, IWP2, wntc59, and Calphostin C are Wnt inhibitors, and they all present a digit phenotype that agrees with the simulation. On the other hand, iCRT14, a Wnt inhibitor, gives a digit sharpening phenotype, even though digit sharpening is only predicted from Wnt activation.

Micromass results from 18 Wnt modulating small molecules/ligands/peptides show that 7 of them agree both in experimental and simulated outcomes (Table 10). In the limb culture 7 agree between experiment and simulation. In micromass, 4 do not result in any experimental change, and 7 modulators show the opposite experimental result relative to the simulation. In the limb culture, 8 modulators do not result in any experimental change.

There are 3 cases in which Wnt modulators result in a limb culture Sox9 digit phenotype implied by the opposite impact: Wnt9a, CHIR99021 and iCRT14 (Highlighted in orange, Table 10). Wnt9a, conventionally known as Wnt activating ligand, generates the webbing phenotype which is expected from Wnt inhibitors. CHIR99021, which exhibits all phenotypes of Wnt inhibitors, is a Wnt activator. Finally, iCRT14, which shows digit sharpening phenotype, would be predicted to demonstrate digit merging because iCRT14 is a Wnt inhibitor. 8 cases do not result in any experimental change.

What is notable is that a set of Wnt inhibitors (wntc59, XAV939, PRI724, Calphostin C) generate opposite experimental outcomes in micromass but matching limb culture outcomes. The result suggests that despite the conflicting results in micromass, these Wnt inhibitors effectively alter Sox9 expression in both micromass and the limb culture.

Impact on the pathway	Name	Micromass			Limb culture		
		Experimental Pattern change	simulated outcome	Agreement	Experimental Pattern change	Simulated outcome	Agreement
↑	CHIR99021	lost	lost	✓	Webbing, Distal digit widening, peripheral digit loss	Digit sharpening	-
↑	QS11	lost	lost	✓	Digit sharpening	Digit sharpening	✓
↑	Wnt3a	lost	lost	✓	-	Digit sharpening	-
↑	Wnt7a	stronger	lost	-	-	Digit sharpening	-
↑	Wnt9a	lost	lost	✓	Webbing	Digit sharpening	-
↑	SB216763	lost	lost	✓	-	Digit sharpening	-

↓	Sfrp1	stronger	stronger	✓	Webbing, distal digit widening	Webbing, distal digit widening, period change, peripheral digit loss	✓
↓	Dkk1	stronger	stronger	✓	-	Webbing, distal digit widening, period change, peripheral digit loss	-
↓	Wntc59	lost	stronger	-	Webbing, Distal digit widening	Webbing, distal digit widening, period change, peripheral digit loss	✓
↓	XAV939	lost	stronger	-	peripheral digit loss	Webbing, distal digit widening, period change, peripheral digit loss	✓
↓	iCRT14	lost	stronger	-	Digit sharpening	Webbing, distal digit widening, period change, peripheral digit loss	-
↓	PRI724	lost	stronger	-	Distal digit widening, peripheral digit loss	Webbing, distal digit widening, period change, peripheral digit loss	✓
↓	Calphostin C	lost	stronger	-	Digit period increase	Webbing, distal digit widening, period change, peripheral digit loss	✓
↓	hsBCL9C T-24	lost	stronger	-	-	Webbing, distal digit widening, period change, peripheral digit loss	-
↓	IWP2	-	stronger	-	webbing	Webbing, distal digit widening, period change, peripheral digit loss	✓
↑	Wnt5a	-	lost	-	-	Digit sharpening	-
↑	Way316606	-	lost	-	-	Digit sharpening	-
↓	1,4 Dibenzo yl piperazines	-	stronger	-	-	Webbing, distal digit widening, period change, peripheral digit loss	-

Table 10. The first two columns for each type of experiment(micromass, limb culture) outline experimental and simulated Sox9 change outcomes respectively. The third column indicates whether these have agreed or not. Overall, 7 Wnt modulators have agreed experimental and simulated outcomes in micromass, and 8 in the limb culture.

To find out whether Wnt signalling is actually downregulated in the micromass from the above set of inhibitors(wntc59, XAV939, PRI724, CalphostinC), immunostaining using antibody against active, dephosphorylated β -catenin was performed on fixed micromass(Supplementary Figure 3). Application of PRI724, for instance, decreases the global intensity of active β -catenin antibody expression level by around 50%. Using the Sox9 antibody against the fixed micromass culture confirms again that the Sox9 condensation pattern in PRI724 is lost.

4.6 Webbing, Distal digit widening, and Peripheral digit loss could be variations of a global digit merging model

Next, I set out to investigate whether different digit merging phenotypes - especially webbing, distal digit widening, peripheral digit loss - can generate identical phenotypes. The idea comes from the fact that these three digit merging phenotypes are from one model, which integrates an additional Wnt inhibitor into the partial differential equation that defines Wnt expression at a given tissue mesh(Materials and methods). The only difference between the webbing and distal digit widening model is the inhibitor concentration, and peripheral digit loss model involves additional modulation in lambda, which sets the period. On the other hand, the period change pattern is generated by directly modulating the degree of Wnt influence on Sox9.

On the experimental side, certain inhibitors can generate multiple digit merging phenotypes(Section 4.2). For instance, applying CHIR99021 on limb culture can produce webbing, distal digit widening, and peripheral digit loss. Wntc59 and PRI724 also demonstrate multiple digit merging phenotypes(Table 5).

There are two variables used in the simulation : the strength of the Wnt inhibitor, and the starting time point when the inhibitor is applied. Each of the original limb culture phenotype simulation results(webbing, distal digit widening, and peripheral loss) are in the leftmost column, which corresponds to recapitulation of the experimental results(Figure 29). Increasing Wnt amount led to closing of the Sox9- regions in all models and generated a global expression of Sox9+ area in the whole autopod. Interestingly, moderate increase in Wnt inhibition(Figure 29, column ++) can be recapitulated to some degree by introducing the inhibitors earlier. However, the uniform and global Sox9+ phenotype(column +++) could not be regenerated even by combination of higher concentration and earlier introduction.

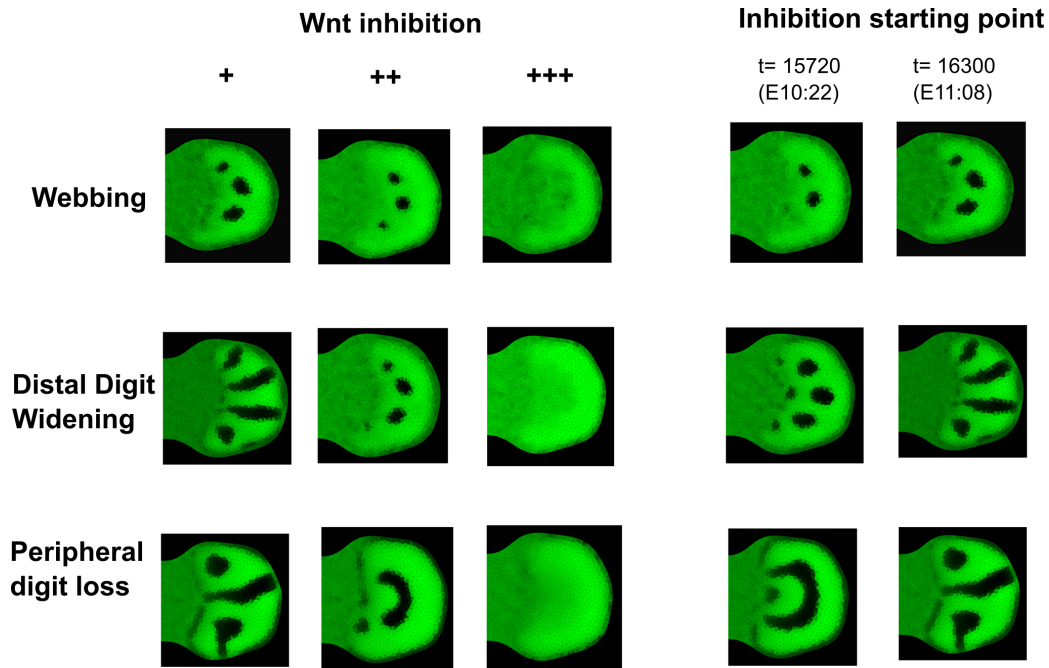


Figure 29. Upon stronger Wnt inhibition, The pattern is completely lost and shows uniform and global expression of Sox9+ area across the autopod.

Experimentally, global Sox9+ expression in the autopod is observed when the inhibitor is applied before the digit forming stage(Figure 29). Both IWP2 and Sfrp1 experiments(Figure 30) started around E11:00. Experimental results suggest that uniform Sox9 expression could be in principle modelled in the LimbNET with a few adjustments(e.g. allowing modelling from earlier stages, and closely matching virtual timepoints to experimental timepoints).

Global autopod Sox9+ expression can be also observed when a sufficient amount of inhibitor is applied during the digit forming stage(Figure 30, Wntc59 column). Nearly complete merging of the three initial digits is observed. The result indicates that Wnt modulators that give webbing/distal digit widening/peripheral digit loss have the potential to display global Sox9 expression, with complete loss of Sox9 pattern, at a suitable concentration and incubation time.

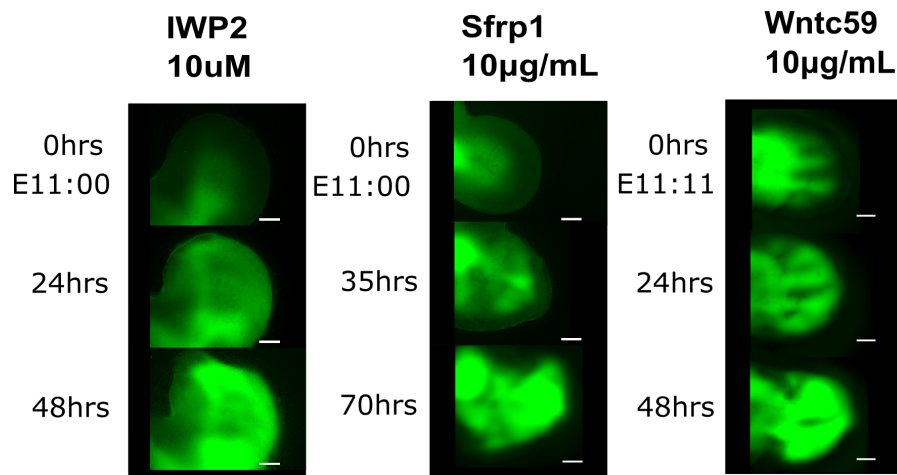


Figure 30. Experimental examples of global Sox9+ expression throughout the autopod(Figure 29, Column +++).

4.7 Partial ectoderm removal locally reorganises Sox9 pattern

So far I have addressed not only which molecular targets/types of the Wnt pathway are relevant to the digit patterning, but also which ligands experimentally changed digit patterning.

One of the unaddressed questions was that while Wnt3a expression is exclusive to the ectoderm, basic conditions of a Turing model require that the diffusible molecules should be expressed throughout the tissue, and these diffusible molecules of the Turing network should form periodic patterns.

My experiments identify another ectodermal ligand [141], Wnt7a, that behaves similarly to Wnt3a in a sense that it also elicits changes in the micromass pattern but not in the limb culture(Table 11). Wnt9a, like Wnt5a, is a pan-mesenchymally expressed ligand in mouse embryonic limb during the digit patterning stage [142].

Since Wnt9a alters both micromass and limb culture patterning and is mesenchymal expressed (Table 11), it is a strong candidate for enabling Turing network in digit patterning. Wnt9a could perform this role by being a canonical Wnt pathway ligand that promiscuously interacts with Fzd4/7/9 and WIF-1 [132].

Still, there is a need to further investigate why and how ectodermal ligands such as Wnt3a and 7a are able to impact digit patterning. It is critical to find out whether previous hypotheses in different systems, such as ectodermal specific signals generating an activating cue of Wnt signalling, also apply to the limb mesenchyme.

In this section, to investigate the role of ectodermal Wnts, I performed ectoderm removal on mouse embryonic limbs. The experiments are expected to provide insight on whether removing ectoderm impacts Wnt signalling in the mesenchymal area.

Ectodermal/Mesenchymal	Name	Micromass	Limb culture	Bead insertion
Ectodermal	Wnt3a	lost	-	Sox9 downregulation in limb
Mesenchymal	Wnt5a	-	-	- [28]
Ectodermal (dorsal only) [141]	Wnt7a	stronger	-	- [28]
Mesenchymal [142]	Wnt9a	lost	Webbing	Not tried

Table 11. Expression patterns of Wnt ligands and their experiment/simulation result summary.

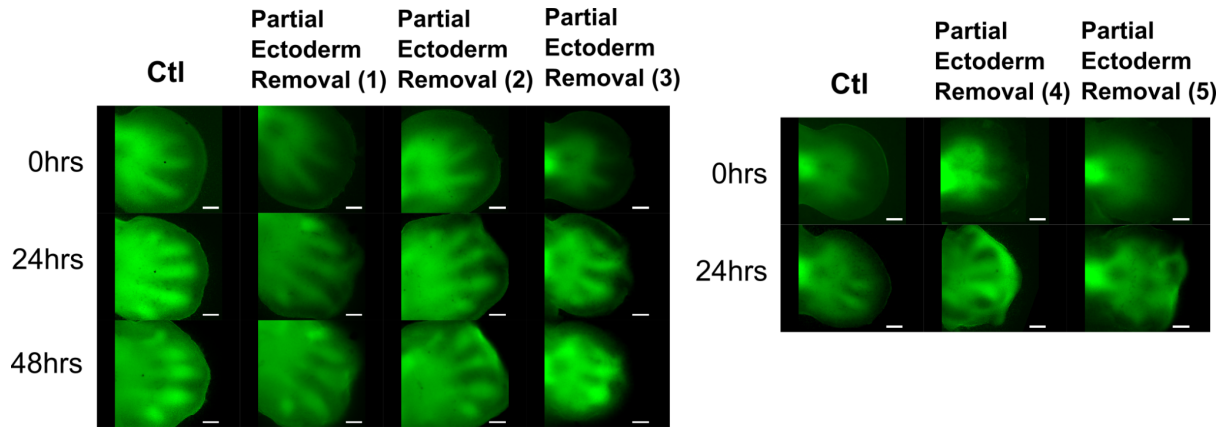
Previously, In the case of Wnt7a, a partial ectoderm removal method has already been applied to investigate Wnt7a role[143]. Following dorsal ectoderm removal in stage 20-21 chick limb buds(equivalent to E10-10.5 mouse limb buds, before digit patterning stage), digits are fused into one another, leaving only 2-3 digits. Zeugopod can be also characterised by partial fusion. This result is thought to be comparable to Wnt7a conditional knockout, which demonstrates variable loss or malformation of posterior digits and ulna[141].

Wnt3a is expressed throughout the entire ectoderm, but complete ectoderm removal around the whole limb before digit patterning stage prevents assessment of accurate limb patterning in the limb culture, because mesenchymal cells lose their orientation and spread out to the culture mesh(Supplementary Figure 4). Therefore, I removed about 30-50% of the distal tip ectoderm, and 50-200µm of ectoderm from the tip towards both dorsal and ventral side. The ectoderm removed area is indicated in red in the brightfield images section(Figure 31).

In all partial ectoderm removal experiments, the mesenchymal area adjacent to the removed ectoderm demonstrates increased Sox9 expression(Figure 31). Increased Sox9 expression along the distal end of mesenchyme can be found in both young disrupted limbs during the early digit patterning stage(Partial ectoderm removal experiment 4 and 5), and in older limbs (Partial ectoderm removal experiment 1 and 2). The impact is the most pronounced in the earliest interrupted experiment 4, and to lesser degrees in all other experiments. Another phenotype is the spreading or blurring of digital Sox9. Sox9 expression at the distal tip of the affected digits either shows an enlarged tip(experiment 3,5), or distally spreads out(experiment 1,4) and forms bridges, or connects to the adjacent digits. In experiment 5, this enlargement is combined with the near-ectoderm mesenchymal Sox9 expression.

The second phenotype - localised enlarged tip or digital spreading, is similar to 'distal digit widening' phenotype upon application of Wnt inhibitors(Figure 32). The result implies that local removal of ectoderm leads to decreased Wnt delivery in the mesenchymal cells in the affected area.

Sox9-GFP



Brightfield

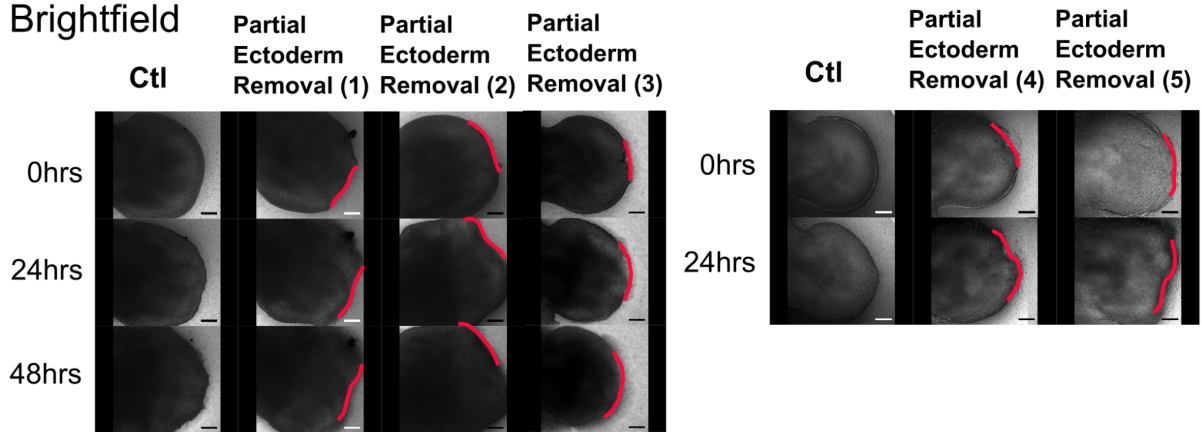


Figure 31. Sox9-GFP and Brightfield images of partial ectoderm removed embryonic limbs. Two distinct phenotypes following partial ectoderm removal experiments are local upregulation of Sox9 in the distal mesenchyme, and spreading of Sox9 in the digital area.

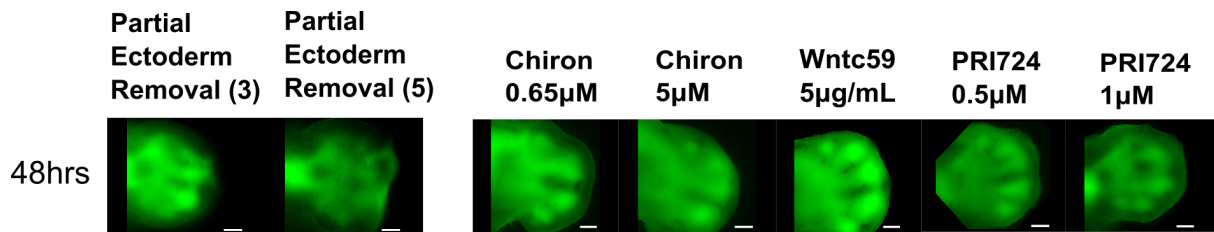


Figure 32. Some phenotypes of partial ectoderm removal, which shows distally enlarged tip or digital spreading, is similar to 'distal digit widening' phenotype upon application of Wnt inhibitors.

4.8 Retinoic acid and Notch pathway modulates digit patterning

The original BSW model states that Bmp, Sox9 and Wnt signalling are the minimum components to establish digit patterning, it is necessary to confirm whether the Wnt pathway has primary importance over other pathways, in a screening approach. Previous microarray analysis, which searched for differentially expressed genes between Sox9+ and Sox9- cells, looked at a few signalling pathways including Wnt, Bmp, TGF, and FGF [28], but Retinoic acid and Notch pathway have not been looked at.

To assess the impact of RA and Notch pathways, three RA pathway modulators and two Notch pathways are tested. Both RA activators and inhibitors were able to alter the periodicity in micromass, and change digit patterns in the limb culture. The result suggests that all RA modulation mechanisms -retinoic acid receptor activation, inhibition, and Cyp26b1 inhibition- effectively interrupt digit patterning.

RA pathway component conditional knockout/conditional activation experiments result in mild changes in digit patterning, ranging from digit merging [89] to digit loss [94]. These mild digit patterning changes are replicated in all limb culture experiments, both in RA pathway activation and inhibition. (Table 12, Supplementary Table 1). Micromass experiments, upon RA pathway activation, show clear disruption of pattern in both literature [91] and the limb culture experiments.

There is a possibility that RA could act on anterior-posterior digit patterning indirectly through proximal-distal patterning, as some models suggest that the proximal-distal identity of the limb is determined by two signals : a distal FGF signalling from AER and a proximal RA signal from the flank[144]. These upstream signals are thought to control the proximal-distal markers/homeobox genes: Meis1 and Meis2 for stylopod, Hoxa11 for zeugopod and Hoxa13 for autopod[145]. Uzkudun *et al* [84] further used reverse engineering to identify a “crossover model” that reveals RA role in defining Hoxa11-Hoxa13 boundary. Since Hoxa13 expression region is critical for determining digit forming region, there is a change of RA defining digit forming region and modulating digit patterning.

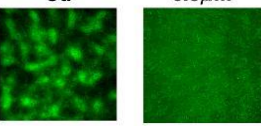
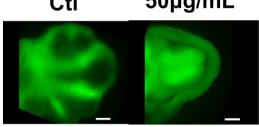
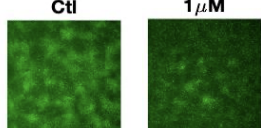
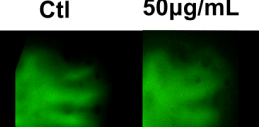
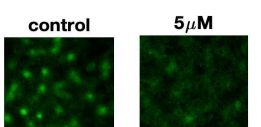
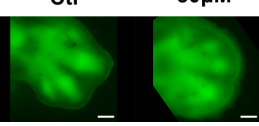
Name	Method of Modulation	Impact on the pathway	Mechanism & Target molecule	Micromass		Limb culture	
				Experimental Results	Periodicity change	Experimental Results	Digit shape change
Retinoic Acid	Ligand	↑	Retinoic acid Receptors agonist	48hrs 	Lost	48hrs 	Digit merging-peripheral digit loss
R115866	Small molecule inhibitor	↑	Cyp26 antagonist	48hrs 	Lost	24hrs 	Digit merging-peripheral digit loss
BMS493		↓	Pan-RA receptor inverse agonist	48hrs 	Lost	48hrs 	5μM - No change 50μM - Distal Digit Widening

Table 12. Experimental result summary table for Retinoic acid pathway interruption. More results in Supplementary Figure 1 and 2.

None of the Notch pathway inhibitors, which are both gamma secretase inhibitors, induced any pattern change in both limb culture and micromass. It is difficult to make a conclusion about whether Notch-Delta signalling modulates digit patterning, because only gamma secretase inhibitors were tried to inhibit Notch-Delta signalling (Table 13). One major difference is that day3 DAPT applied micromass does not show any pattern change, indicating that the impact of Notch signalling inhibition in micromass is stronger on later stages of cartilage differentiation/development. Higher concentrations of DAPT (0.1µM, 0.5µM, 1µM, 5µM, and 10µM) than that of the literature (0.1µM) are applied and none of them, at day3, changed micromass pattern. The results were identical in another Gamma secretase inhibitor, Compound E. Limb culture application of gamma secretase inhibitors did not change digit patterns.

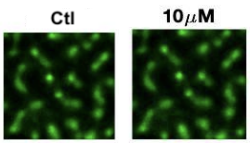
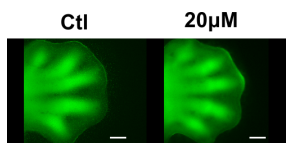
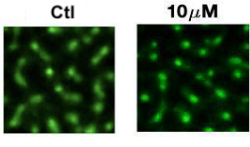
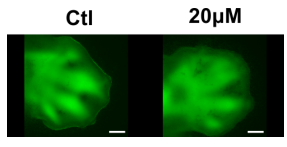
Name	Method of Modulation	Impact	Mechanism & Target molecule	Micromass		Limb culture	
				Experimental Results	Periodicity change	Experimental Results	Digit shape change
DAPT	Small molecule inhibitor	↓	Gamma secretase inhibitor	72hrs 	Lost	48hrs 	Digit merging - peripheral digit loss
Compound E		↓		72hrs 	Lost	48hrs 	Digit merging - peripheral digit loss

Table 13. Experimental result summary table for Notch pathway interruption. More results in Supplementary Figure 1 and 2.

Overall, out of all the experiments performed, RA pathway modulation changed Sox9 patterns in all experiments(6/6), whereas Notch pathway inhibition did not alter Sox9 patterns(0/4) (Table 14).

Pathway	Impact on the pathway	Name	Micromass			Limb culture			Number of experiments resulted in Sox9 pattern change
			Experimental Pattern change	Literature	Agreement	Experimental Pattern change	Literature	Agreement	
RA	↑	Retinoic Acid	lost	lost	✓	Digit merging-peripheral digit loss	Digit merging	✓	6/6
	↑	R115866	lost	lost	✓	Digit merging-peripheral digit loss	Digit loss	✓	
	↓	BMS493	lost	stronger	-	5µM - No change 50µM - Digital Digit Widening	-	-	
Notch	↓	DAPT	-	stronger	-	-	Mild Digit curving	-	0/4
	↓	CompoundE	-		-	-			

Table 14. Micromass-experimental agreement, and the number of experiments that lead to any Sox9 pattern change. All 6 RA modulator experiments resulted in Sox9 pattern changes, and 4 of them agree with the existing literature. The summary for the existing RA literature is found in Table 1 and Supplementary Table 1.

4.9 Part II Summary

In this section, using an unbiased screening approach, I have answered all of the initially proposed questions : How strong is the evidence for WNT being a major player? Can we pin-down whether this is canonical versus non-canonical signalling? What are the different impacts on patterning caused by different types of Wnt perturbation?

On top of demonstrating that while Wnt signalling is absolutely necessary for digit patterning(out of 18 modulators, 15 resulted in either micromass or limb pattern change), I also show that other previously uninvestigated pathways such as retinoic acid and notch are limited to modulation of digit patterning. I pinned down that inhibiting not only extracellular but also intracellular part of canonical Wnt signalling, such as cytosolic components and β -catenin- co-activator interaction, impact digit patterning. Through the screening approach, I also identified another strong candidate ligand for digit patterning, Wnt9a. Then I have successfully replicated different digit patterning phenotypes *in silico*, and identified through modelling that three of these phenotypes(webbing ,distal digit widening, peripheral digit loss) can generate an identical phenotype upon strong inhibition.

In addition to the screening approach, I have also designed and performed partial ectoderm removal experiments to investigate the role of the ectodermal Wnts. I show that some partial ectoderm removal experimental results are identical to the 'distal digit widening' phenotype generated upon Wnt inhibition.

5. Discussion

This thesis is dedicated to the question “To what extent is digit patterning a Turing system?”. I explored two different approaches to answer this:

First, a conceptual approach of probing how long is the digit patterning a self-organising system, relating the ‘Turingness’ or the degree of reaction-diffusion with the classic concept of plasticity. By developing a novel image analysis method, I quantified plastic behaviour of mouse embryonic digit patterning process. Then I successfully incorporated quantified plasticity values into reaction-diffusion based computer simulations, confirming that if plasticity is programmed to decrease in a sigmoidal manner very similar to my empirical quantifications, it is able to recreate patterns very similar to those observed experimentally. Furthermore, Sox9 intensity analysis of cryosectioned limbs showed that molecular digit patterning is fully established before the cell density changes - which lends weight to the idea that the initial patterning is purely molecular, rather than mechanical. These findings provide an insight into not only how long is digit patterning a Turing system, but how fast the mesenchymal limb tissue loses plasticity and when this molecular patterning happens in the context of organogenesis.

The second approach - an unbiased screening of pathways and components critical for the digit patterning. It is non-hypothesis driven and provides complementary insight to the first approach. Although the Wnt pathway has previously been identified as one of the strongest candidates for the Turing mechanism, this evidence still rested on only a few specific observations. The screening approach pursued here identified more specific components of the Wnt pathway, such as the canonical signal transduction and Wnt production, which were important for digit patterning. Interestingly, a variety of different Wnt signalling modulators were converging into just a few distinct patterning results. Although these 4 categories look visually different, computer simulations were able to reveal that they can all be produced by modifications to the same underlying Turing mode. Overall, the screening approach provided ample evidence Wnt signalling is indeed a critical part of Turing network in charge of the self-organising digit patterning.

5.1 For how long is the digit patterning a dynamic self-organisation process?

In this section, I highlight the novelty and importance of our 2D pattern analysis method, discuss the core message of why tissue plasticity in embryonic limbs decreases gradually, and how earlier molecular patterning might have led to mesenchymal condensations.

5.1.1 Novel and quantitative analytic method of tissue plasticity

In this study, a novel and quantitative analytic method of digit pattern was developed to assess dynamic 2D gene expression changes in a tissue upon controlled perturbation: insertion of wnt- or bmp-soaked beads into the tissue. The dynamicity of patterning upon perturbation of the tissue comes from a degree of reaction-diffusion in the system. Tissue plasticity in mouse embryonic limbs gradually decays in a sigmoidal manner, yet plasticity is sustained above zero until E12:00, hours after the digit emerging stage(E11:05-E11:12). Further, through extensive interplay between modelling and experiment, I confirmed that the

mechanism behind digit patterning involves gradual loss of influence from the reaction-diffusion mechanism.

Visually, it is already possible to distinguish both local plasticity change and global tissue plasticity change without quantification. Local changes in plasticity occur in the region immediately surrounding the bead and generate concentric circles of Sox9 upregulation or downregulation (Figure 33A). The global rearrangement involves a) change in Sox9 expression in the distant area from the perturbation source and b) Upregulation of Sox9 in the absence of additional Sox9 source. For instance, in Figure 33A, the region further away from the digit (P1) has its Sox9 upregulated in response to a Sox9 repressor (Figure 33A). This again strengthens the idea that digit patterning is a true Turing system, as this is the type of non-intuitive and long-range behaviour displayed by such RD systems; morphogen-containing bead insertion interrupts the reaction-diffusion of the field as a whole, not solely locally. Global rearrangement demonstrates significantly higher Sox9 upregulated areas (Figure 33B, last row).

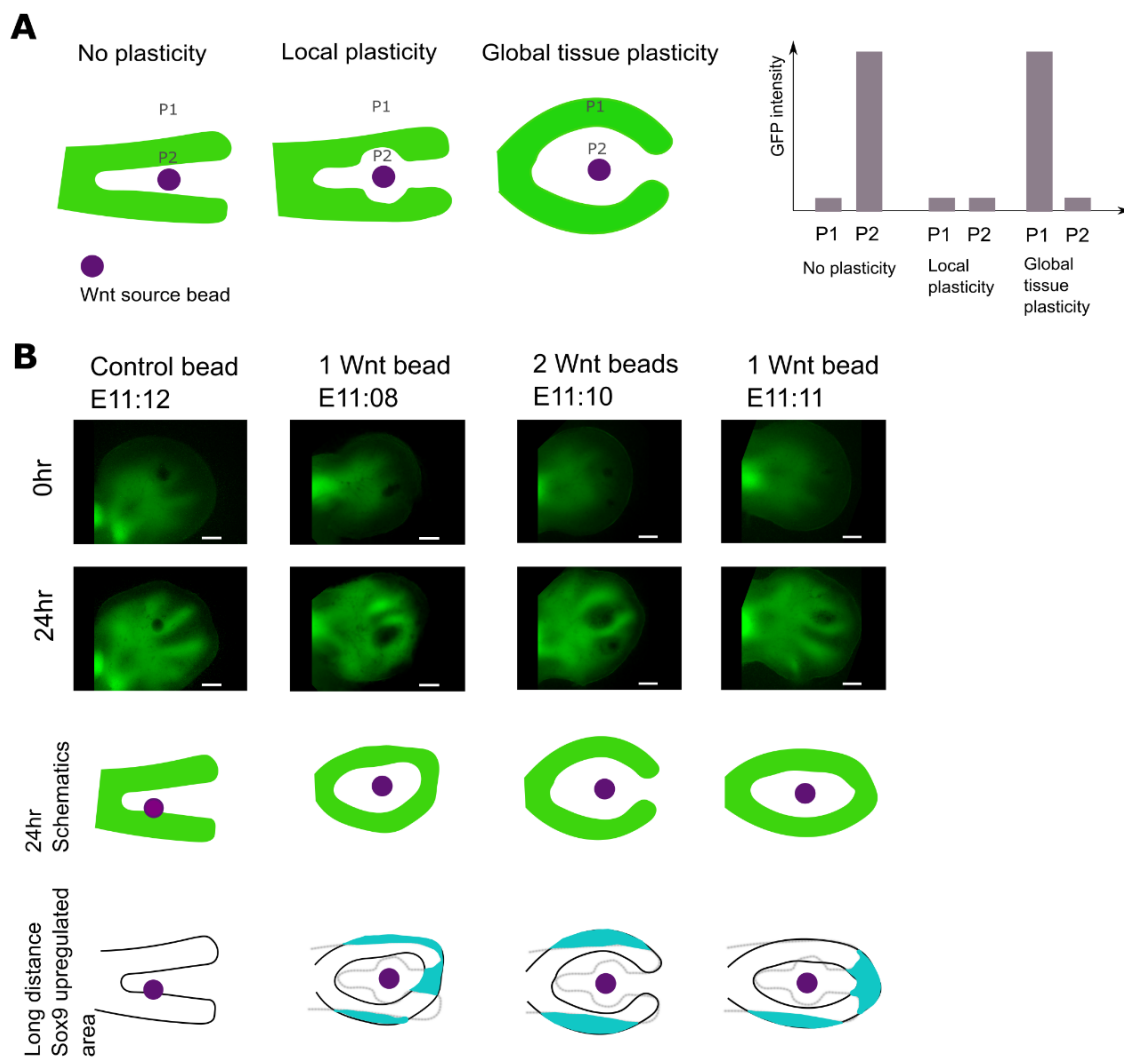


Figure 33. Global rearrangement of Sox9-GFP patterns. (A) Schematic illustration comparing Sox9 levels at different positions of the limb, upon Wnt bead insertion. Tissue P1 is a part of the limb distal

from the Wnt source bead, whereas P2 is closer. Global tissue plasticity changes tissue in P2 to become Sox9-GFP-, while turning P1 into Sox9-GFP+ cells, despite the fact that Wnt bead can only turn off Sox9 expression. (B) Experimental GFP expressions at 0hr and 24hrs. The third row is a schematic of the 24hr GFP pattern in the digits surrounding the beads. The final row highlights the long-distance impact of Wnt beads, which are shown as the difference between the potential local plasticity pattern and the experimental Sox9 pattern.

Our novel method to quantify changes in the 2D tissue pattern reveals quantitative, novel information about the pattern changes as it can distinguish global pattern rearrangements via topological changes. The method focuses on the overall reorganisation of the pattern, and establishes that the 2D tissue plasticity falls to 0 by E12:20. At E12:20, there is no topology difference between the patterns of control and the bead inserted limbs. However, it is important to note that all limbs including those at relatively later developmental timepoint demonstrate individual cellular plasticity. For instance, even around E12:00 and E12:15, Sox9-GFP upregulation/downregulation of the cells immediately surrounding the beads can be observed (Figure 19D). This indicates that individual cells may nonetheless have reversible Sox9 fate around E12:15. Depending on the system, there might be a need to incorporate additional parameters for local plasticity change in order to distinguish the difference in pattern change without an actual change in topology.

Another point to be addressed is the overestimation of plasticity at later timepoints. Once the quantified plasticity is fitted into the model ("Original data fit model"), the simulation turns out to be more dynamic than the experiment. The difference indicates that the quantified RD/plasticity could be slightly overestimated during the network formation and minimum cost calculation steps. One of the reasons for overestimation could be that small changes in digit shape generate a network that is topologically quite different from that of a wild-type network. The effect of this variability is more obvious towards the later developmental timepoints, because the majority of data is biased to 0. To account for overestimation, more bead insertion experiments could be done, even though our experiment already contains 81 datapoints.

5.1.2 Why does tissue plasticity in embryonic limbs decrease in a gradual manner?

There are many reasons why the 2D tissue plasticity decrease in limb embryonic tissue appears gradual. It could theoretically be a delayed manifestation of steeper, or even 'switch' like behaviour. Indeed, a delay is critical to biological systems in general. For instance, there is a significant delay from the start of the RNA transcription until the end of protein synthesis. Even though some processes, such as chromatin opening, acts like a switch between open and closed states [100], delays in multiple steps such as nucleotide modification and protein folding makes protein production gradual.

Equally important are the delays that govern coordination of multiple cells, such as signalling cascade and gene regulatory networks. A series of proteins involved in a signalling pathway delays the initial input to the final output [146], and certain network structures such as negative feedback loop create time delay [147]. Our understanding of the patterning principle, reaction-diffusion, also requires delay by its very nature. For instance, diffusion of Bmp/Wnt from the source bead to neighbouring cells requires time [148]. Inside the cell,

Sox9 protein takes time to be expressed, and our observation of Sox9-GFP is effectively followed by GFP expression, maturation and accumulation.

Cells benefit from gradual decreases in plasticity. It has been long known that a fate decision is a dynamic process, as described by Helen Blau, “The differentiated cell, instead of being caught in a groove, appears to require continuous control to prevent it from wandering into another valley.”[149]. As cells slowly integrate new stimuli and inputs, process these inputs, and make decisions, a gradual decrease in plasticity allows them to correct for mistakes and noise. A steep plasticity decrease would not allow enough time to properly employ a control mechanism and to assign itself to a final fate. Moreover, a gradual decrease in plasticity promotes the development of self-organising mechanisms that require noise and dynamicity.

It is striking that the decreasing plasticity measure -illustrating gradual loss of the ability to remodel the spatial pattern of gene expression- corresponds to the decreasing stemness profile. It further highlights the fact that while phenotypic plasticity is compounded by a variety of factors from chromatin remodelling to stochastic gene expression[150], stemness factors provide a good approximation of a cellular state. The close alignment of measured plasticity to stemness factors suggests that reprogramming, stem cell maintenance, and regeneration may all share regulatory elements with plasticity loss. Conversely, this suggests that reprogramming/stem cell maintenance, which traditionally have been analysed underlying molecular mechanisms in cells in isolation, may involve a spatial patterning aspect that has been overlooked.

5.1.3 How can cell density change following molecular patterning?

Now we reconsider another question related to a detailed timing of the molecular patterning. Previously, quantifying Sox9 expression and cell density in limb cryosection concluded that Sox9 digit patterning process happens prior to condensation, and cell movements could be interpreted as a downstream result of molecular patterning.

What could be in charge of the mechanistic link between molecular patterning and mesenchymal condensations? It has been long proposed that canonical Wnt signalling and cadherin-mediated cell adhesion depend on the same pool of cytosolic β -catenin - so β -catenin is considered to be a ‘pivot’ that can switch a cell between adhesion and Wnt signalling [151] (Figure 34). Upon activation of canonical Wnt signalling, the cytosolic β -catenin pool is largely unphosphorylated, and are ‘activated’ to translocate into the nucleus and transcribe downstream targets, potentially depleting the pool for cadherin-bound β -catenin, decreasing cell adhesion, and possibly also decreasing cell density.

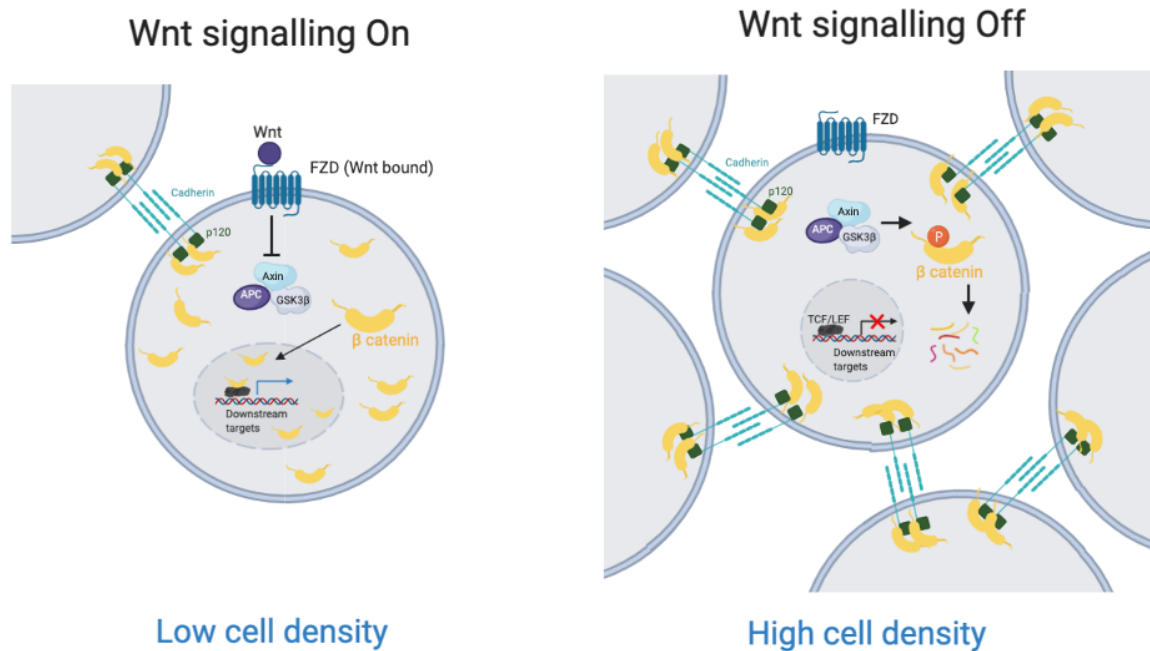


Figure 34. Illustration of Pivot hypothesis. Wnt signalling could decrease cell adhesion and density.

There are some observations that the Wnt signalling and cadherin-mediated cell adhesion depend on the same pool of β -catenin. Pulse-chasing of photoactivatable β -catenin-GFP upon canonical Wnt pathway activation shows that cadherin-bound β -catenin dissociates from adherens junction and accumulates at the perinuclear endocytic recycling compartment (ERC), eventually translocating into the nucleus [152]. Cadherin overexpression experiment on *Drosophila* embryos mimicked the wingless (Wnt) phenotype [153], meaning that increase in cell density could prevent β -catenin mediated Wnt signalling. E-cadherin knockdown in colon cancer cells is known to augment Wnt-mediated, β -catenin-dependent transcription [154].

If the same pool of β -catenin is involved in deciding between low density and high density, visualising subcellular localisation of β -cat can tell whether the pivot hypothesis works or not. However, directly visualising β -catenin signalling/subcellular location has been a challenge in most systems. Although β -catenin localisation in the form of nuclear 'spot' can be detected in *Drosophila* embryos [155], in mouse embryos, β -cat nuclear translocation is not observed even when the canonical Wnt signalling is active [156]. For instance, in mouse colon, cytoplasmic enrichment is detectable, but checking for nuclear translocation requires quantitative tools of colocalization with DAPI with careful threshold tuning with control conditions [156]. More importantly, studies have consistently shown that a very low number of β -catenin molecules are sufficient to activate target gene expression [157], suggesting that visually undetectable levels of nuclear β -catenin can still mean active signalling. High magnification microscopy of β -catenin on mouse embryonic limb was attempted during the course of my PhD, but it did not demonstrate cytoplasmic upregulation nor nuclear localisation (Supplementary Figure 5).

5.2 Unbiased screening of digit patterning pathways

Now I discuss the second part of the study - a non-hypothesis driven, unbiased screening of pathways. The unbiased screening approach I designed for this study is unique in many ways: 1) tissue-level readout(Sox9 pattern) is evaluated 2) Both 2.5D and 3D systems are tested and 3) there is an interplay of modelling and experiments. All of these -18 micromass and 18 limb culture experiments using Wnt modulators- provide new data critical to dissecting the complexity of the digit patterning process, and providing the insight into the mechanism of how Wnt signalling activity represses Sox9.

In the beginning of this study, I have proposed several questions about the mechanism, including which type of Wnt pathway is involved(canonical/non-canonical), which components of Wnt pathways are involved(Wnt ligands/ Wnt receptors/cytosolic components/transcription factors), which specific Wnt ligands are involved(Wnt3a, Wnt5a etc), and which wnt antagonists are involved(Dkk1, Sfrp1, etc).

The study answers all of the initially proposed questions. It is now clear that the canonical pathway and Wnt production step of the Wnt signalling pathways are the most critical to Sox9 digit patterning. In the extracellular environment, Wnt3a and Wnt9a, their target Wnt receptors FZD2/4/5/7/9, are confirmed to be relevant to digit patterning over other ligands, such as Wnt7a and 9a. Sfrp1 and Dkk1 are confirmed to be both effective Wnt antagonists to change digit patterning. Their interacting partners -Wnt&FZD receptors and LRP6 co-receptor respectively- are important targets to generate digit merging phenotypes. In the cytosol, GSK3 β is a candidate that effectively changes digit patterning. Modulating transcriptional role of β -cat, by increasing β -cat nuclear translocation, and inhibiting TCF/CBP - β -cat binding most effectively changed Sox9 digit patterning, with 5 out of 6 modulators in this category.

5.2.1 How does Wnt mediated Sox9 expression work with the rest of the BSW model

Another question proposed is how Wnt repression on Sox9 works in the context of individual molecular interactions(k_2 - k_9) to generate the digit pattern, especially in consideration of the negative feedback from Sox9 to Wnt(k_7). According to the original BSW model, a negative feedback from Sox9 to Wnt(k_7) is required to obtain a Sox9 pattern that is out of phase of Wnt, which is observed from immunostaining. Since Sox9 is a transcription factor and can only act inside the cell[74], the simplest way to generate low Wnt signalling expression in Sox9+ area is that Sox9 promotes a Wnt inhibitor acting in the extracellular environment.

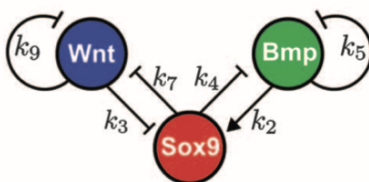


Figure 35. Figure from Raspopovic *et al.*, [28]

Unbiased screening approach from this study(Section 4.1-4.4) successfully identified both sFRP1 and Dkk1 as potential extracellular Wnt inhibitors that effectively change digit patterning upon application. To systematically find out whether both sFRP and Dkk family are involved in digit patterning, rest of the ligands in these families need to be tested for perturbation experiments.

sFRP family of proteins are thought to perform redundant function, because homozygous mutation in *sfrp1* or *sfrp2* has no effect in embryogenesis, but *Sfrp1* and *Sfrp2* double deficiency causes lethality and limb outgrowth defects[158]. *Sfrp2* mediated Wnt signalling downregulation is already known to upregulate Sox9 and promote chondrogenesis. For instance, grafting *Sfrp2* expressing chick embryo fibroblast cells into the interdigit area at E11.5 shows that the grafted area induced expression of *Col2a1*[159]. Interestingly, despite overlapping functions, the expression patterns of *Sfrp1,2* and *3* are quite distinct[160]. Despite *Sfrp1* generating digit merging phenotypes in limb culture, *Sfrp1* is not detected in mesenchyme at E11.5. *Sfrp2* is detected throughout mesenchyme at E11.5. At E11.5, sFRP3 is detected throughout mesenchyme, concentrated towards the distal end[142]. Similarly, despite the overlapping function of *Dkk1* and *Dkk2*[161], the expression patterns of *Dkk1,2* and *3* are different, with *Dkk1* expressed in ectoderm, *Dkk2* expressed interdigitally, and *Dkk3* in joint cells and periarticular perichondrium at E13.5[142].

While their roles as Wnt regulators and downstream actions are extensively studied, how sFRP and Dkk families are regulated in limb mesenchyme remains unclear. While Sox9 itself is a transcription factor, it has not been found yet evidence of its direct regulation upon sFRP and Dkk transcription. CpG hypermethylation is another way many Wnt antagonists - sFRPs DKK1 and also Wif1- are known to be regulated[162], but Sox9 contribution has not been documented. Heparin and heparan sulphate are mammalian glycosaminoglycans that regulate the activities of sFRP1 as well as Wnt proteins by binding them through ionic interactions[163]. Lowering tissue heparan sulphate polyglycan levels has been shown to impair Wnt signalling *in vivo*[164].

To further substantiate the hypothesis that Sox9 promotes a Wnt inhibitor acting in the extracellular environment, alternative ligands such as the WIF family should be screened. Out of Wnt family proteins, Wif1 was previously identified to have different Sox9 expression between positive and negative cells[28], and working in a similar manner to sFRP proteins, by binding to Wnt ligands.

One of the mathematical requirements for the original BSW model was that extracellular or/and diffusible Wnt components are liable for Sox9 mediated Wnt repression. This assumption comes from the mathematical requirement for Turing patterning that the feedback from Sox9 to Wnt has to be extracellular - in other words, this feedback has to impact the diffusing signal.

On the other hand, my results(section 4.4) clearly show that inhibiting cytoplasmic and nuclear cell-autonomous components of the Wnt canonical pathway changes Sox9 patterns. In fact, inhibiting the Wnt transcriptional component most effectively modifies the Sox9 pattern in all 6 experiments performed. 8 out of 12 experiments using cytoplasmic Wnt pathway inhibitors/activators changed digit patterning.

Such finding is critical because it expands our previous understanding of the BSW model that cell-autonomously mediated Wnt signalling is not mathematically required for

generating Turing based digit patterns. Although not required, inhibiting cell-autonomous Wnt components still change the digit patterning, and this suggests that the intracellular pathway disruption might also inhibit the cell's ability to sense extracellular signals. Another interpretation is that some downstream components of β -catenin mediated transcription can impact the diffusible component of Wnt pathways. For instance, DKKs are already known to be downstream targets of Wnt/ β -catenin signalling [165]. It should be further dissected whether this self negative feedback mechanism on the Wnt signalling is relevant to the digit patterning. My results do not exclude the scenario of Sox9 inhibition of Wnt signalling by physical binding on β -catenin [166], but the role of such cell-autonomous mechanism would be unclear, as its impact on the diffusible part of Wnt signalling is not known.

5.2.2 Limitations of the study

5.2.2.1 Addressing conflicting results

There are two types of conflicting results observed in the experiments: the mismatch between the micromass and limb culture experiment (Table 6), and the mismatch between the experiment and computer model simulations (Table 10). There are 4 small molecules/ligands/peptides (Wnt3a, SB216763, hsBCL9CT-24, Dkk1) in which the micromass pattern has changed but limb pattern has not been impacted, and 1 case (IWP2) in which the limb pattern showed Sox9 pattern difference but not in the micromass (Table 6).

The difference in the setup of limb culture and micromass system largely contributes to the mismatches in their experimental outcomes. The major difference between the two can be summarised as: 1) removal of ectoderm in micromass 2) direct contact of Wnt modulators with mesenchymal cells in micromass, and 3) resuspension and reorganisation of cells before the seeding process in micromass. Out of these factors, I propose that the presence of an ectoderm in the limb culture poses a barrier from generating pattern change with the following externally applied ligands (Wnt3a, Wnt5a, Wnt7a, Dkk1, Way316606, SB216763, hsBCL9CT-24, 1,4 Dibenzoyl piperazines). Conversely, the absence of ectoderm could have resulted in some modulators (Wnt3a, SB216763, hsBCL9CT-24, Dkk1) to selectively work only in the micromass system. I suggest that ectoderm, already consisting of the embryonic basal layer, intermediate layer, and periderm (a layer of tightly adhered cells overlying the ectoderm) [167] during the digit patterning stage, works as a physical barrier.

In micromass, 7 modulators show the opposite experimental result relative to the simulation (Wnt7a, Wntc59, XAV939, iCRT14, PRI724, Calphostin C, hsBCL9CT-24), and 4 does not result in any experimental change (IWP2, Wnt5a, Way316606, 1,4 Dibenzoyl piperazines). In the limb culture, 3 Wnt modulators result in opposite experimental results compared to simulation (Wnt9a, CHIR99021, iCRT14). There are 8 cases in which limb culture did not result in any phenotype changes (Wnt3a, Wnt5a, Wnt7a, Dkk1, Way316606, SB216763, hsBCL9CT-24, 1,4 Dibenzoyl piperazines) (Table 10).

There might be several reasons why there are conflicting results between the experiment and the simulation. First, a Wnt modulator can both activate and deactivate the Wnt pathway. For instance, a Wnt ligand could behave as a Wnt inhibitor specifically in the mouse limb, depending on the presence of specific receptors and coreceptors, although they have not been identified. It has already been shown that in primary human articular chondrocytes, either activation or inhibition of the Wnt/ β -catenin pathway resulted in loss of

cartilage [168]. At low concentrations, Wnt3a can activate Wnt/Ca²⁺ signalling, while high concentrations of Wnt3a activate Wnt/ β -catenin signalling [169], eventually targeting different downstream genes. This concentration dependency also applies to sFRP. At lower concentrations, sFRP is known to enhance long range diffusion of Wnt by increasing Wnt solubility and aiding diffusion, while at high concentrations they sequester Wnt proteins [170].

Another reason behind the conflicting results could be that my adaptation of the BSW model does not accommodate certain experimental outcomes. For instance, to introduce Wnt inhibitors in micromass, I put an inhibitor term onto the partial differential equation that governs Wnt signalling strength in relation to Bmp and Sox9. This method might not correspond to the molecular mechanism. To more accurately model inhibitor actions, it might be required to separately address mesenchymal/ectodermal Wnt signalling, or incorporate quantitative, time-coursed expression pattern of a diffusible Wnt component.

Another possibility is that the current version of the BSW model does not fully address complex aspects of Wnt signalling. Originally, the aim was to build the simplest dynamical model that is compatible with the *in situ*, microarray and immunostaining data, and so far a model with three state variables (Bmp, Sox9, Wnt) was used to make predictions. While it is not my goal to incorporate every known molecular state of the system, it might be necessary to parameterise certain aspects of the Wnt signalling system, for instance, diffusibility change upon inhibitor application such as sFRPs.

Another reason might lie in difficulties of disrupting already strongly established regulatory networks or feedback loop characteristic of the limb tissue. For instance, throughout the limb development, ectodermal FgfR2b receptor, Wnt/ β -cat signalling, and mesodermal Fgf10 constantly feedback [171]. Fgf10 can bind the Fgfr2b receptor in the ectoderm, whose activation results in active Wnt/ β -cat signalling in the AER. This results in activation of ectodermal Fgf8, feeding back into mesodermal Fgf10 and finishing the loop. In case of ligands Wnt3a/7a, even though they could effectively upregulate Wnt signalling in the ectoderm, strong feedback loop might prevent delivering the effect on the mesenchyme. This also promotes the need in our model to incorporate feedback loops that are relevant to limb growth and relate it to our digit patterning. Once we have an idea of how ectodermal Wnt signal is transduced to mesenchyme, a model testing this might be incorporated into the digit patterning, potentially separating the Wnt signalling and its strength in the ectodermal and mesenchymal parts. This discussion will be continued in the next section 5.2.4.

5.2.2.2. Validation of experimental results

To further validate the experimental results, there are many factors to be considered including the concentration of the applied modulators, biological replicates, molecular evidence of Wnt modulation and off-target effects.

All micromass and limb culture results are tested at 3-8 different concentrations of a modulator (Supplementary Figure 1), demonstrating a grade of response upon different dosage. About half of the micromass experiments have two biological replicates, and the rest is performed once. About half of the limb culture experiments were repeated, providing biological replicates. The exact number of repeats per each modulator and experiment is listed on the Supplementary Figure 1.

The range of concentration for each experiment was determined from literature which suggests *in vivo* or *in vitro* use of each small molecule/ligands/peptide. For some of the

experiments, the applied range was wide enough to demonstrate impact on the patterning at the low-moderate level, and toxicity to the cells/tissue at a higher level. Some do not show any patterning change until the modulators reach the toxic level, and some still need to be tested for higher concentration of modulators(Table 15).

Examining the molecular response would be particularly useful to address contradicting experimental results from the simulation. For a few micromass experiments, immunostaining using antibodies against active β -cat was performed in order to find whether Wnt signalling activity is actually altered in the micromass(Supplementary Figure 3, Table 15). Active β -cat immunostaining experiments need to be performed on the rest of the micromass in order to confirm the molecular impact of the modulator. For the limb culture experiments, the process of separating the limbs from the mesh following a 48hrs culture(Materials and Methods) followed by cryosectioning have damaged most of the limbs. So far, I have confirmed that micromass experiments with PRI724 and Calphostin C leads to downregulation in Wnt signalling, showing that loss of pattern coming from these Wnt inhibitors are due to Wnt downregulation, despite their conflicting experimental result from the simulation. The result suggests that Wnt downregulation genuinely results in loss of Sox9 condensating pattern.

While most Wnt modulators used in this study do not have clear off target effects(Table 15), some Wnt inhibitors such as Calphostin C have a low IC50 value of 317nM against Protein kinase C. Since Calphostin C generates a unique phenotype of increased periodicity of digits, this phenotype could be possibly an influence of lower PKC activities. IWP2 activates casein kinase, with higher IC50 value compared to its action against porcupine but still in the nM range. Still, it is difficult to predict how PKC and casein kinase activity alter Wnt signalling or their direct impact on digit patterning.

Type	Type of exp	Modulator	# of experiments	# of biological replicates	Wide concentration range tried	Active β -cat immunostaining	Documented off-target effects
Contradicting simulation	Micromass	Wnt7a	1	1	-	-	-
		Wntc59	2	2	✓	-	-
		XAV939	2	2	✓	-	-
		iCRT14	1	1	-	-	-
		PRI724	1	1	✓	✓	-
		Calphostin C	2	2	✓	-	Protein Kinase C inhibitor, IC50 = 317nM[139]

		hsBCL9CT-24	1	1	✓	-	-
No pattern change		IWP2	1	1	-	-	CK1δ(casein kinase - Se/Th selective), IC50 = 317nM [172]
		Wnt5a	1	1	-	-	-
		Way316606	2	2	-	-	-
		1,4 Dibenzoyl piperazines	1	1	-	-	βcat-Ecadherin interaction. IC50=510μM [126]
Contradicting simulation	Limb Culture	Wnt9a	1	2	-	-	-
		CHIR99021	3	2-3	✓	-	-
iCRT14		1	2-3	✓	-	-	
No pattern change		Wnt3a	3	3-4	✓	-	-
		Wnt5a	1	2	-	-	-
		Wnt7a	1	1	-	-	-
		Dkk1	1	2-3	-	-	Localises to adhesion complex, mediate cell-cell interaction [173]
		Way316606	1	2-3	✓	-	-
		SB216763	1-2	1-2	✓	-	Promotes pluripotency in mouse ESC [174]
	hsBCL9CT-24	4	4	✓	-	-	
1,4 Dibenzoyl piperazines	2	2	✓	-	-		

Table 15. Actions required to further validate the experimental results.

5.2.3 How is ectodermal signal transduced to mesenchyme?

Despite the advances made in this thesis, there is still rather a big mystery. Some Wnt ligands with the most evidence in favour of their involvement in digit patterning (in particular *Wnt3a*), are not expressed in the mesenchyme - only the ectoderm (Section 4.7). And yet the Turing model only works if their signalling activity is regulated in the mesenchyme.

Understanding the nature of ectodermal-mesenchymal interaction will reveal the functional mechanism of various Wnt components that are specifically expressed in the ectoderm, including *Wnt3a/9a* ligands and Wnt antagonist *Dkk1*. Partial ectoderm removal experiments demonstrated two different digit perturbation phenotypes: first, increased Sox9 expression immediately surrounding the removed ectoderm, and second, spreading or blurring of digits. The result is time dependent - the global impact of digit blurring happens exclusively to the limbs that are interrupted before or during the digit forming stage. When the removal is performed post digit patterning stage Sox9 upregulation is only observed in the mesenchymal cells adjacent to the removed ectoderm.

The results generally align with our current digit patterning model in the sense that a loss of Wnt/ β -catenin signalling pathways leads to increase in Sox9. Spreading, blurring or distal enlargement of digits following partial ectoderm removal resembles that of a Wnt signalling inhibited limbs (Figure 32). However, the limited Sox9 upregulation post digit patterning stage indicates that ectodermal Wnt signalling facilitated through the mesenchyme is less critical to digit patterning.

Studies in related systems, such as in embryonic mouse heads, reveal that cranial ectodermal Wnts are an initiating factor for mesenchymal Wnt ligand expression [175]. Early ectoderm specific conditional Wntless knockout mice abolished mesenchymal expression of Wnt ligands mRNA transcript, including *Wnt5a*, *Wnt11*, and *Wnt16* [175]. Early conditional deletion of cranial mesenchyme β -catenin also resulted in an absence of *Wnt5a* and *Wnt11* expression, suggesting that phenotype of ectodermal Wnt conditional knockout is equivalent to that of a mesenchymal loss of Wnt/ β -catenin signalling. On the other hand, mesenchyme specific Wntless knockout mice retained wild type expression patterns of multiple Wnt ligands such as *Wnt5a*, *Wnt11*, and *Wnt4* [175]. The study suggests that ectodermal, not mesenchymal Wnt signal, is necessary for correct mesenchymal Wnt ligand expression pattern, and ectodermal Wnts act as initiating factors. Although the precise mechanism is not known, the study proposes that two sources of Wnt ligands perform distinct functions - ectodermal wnt triggering mesenchymal wnt expression, and mesenchymal wnts required in later stages for osteoblast differentiation.

Interestingly, the phenotype of early surface ectoderm conditional Wntless knockout [175] replicates my partial ectoderm experimental result, in which Sox9 expression is enhanced right beneath the surface ectoderm (Figure 31). This observation suggests that in mouse embryonic limb, like in mouse embryonic head, ectodermal Wnts might be responsible for inducing mesenchymal Wnt expression.

6. Outlook

In the first part of this thesis, I show that plasticity during digit patterning smoothly decreases in a sigmoidal manner, by quantification of experimental data, followed by modelling based on the result and confirmation of experimental findings by simulation. Then with other members of the lab, I identify gene candidates with a similarly decreasing profile in their transcriptome expression over time.

It would be interesting to extend this analysis pipeline to other developmental processes. It would be particularly interesting to compare levels of plasticity decrease between different processes. To do that, the precise dimension of the perturbations, and some steps in the quantification pipeline such as binarization at different thresholds, should be normalised across these processes. The plasticity measure featured in this thesis intrinsically has no units, because it is based on calculating the minimum difference between the control and perturbed networks (it is a normalised score from 1.0 to 0.0 in which 1.0 represents the maximum observed degree of plasticity, and 0.0 represents a complete absence of plasticity). If these challenges could be overcome, it would be possible to find out a certain developmental process, or organogenesis that is more plastic than the others despite happening around a similar biological timeframe. So far, we have discussed that gradual plasticity decrease is advantageous to correct for error, but it would be meaningful to investigate whether there is any organogenesis or developmental process that demonstrates steeper plasticity decay.

Current molecular understandings of digit patterning formation should be eventually coupled with growth and tissue movements. Indeed, this is especially relevant in the latter stages of limb development where tissue structures begin to differentiate (e.g., to bone/cartilaginous tissue); changes to material properties would strongly affect tissue morphology and cell movement, and therefore subsequent patterning. Understanding if and how signalling pathways/molecular patterning impact cell movements and tissue organisation will significantly help achieving a complete organogenesis model of limb development. As previously addressed, there are many ideas regarding the role of Wnt signalling pathway roles in cell movements, including the pivot hypothesis. To further elucidate the mechanistic role of β -catenin and to relate it to the ectodermal-mesenchymal interaction, I have discussed that a clear global and high resolution readout of active β -catenin time course should be obtained, and possibly those without certain ectodermal or mesenchymal Wnt components.

Further extending our existing in-silico experiments, I would be able to incorporate various signalling pathway component expression and activity patterns into the existing BSW model, and suggest a model that explains the remaining questions from this study such as the mechanism of ectodermal-mesenchymal interaction. An initial approach could be to extend or modify our existing gene regulatory network model piece-by-piece, starting from the simplest possible extensions to the wnt-related pathways in the model. For example, the existing BSW network incorporates only a single globally-expressed (non-specific) Wnt. Further data driven modelling - in which the expression/activity patterns of specific wnt-related signalling pathways are mapped to predict underlying regulatory mechanisms or gene regulatory networks - would ideally allow us to model both a specific (as opposed to generic) mesenchymal Wnt as well as a separate ectodermal Wnt. Then multiple versions of these extended networks could be simulated to find the best phenotypes that describe the

wild type digit pattern or the perturbed phenotype. This way, hypothetical interactions between the ectodermal and mesenchymal components can be tested with LimbNET. Eventually, I aim to fully integrate the experimental results from this study into dynamic simulations of the gene regulatory circuits, and to further relate cellular proliferation and tissue movements.

7. Materials and Methods

Animals

Embryos were harvested from Sox9-eGFP pregnant female mice, at different gestation stages in between E10:16-E12:15. Sox9-eGFP mouse has a knock-in mutation in which IRES-EGFP has been inserted into the 3'UTR of the Sox9 locus. All procedures in this study have been approved by EMBL Institutional Animal Care and Use Committee (IACUC). All mice were kept in the PRBB Animal Facility, which is accredited by the International Association for Assessment and Accreditation of Laboratory Animal Care (AAALAC).

Limb Bud Cultures

Limb buds were dissected from Sox9-EGFP embryos in PBS 1x, and transferred onto PET membrane inserts (1.0µm pore size) (Falcon) located in a 6-well plate. Each well was filled with 1.5ml DMEM/F12 (1X) L-Glu medium(Gibco) (with 10% FCS, 5% Penicillin-Streptomycin), letting the bottom side of the PET membrane touch top of the medium, allowing air-liquid interface.

Bead Implantations

Affigel blue beads (Bio Rad) were incubated for 1h at RT in a 5µl of dissolved protein. Recombinant Human/Mouse/Rat BMP-2 protein(R&D systems) was used at 100µg/ml and recombinant mouse Wnt-3a protein(R&D systems) were used at 40µg/ml. Control beads were incubated in 5µl of PBS. Beads were manually implanted in dissected Sox9-EGFP limb buds using tweezers.

Limb bud culture image acquisition

Limb culture imaging and time-lapses were done in Zeiss Cell Observer HS, with 5x objective NA 0.3, with CCD AxioCam camera. Timelapses were done at 37 °C in a CO₂ chamber with 5% CO₂, and pictures were taken every five minutes. Both brightfield and GFP images were taken, with GFP excitation at 488nm.

Digit patterning quantification

Both control and experimental microscopy images were first binarized at different GFP intensity thresholds at around 25 different intensity thresholds. The binarized images were then skeletonised using the "Skeletonize 2D/3D" Fiji plugin. All the skeletonised images were then overlaid, smoothed 6 times, and gaussian blurred 5 times with sigma value of 7. The blurred image was then re-skeletonised using the "Skeletonize 2D/3D" Fiji plugin, generating the final representative topology of the digit patterning.

Wild type digit patterning simulation

LimbNET describes limb tissue as a collection of triangular meshes. For each developmental time point from E10.5 to E12.5, limb tissue filled with triangular meshes are generated, Each mesh is deformed into meshes in the next timepoint with a velocity vector field derived from experimental clonal data, that recapitulates the tissue movements underlying the normal limb outgrowth. LimbNET solves the following reaction-diffusion Partial Differential Equations (PDEs) of the Bmp-Sox9-Wnt model. Fgf8 and Hoxd13 are fixed values, and are introduced to limit the reaction-diffusion model to the autopod. d is introduced to take account of the diffusion differences between Bmp and Wnt.

Reaction	Diffusion
$\frac{dSox9}{dt} = (k2(Bmp - Bmp_0) - k3(Wnt - Wnt_0) - (Sox9 - Sox9_0)^3)$	0
$\frac{dBmp}{dt} = -((k4 - 2.50 * fgf8 * hoxd13) * (Sox9 - Sox9_0)) - k5(Bmp - Bmp_0)$	$\gamma * d$
$\frac{dWnt}{dt} = -((k7 + 1.25 * fgf8 * hoxd13) * (Sox9 - Sox9_0)) - k9(Wnt - Wnt_0)$	γ

Variable	Value
$k2$	0.5
$k3$	0.5
$k4$	7
$k5$	0.1
$k7$	0.45
$k9$	0.1
γ	500
d	10

h_0	10
p_0	10
q_0	10

To account for delayed GFP expression in Sox9-GFP mouse line, GFP is separately expressed with its own expression and degradation values.

$$\frac{dGFP}{dt} = P_{GFP} * (Sox9 - Sox9_0) - D_{GFP} * GFP$$

Variable	Value
P_{GFP}	0.001
D_{GFP}	0.001

Simulation of bead insertion experiments

The position of the bead in the models can be defined from the bead editor function of LimbNET. The trajectory of the bead was automatically determined by the predefined mesh movements. The bead can be inserted at the desired timepoints, meaning that bead insertion throughout different developmental timepoints could be simulated.

Bead editor | mouse limb coarse | Background (optional) | CLEAR ALL | SAVE PATTERN

Pattern name
E11.08 Bmp Bead

1. Bead trajectory

Point selected at 17520 (E12:04)

GO TO TIME | CLEAR SELECTION

2. Restrict bead time range

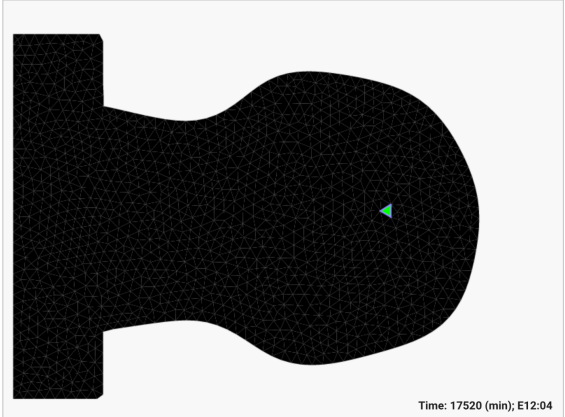
From 14960 (E10:09) to 17760 (E12:08)

NOW | NOW

3. Paint bead

FILL SELECTED

Fill



Time: 17520 (min); E12:04

Then the designated bead was imported as an independent predefined pattern (BMP pattern, Wnt pattern). Each beads were given their production and degradation values.

$$\frac{dBMPbead}{dt} = P_{BMPbead} * (BMPpattern) - D_{BMPbead} * BMPbead$$

$$\frac{dWNTbead}{dt} = P_{WNTbead} * (WNTpattern) - D_{WNTbead} * WNTbead$$

Variable	Value
$P_{BMPbead}$	50
$P_{WNTbead}$	50
$D_{BMPbead}$	0,1
$D_{WNTbead}$	0,1

Wnt and Bmp productions from the beads are integrated to the reaction equations.

Reaction
$\frac{dSox9}{dt} = (k2((Bmp + Bmpbead) - Bmp_0) - k3((Wnt + Wntbead) - Wnt_0) - (Sox9 - Sox9_0)^3)$
$\frac{dBmp}{dt} = - ((k4 - 2.50 * fgf8 * hoxd13) * (Sox9 - Sox9_0)) - k5((Bmp + Bmpbead) - Bmp_0)$
$\frac{dWnt}{dt} = - ((k7 + 1.25 * fgf8 * hoxd13) * (Sox9 - Sox9_0)) - k9((Wnt + Wntbead) - Wnt_0)$

Changing plasticity

In the original BSW model, plasticity is set to 1, or the maximum level. We introduce plasticity as a variable that controls the degree to which any molecular component of the model can change, scaling both reaction and diffusion. Plasticity is multiplied to all the reaction equations and diffusion values, and can vary from zero to one.

Reaction	Diffusion
$\frac{dSox9}{dt} = plas * (k2(Bmp - Bmp_0) - k3(Wnt - Wnt_0) - (Sox9 - Sox9_0)^3)$	0

$\frac{dBmp}{dt} = plas * (- (k4 - 2.50 * fgf8 * hoxd13) * (Sox9 - Sox9_0)) - k5(Bmp - Bmp_0)$	plas*γ*d
$\frac{dWnt}{dt} = plas * (- (k7 + 1.25 * fgf8 * hoxd13) * (Sox9 - Sox9_0)) - k9(Wnt - Wnt_0)$	plas*γ

Turing spot model simulation

The Turing spot model proposes that the initial brief Turing moment to generate Sox9 spots is followed by complete stop in reaction-diffusion. Subsequent digit formation depends on growth mediated elongation of the digit organising centre. Here we defined plasticity to reach zero immediately after a certain time point, which is t_{plas_start} .

$$plas = \max(0, 1 - (t > t_{plas_start}))$$

“Data fit” model simulation

We fitted all quantified plasticity data to a sigmoidal decay function. We used `scipy.optimize.curve_fit` function to the following equation :

$$plas = \frac{e^{-\mu(t-k)}}{1+e^{-\mu(t-k)}}$$

The fitting gives the following values. k is the x value(time value) of the sigmoid’s midpoint. In other words, the plasticity reaches half when the developmental time is Day 11, 12 hours and 50 minutes. μ describes the steepness of the curve.

variable	value
μ	$4.69 * 10^3$
k	16610 (=E11:12:50)

The above equation is then implemented into LimbNET.

“Optimised Data fit” model simulation

We generated an ‘optimised data fit’ model that decays faster and has lower values of plasticity after E11:12:50. We came up with an asymmetric Hill decay function where we can modulate the time that the plasticity reaches 0 (t_{cut} and k), the steepness of the curve (m and k), and the plasticity level when $t=E11:12:50$ (n). The following set of parameters represent

the graph in Figure 6A. Supplementary information explores different variables and finds the curve that is comparable to the ‘data fit’ model.

$$plas = \left(\frac{(t_{cut} - \min(x, t_{cut}))^m}{k^m + (t_{cut} - \min(x, t_{cut}))^m} \right)^n$$

variable	value
t_{cut}	17410
k	800
m	4.5
n	1

“Steeper” model simulation

Steeper model is also generated from the optimised data fit equation. The steeper model gives slower plasticity decay before E11:12:50 and faster decay after E11:12:50.

variable	value
t_{cut}	17410
k	800
m	16
n	1

Micromass culture

At E11.5, mouse embryonic limb bud autopods are dissected in PBS 1x. The dissected limbs are left with 0.5% Trypsin-EDTA for 4min at RT. Limbs are then moved to RT PBS 1x. Forceps are used to manually remove the ectoderm that surrounds the ectoderm. The mesenchymal tissue is then dissociated by pipetting. The number of cells in the unit mL is measured, and the cell suspension is diluted to 2×10^7 cells/mL, in DMEM/F12 (1X) L-Glu medium(Gibco) (with 10% FCS, 5% Penicillin- Streptomycin). The cell suspension is cultured as 10 μ l drops in 8-well plates(Ibidi). After 1h of incubation at 37°C and 5% CO₂, 250 μ l of DMEM/F12 (1X) L-Glu medium(Gibco) is added from the corner of each well, slowly, to prevent disruption of the cells attached on the bottom.

Immunohistochemistry

For wild type limbs, Sox9-EGFP limbs at different stages were fixed in 4% PFA for 1h. If the limbs are harvested following limb culture, the limbs are detached from the mesh using forceps and transferred to PFA to be fixed. PFA is washed with 1x PBS, 3 times, 5 min each. Following the washing, limbs are then incubated in 30% sucrose/PBS overnight at 4°C. Limbs are taken out and embedded in tissue-tek OCT (Sakura). The OCT block is submerged in 2-methylbutane held by a small metal container, which is put on a dry ice for quick freezing. OCT blocks stored at -80°C or immediately cryosectioned. During the transport the blocks should be placed in dry ice.

Cryosections were cut coronally at 14µm. Sections were permeabilized in 10% FBS, 0.3% Tx, 0.5% milk, 0.3M glycine in PBS, for 1-2h at RT in a wet chamber. Before primary antibody application, a blocking solution composed of 0,1% Triton X PBS 1x solution - 1% BSA, 5% DMSO, 2.5% Donkey serum, 2.5% FBS or Goat serum , 1% Gelatin from fish skin, and 0,1% Sodium Azide are used for 1-2h at RT in a wet chamber. Primary antibody incubation was done in a wet chamber in the above blocking solution overnight at 4°C. Secondary antibodies incubation was done in 10% FBS, 0.1% BSA in PBS 2h, RT in dark in a wet chamber. Slides were mounted in VectaShield. Primary antibodies used are : anti Sox9 AB5535 Sigma-Aldrich (1:300) and anti-active β -catenin clone 8E7 (Millipore) antibody (1:100). Secondary antibody used are Alexa Fluor 486 Anti-donkey(1:250) and Alexa fluor-568 anti-Rb (1:250). For supplementary figure 5, tyramide conjugation system (Tyramide superbust kit, Thermofisher, B40915) was used for secondary antibody, with the tyramide incubation time of 11min.

Micromass / immunohistochemistry Image acquisition

Images taken with Leica TCS SP5 with an HCX PL APO CS 10x air objective, NA 0.4 on the centre of the culture. Excitation at 488nm were provided by Argon laser. The same confocal microscope was used for imaging immunohistochemistry results on immunostained micromass(Supplementary Figure 3) and cryosectioned mouse limb(Supplementary Figure 5). For the latter, Plan Apo Oil 63x (1.4 NA Blue) is used to obtain higher magnification images. Effective 100x image was obtained by enlargement of 63x images without sacrificing the resolution, using LASX.

Simulating Wild Type micromass

Using LimbNET, micromass is modelled in a fixed size square mesh, instead of a limb-shaped mesh that grows over time. Identical reaction-diffusion BSW model is simulated - the only difference is introduction λ , which scales all the reaction equations. To effectively simulate micromass, λ value is given as 1.3. GFP expression equation is omitted as the speed of pattern formation in micromass is less delayed.

Reaction	Diffusion
$\frac{dSox9}{dt} = \lambda(k2(Bmp - Bmp_0) - k3(Wnt - Wnt_0) - (Sox9 - Sox9_0)^3)$	0
$\frac{dBmp}{dt} = \lambda(-(k4 - 2.50 * fgf8 * hoxd13) * (Sox9 - Sox9_0)) - k5(Bmp - Bmp_0)$	$\gamma * d$
$\frac{dWnt}{dt} = \lambda(-(k7 + 1.25 * fgf8 * hoxd13) * (Sox9 - Sox9_0)) - k9(Wnt - Wnt_0)$	γ

Variable	Value
k_2	0,5
k_3	0,5
k_4	7
k_5	0,1
k_7	0,45
k_9	0,1
γ	300
d	10
λ	1,3
h_0	10
p_0	10
q_0	10

Simulating Wnt activation/ inhibition in micromass

Wnt activation is achieved by inserting a Wnt activator term(WA) as a production term in the differential equation defining the Wnt reaction. WA can be introduced to the micromass during the duration of t_{WA} , which is defined by t_{WA_start} and t_{WA_end} . t_{WA_start} is set equal to the biological age of when the mice mesenchymal cells are harvested - around E11:11.

Reaction	Diffusion
$\frac{dSox9}{dt} = \lambda(k2(Bmp - Bmp_0) - k3(Wnt - Wnt_0) - (Sox9 - Sox9_0)^3)$	0
$\frac{dBmp}{dt} = \lambda(-(k4 - 2.50 * fgf8 * hoxd13) * (Sox9 - Sox9_0)) - k5(Bmp - Bmp_0)$	$\gamma * d$
$\frac{dWnt}{dt} = \lambda(WA * t_{WA} - (k7 + 1.25 * fgf8 * hoxd13) * (Sox9 - Sox9_0)) - k9(Wnt - Wnt_0)$	γ

$$t_{WA} = (t > t_{WA_start}) * (t < t_{WA_end})$$

Variable	Value
k_2	0,5
k_3	0,5
k_4	7
k_5	0,1
k_7	0,45
k_9	0,1
γ	300
d	10
λ	1,3
h_0	10
p_0	10
q_0	10
WA	0,8
t_{WA_start}	16500 (=E11:11)
t_{WA_end}	17760 (=E12:08)

The principle of Wnt inhibition simulation is identical, except a minor difference in the equation in which the sign of the Wnt inhibitor(WI) term is negative, as the production of WI gives negative impact to the overall activity of Wnt signalling. All values of the variables are identical.

Reaction	Diffusion
$\frac{dSox9}{dt} = \lambda(k2(Bmp - Bmp_0) - k3(Wnt - Wnt_0) - (Sox9 - Sox9_0)^3)$	0
$\frac{dBmp}{dt} = \lambda(-(k4 - 2.50 * fgf8 * hoxd13) * (Sox9 - Sox9_0)) - k5(Bmp - Bmp_0))$	$\gamma*d$
$\frac{dWnt}{dt} = \lambda(- WI * t_{WI} - (k7 + 1.25 * fgf8 * hoxd13) * (Sox9 - Sox9_0)) - k9(Wnt - Wnt_0))$	γ

$$t_{WI} = (t > t_{WI_start}) * (t < t_{WI_end})$$

Simulating distal digit widening phenotype

Distal digit widening is a phenotype from Wnt inhibition. Parameters listed below.

Reaction	Diffusion
$\frac{dSox9}{dt} = \lambda(k2(Bmp - Bmp_0) - k3(Wnt - Wnt_0) - (Sox9 - Sox9_0)^3)$	0
$\frac{dBmp}{dt} = \lambda(-(k4 - 2.50 * fgf8 * hoxd13) * (Sox9 - Sox9_0)) - k5(Bmp - Bmp_0))$	$\gamma*d$
$\frac{dWnt}{dt} = \lambda(- WI * t_{WI} - (k7 + 1.25 * fgf8 * hoxd13) * (Sox9 - Sox9_0)) - k9(Wnt - Wnt_0))$	γ

$$t_{WI} = (t > t_{WI_start}) * (t < t_{WI_end})$$

Variable	Default value (+, Figure 29)	++ (Figure 29)	+++ (Figure 29)	Inhibition starting point t=15720 (Figure 29)
<i>k2</i>	0.5	0.5	0.5	0.5
<i>k3</i>	0.5	0.5	0.5	0.5
<i>k4</i>	7	7	7	7
<i>k5</i>	0.1	0.1	0.1	0.1
<i>k7</i>	0.45	0.45	0.45	0.45
<i>k9</i>	0.1	0.1	0.1	0.1
γ	500	500	500	500
<i>d</i>	10	10	10	10
λ	1	1	1	1
<i>h0</i>	10	10	10	10
<i>p0</i>	10	10	10	10
<i>q0</i>	10	10	10	10
WI	0,9	2,1	3	0,9
t_WI_start	16500 (=E11:11)	16500 (=E11:11)	16500 (=E11:11)	15720 (=E10:22)
t_WI_end	17760 (=E12:08)	17760 (=E12:08)	17760 (=E12:08)	17760 (=E12:08)

Simulating webbing phenotype

Webbing is a phenotype from Wnt inhibition. Parameters listed below.

Reaction	Diffusion
$\frac{dSox9}{dt} = \lambda(k2(Bmp - Bmp_0) - k3(Wnt - Wnt_0) - (Sox9 - Sox9_0)^3)$	0
$\frac{dBmp}{dt} = \lambda(- (k4 - 2.50 * fgf8 * hoxd13) * (Sox9 - Sox9_0)) - k5(Bmp - Bmp_0)$	$\gamma*d$
$\frac{dWnt}{dt} = \lambda(- WI * t_{WI} - (k7 + 1.25 * fgf8 * hoxd13) * (Sox9 - Sox9_0)) - k9(Wnt - Wnt_0)$	Υ

$$t_{WI} = (t > t_{WI_start}) * (t < t_{WI_end})$$

Variable	Default value (+, Figure 29)	++ (Figure 29)	+++ (Figure 29)	Inhibition starting point t=15720 (Figure 29)
<i>k2</i>	0.5	0.5	0.5	0.5
<i>k3</i>	0.5	0.5	0.5	0.5
<i>k4</i>	7	7	7	7
<i>k5</i>	0.1	0.1	0.1	0.1
<i>k7</i>	0.45	0.45	0.45	0.45
<i>k9</i>	0.1	0.1	0.1	0.1
γ	500	500	500	500

d	10	10	10	10
λ	1	1	1	1
h_0	10	10	10	10
p_0	10	10	10	10
q_0	10	10	10	10
WI	2	2,4	3,5	2
t_WI_start	16500 (=E11:11)	16500 (=E11:11)	16500 (=E11:11)	15720 (=E10:22)
t_WI_end	17760 (=E12:08)	17760 (=E12:08)	17760 (=E12:08)	17760 (=E12:08)

Simulating peripheral digit loss phenotype

Peripheral digit loss is a phenotype from Wnt inhibition. Parameters listed below.

Reaction	Diffusion
$\frac{dSox9}{dt} = \lambda(k_2(Bmp - Bmp_0) - k_3(Wnt - Wnt_0) - (Sox9 - Sox9_0)^3)$	0
$\frac{dBmp}{dt} = \lambda(-(k_4 - 2.50 * fgf8 * hoxd13) * (Sox9 - Sox9_0) - k_5(Bmp - Bmp_0))$	$\gamma * d$
$\frac{dWnt}{dt} = \lambda(-WI * t_{WI} - (k_7 + 1.25 * fgf8 * hoxd13) * (Sox9 - Sox9_0) - k_9(Wnt - Wnt_0))$	γ

$$t_{WI} = (t > t_{WI_start}) * (t < t_{WI_end})$$

Variable	Default value (+, Figure 29)	++ (Figure 29)	+++ (Figure 29)	Inhibition starting point t=15720 (Figure 29)
<i>k2</i>	0.5	0.5	0.5	0.5
<i>k3</i>	0.5	0.5	0.5	0.5
<i>k4</i>	7	7	7	7
<i>k5</i>	0.1	0.1	0.1	0.1
<i>k7</i>	0.45	0.45	0.45	0.45
<i>k9</i>	0.1	0.1	0.1	0.1
γ	500	500	500	500
<i>d</i>	10	10	10	10
λ	1.2	1.2	1.2	1.2
<i>h0</i>	10	10	10	10
<i>p0</i>	10	10	10	10
<i>q0</i>	10	10	10	10
WI	0,9	1,8	3	1,8
t_WI_start	16500 (=E11:11)	16500 (=E11:11)	16500 (=E11:11)	15720 (=E10:22)
t_WI_end	17760 (=E12:08)	17760 (=E12:08)	17760 (=E12:08)	17760 (=E12:08)

Simulating digit sharpening phenotype

Digit sharpening is a phenotype from Wnt activation. Parameters listed below.

Reaction	Diffusion
$\frac{dSox9}{dt} = \lambda(k2(Bmp - Bmp_0) - k3(Wnt - Wnt_0) - (Sox9 - Sox9_0)^3)$	0
$\frac{dBmp}{dt} = \lambda(-(k4 - 2.50 * fgf8 * hoxd13) * (Sox9 - Sox9_0) - k5(Bmp - Bmp_0))$	$\gamma * d$
$\frac{dWnt}{dt} = \lambda(WA * t_{WA} - (k7 + 1.25 * fgf8 * hoxd13) * (Sox9 - Sox9_0) - k9(Wnt - Wnt_0))$	γ

$$t_{WA} = (t > t_{WA_start}) * (t < t_{WA_end})$$

Variable	Value
$k2$	0.5
$k3$	0.5
$k4$	7
$k5$	0.1
$k7$	0.45
$k9$	0.1
γ	500
d	10

λ	1.2
$h0$	10
$p0$	10
$q0$	10
WA	0,9
t_WA_start	16500 (=E11:11)
t_WA_end	17760 (=E12:08)

Simulating period change phenotype

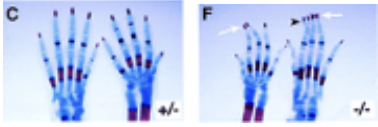
Period change is a phenotype from Wnt activation. Parameters listed below.

Reaction	Diffusion
$\frac{dSox9}{dt} = \lambda(k2(Bmp - Bmp_0) - k3(Wnt - Wnt_0) - (Sox9 - Sox9_0)^3)$	0
$\frac{dBmp}{dt} = \lambda(- (k4 - 2.50 * fgf8 * hoxd13) * (Sox9 - Sox9_0) - k5(Bmp - Bmp_0))$	$\gamma*d$
$\frac{dWnt}{dt} = \lambda(- (k7 + 1.25 * fgf8 * hoxd13) * (Sox9 - Sox9_0) - k9(Wnt - Wnt_0))$	γ

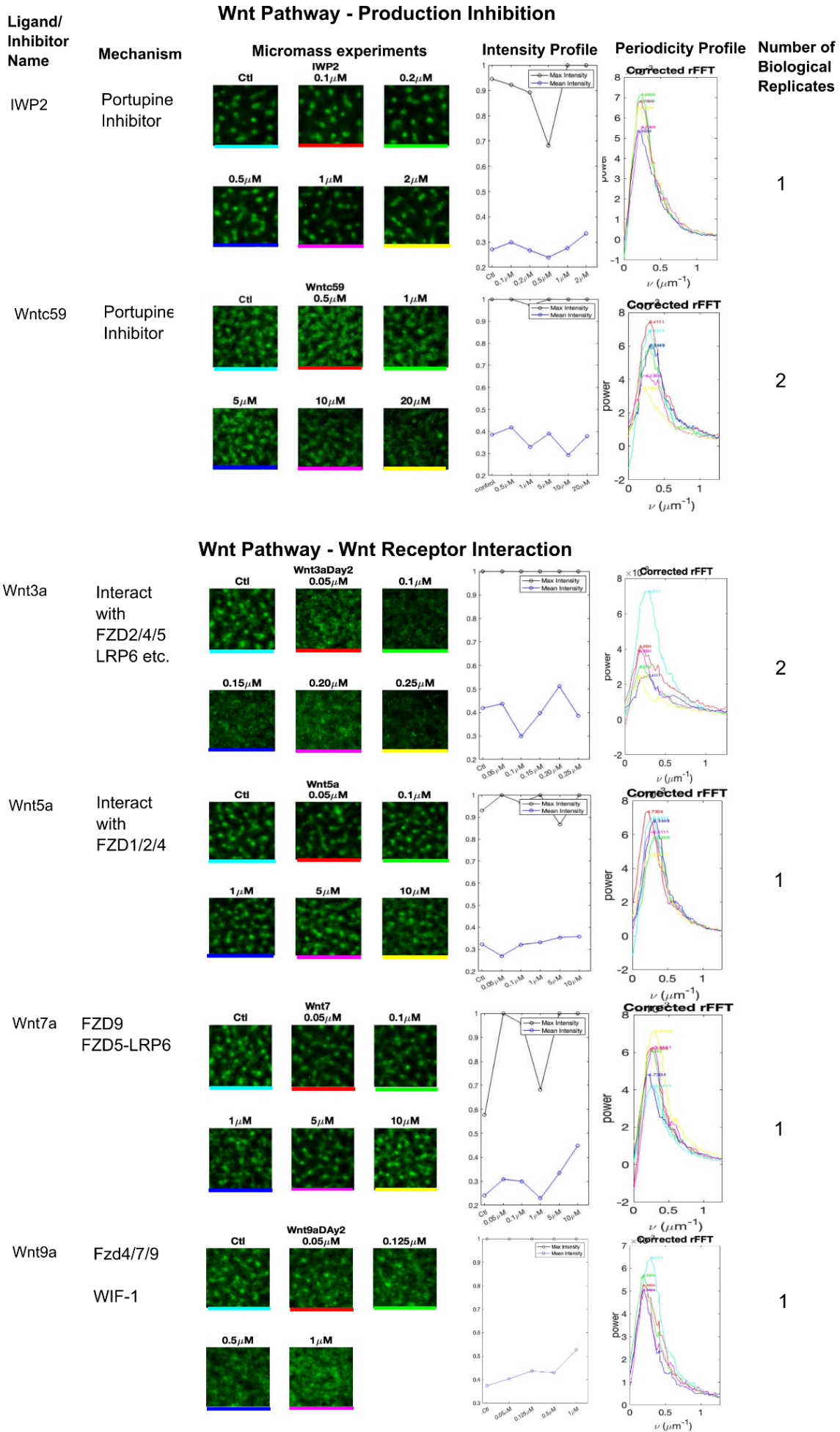
Variable	Value
$k2$	0.5

$k3$	1.05
$k4$	7
$k5$	0.1
$k7$	0.45
$k9$	0.1
γ	500
d	10
λ	1
$h0$	10
$p0$	10
$q0$	10

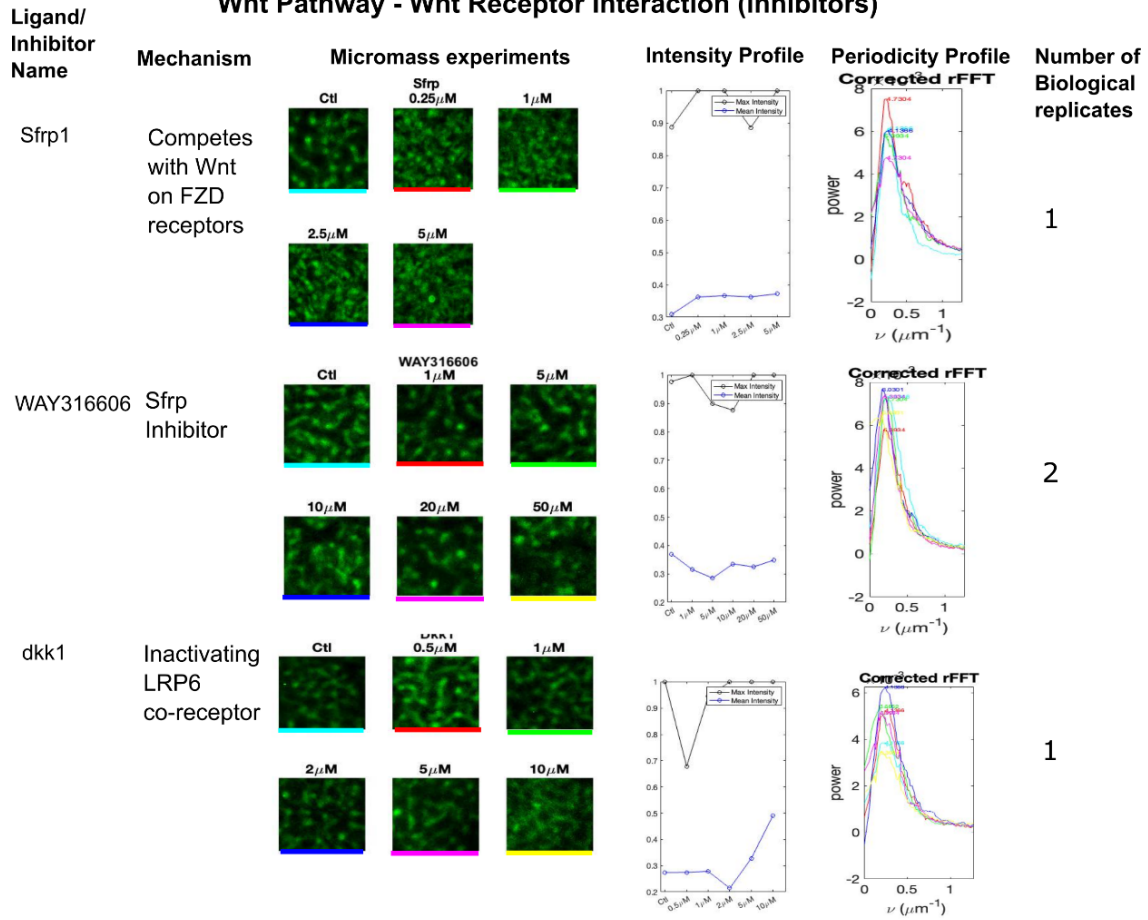
8. Appendix

Pathway	Component	perturbation phenotype or <i>in situ</i>
Retinoic acid	Cyp26b1 Degrades RA to inactive forms. Activated by FGF signalling.	 <p>E15.5, Alcian Blue and Alizarin Red stained. Left : WT, Right : <i>cyp26b1</i>^{-/-} Image from Dranse <i>et al</i> [94]</p>
Notch-delta	Jagged2 Ligand for the Notch family of transmembrane receptors	 <p><i>Jag2</i>^{ΔDSL} mutant. Neonatal mouse limb. Image from Jiang <i>et al.</i> [98]</p>

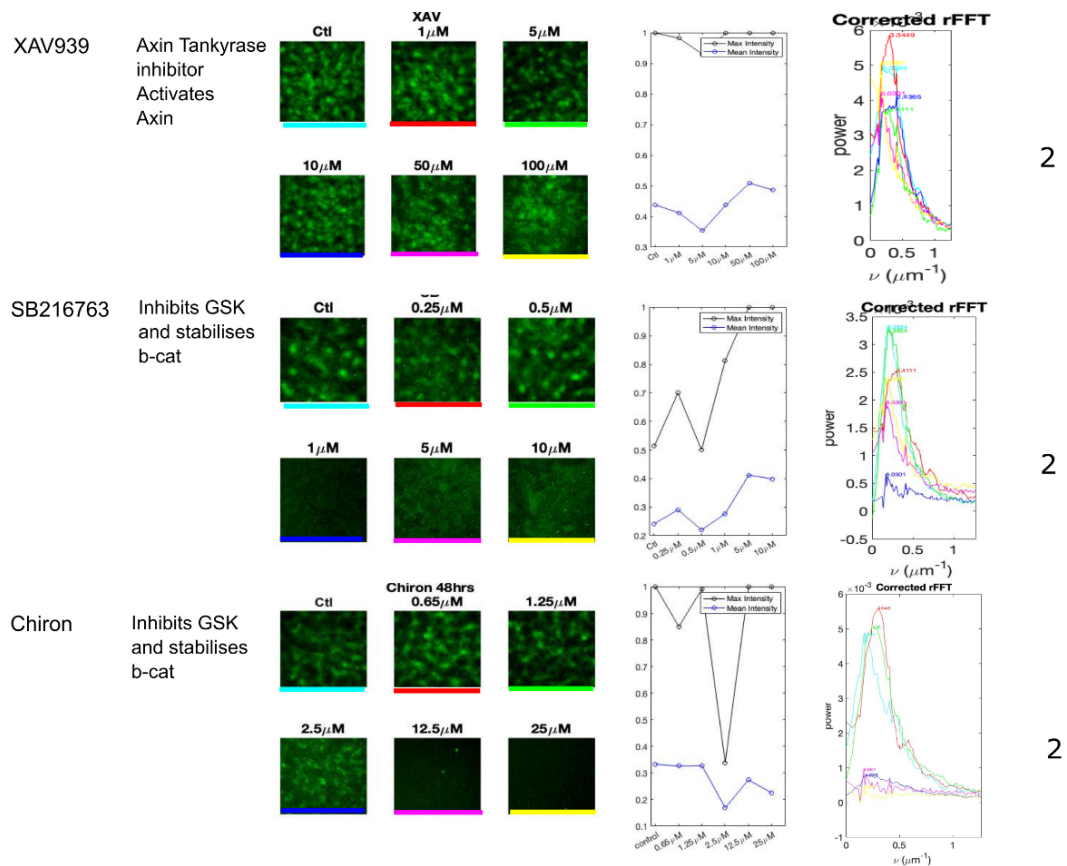
Supplementary Table 1. mutant/conditional phenotypes of Retinoic acid pathway components and Notch pathway components.

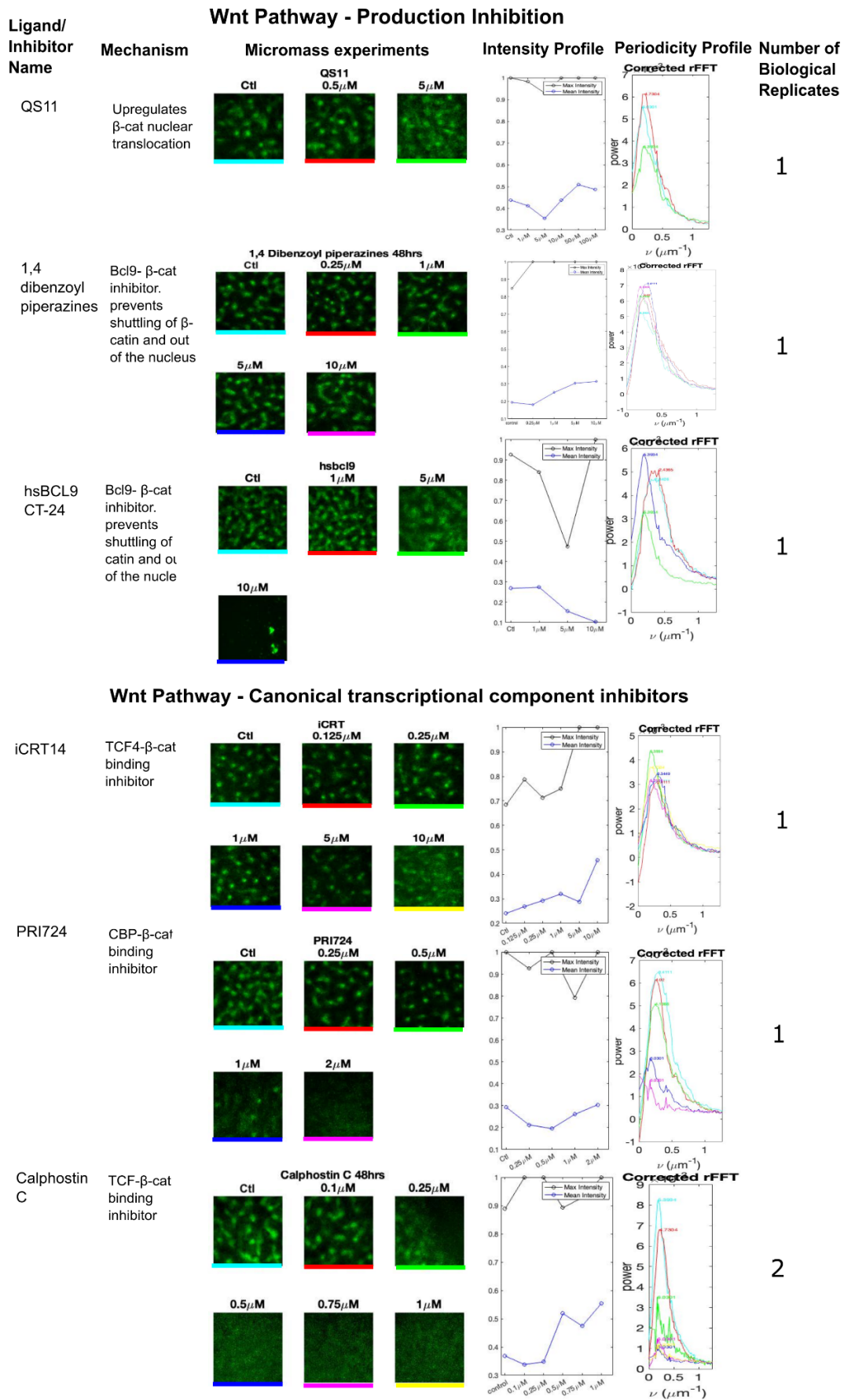


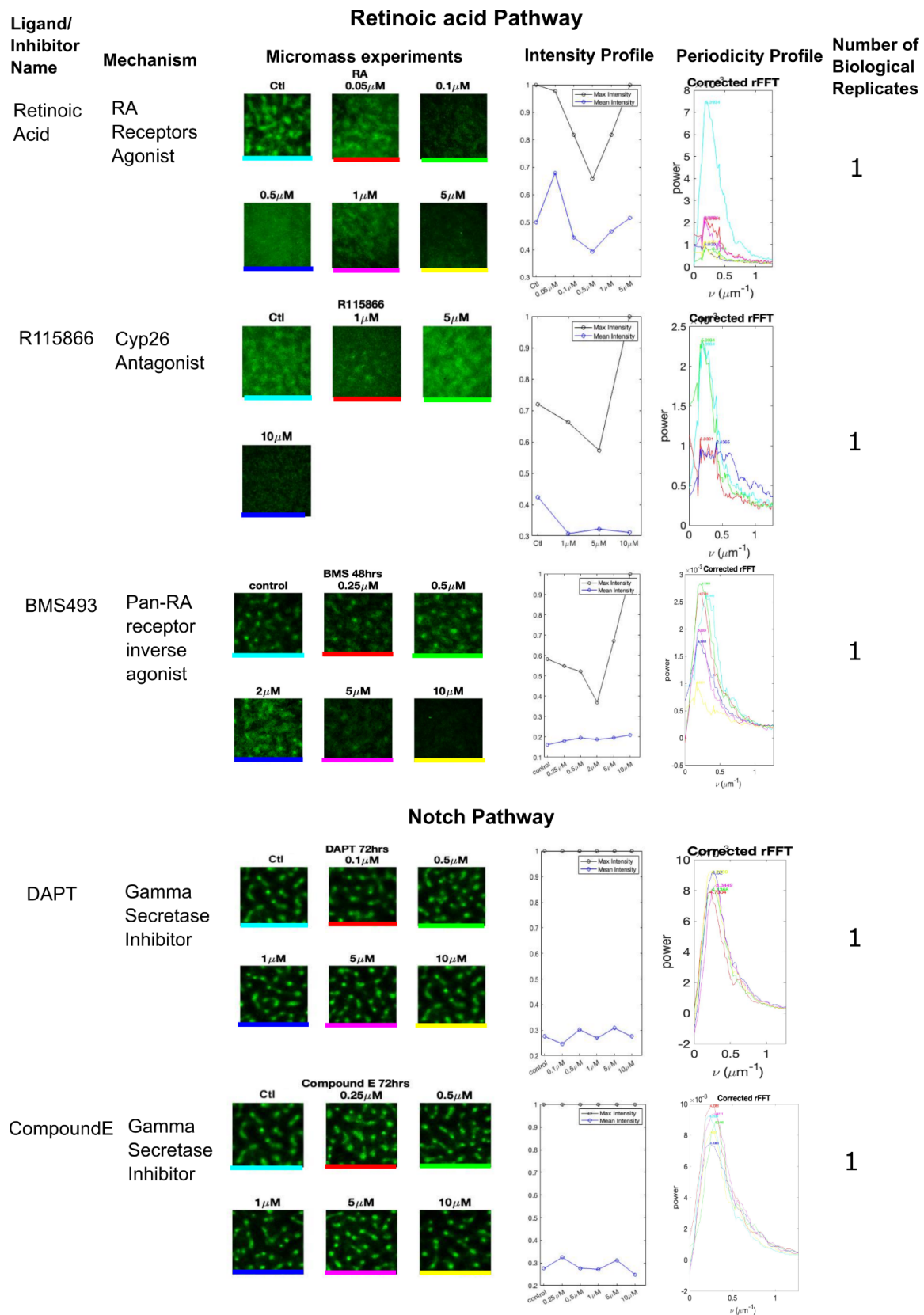
Wnt Pathway - Wnt Receptor Interaction (inhibitors)



Wnt Pathway - Canonical cytosolic component inhibitors







Supplementary Figure 1. Micromass raw experimental images, intensity and periodicity Profiles.

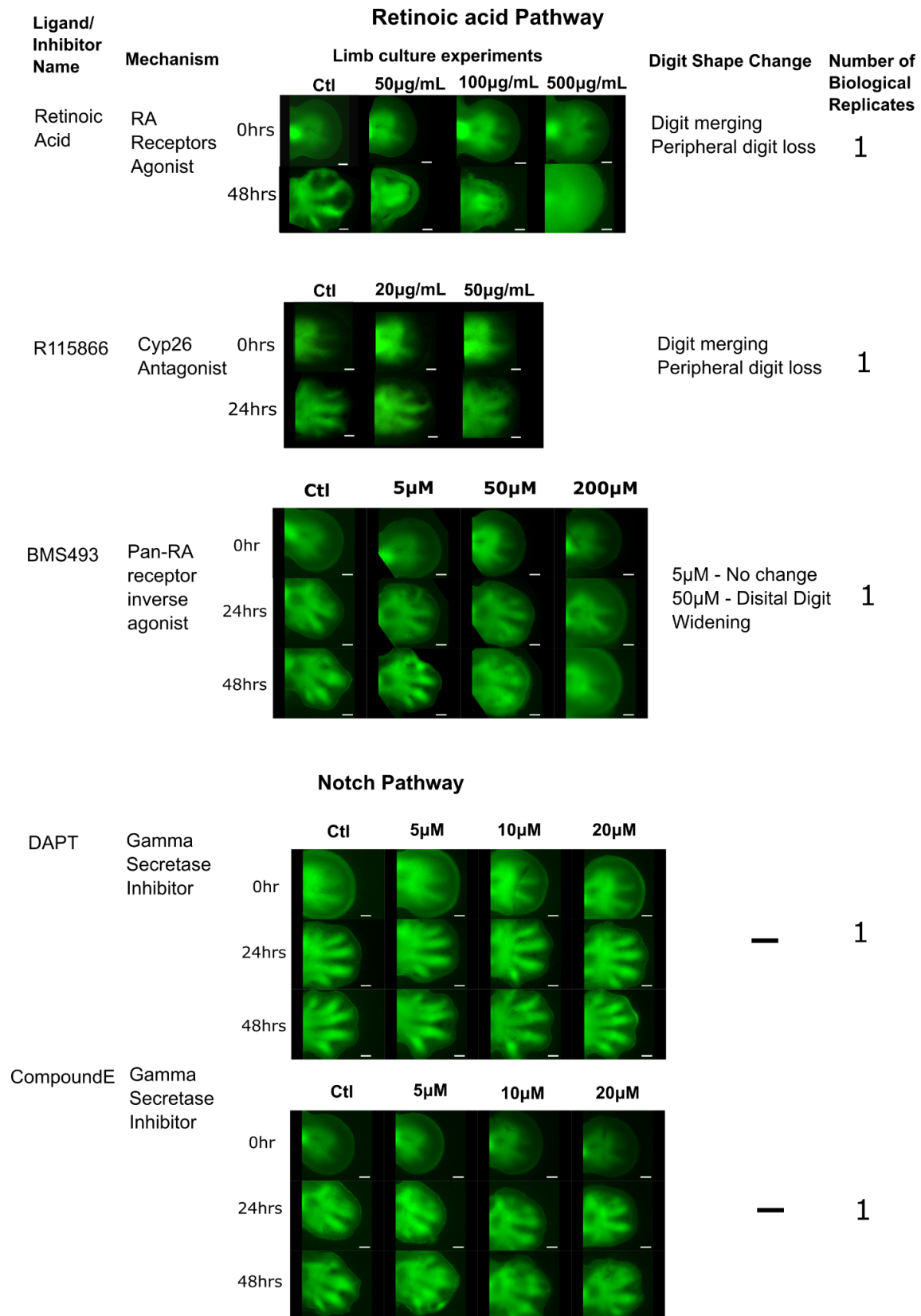
Ligand/ Inhibitor Name	Mechanism	Limb Culture Experiment				Digit Shape changes	Number of biological replicates
		Ctl	5 μ M	25 μ M	50 μ M		
IWP2	Porcupine Inhibitor					Digit Merging Webbing	3-4
Wntc59	Porcupine Inhibitor					Digit Merging 2 μ g/mL : webbing 5, 10 μ g/mL: Distal digit widening	4-5
Wnt Pathway - Wnt Receptor Interaction							
			Ctl	3 μ g/mL	20 μ g/mL		
Ligand/ Inhibitor Name	Mechanism					—	3-4
Wnt3a	Interact with FZD2/4/5 LRP6 etc.	0hr 24hrs 48hrs					
			Ctl	1 μ g/mL	10 μ g/mL		
Wnt5a	Interact with FZD1/2/4	0hr 24hrs 48hrs				—	2
			Ctl	1 μ g/mL	10 μ g/mL		
Wnt7a	unknown	0hr 24hrs 48hrs				—	1
			Ctl	0.1 μ g/mL	1 μ g/mL		
Wnt9a	unknown	0hr 48hrs				Digit Merging Peripheral digit loss	2

Wnt Pathway - Canonical cytosolic component inhibitors

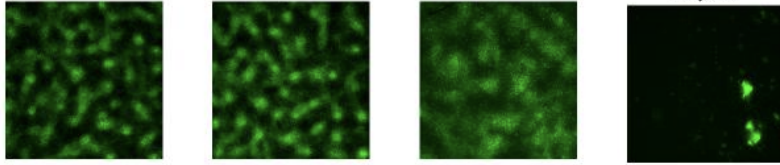
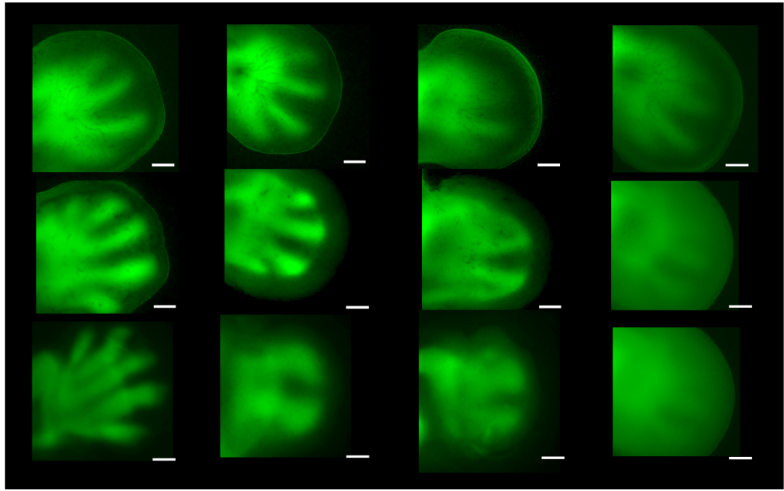
Ligand/ Inhibitor Name	Mechanism	Limb Culture Experiment				Digit Shape changes	Number of Biological Replicates
		Ctl	100µg/ml	500µg/ml	1mg/ml		
QS11	Upregulates β-cat nuclear translocation					Digit Sharpening	2-4
1,4 dibenzoyl piperazines	Bcl9- β-cat inhibitor. prevents shuttling of β- catin and out of the nucleus					—	2
hsBCL9 CT-24	Bcl9- β-cat inhibitor. prevents shuttling of β- catin and out of the nucleus					—	3-4

Wnt Pathway - Canonical transcriptional component inhibitors

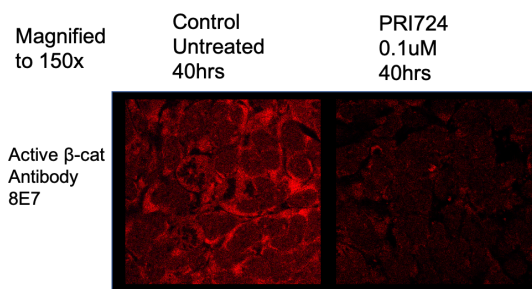
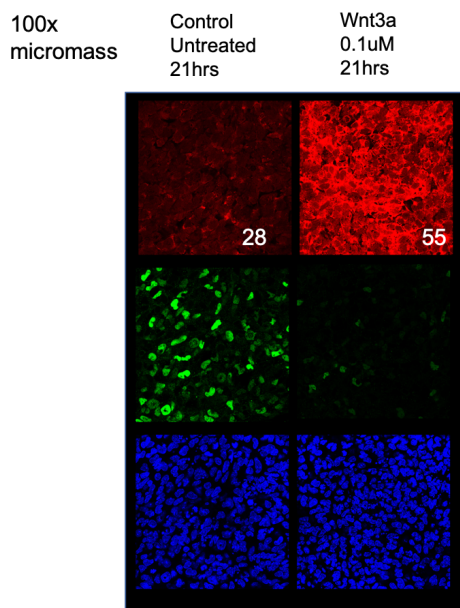
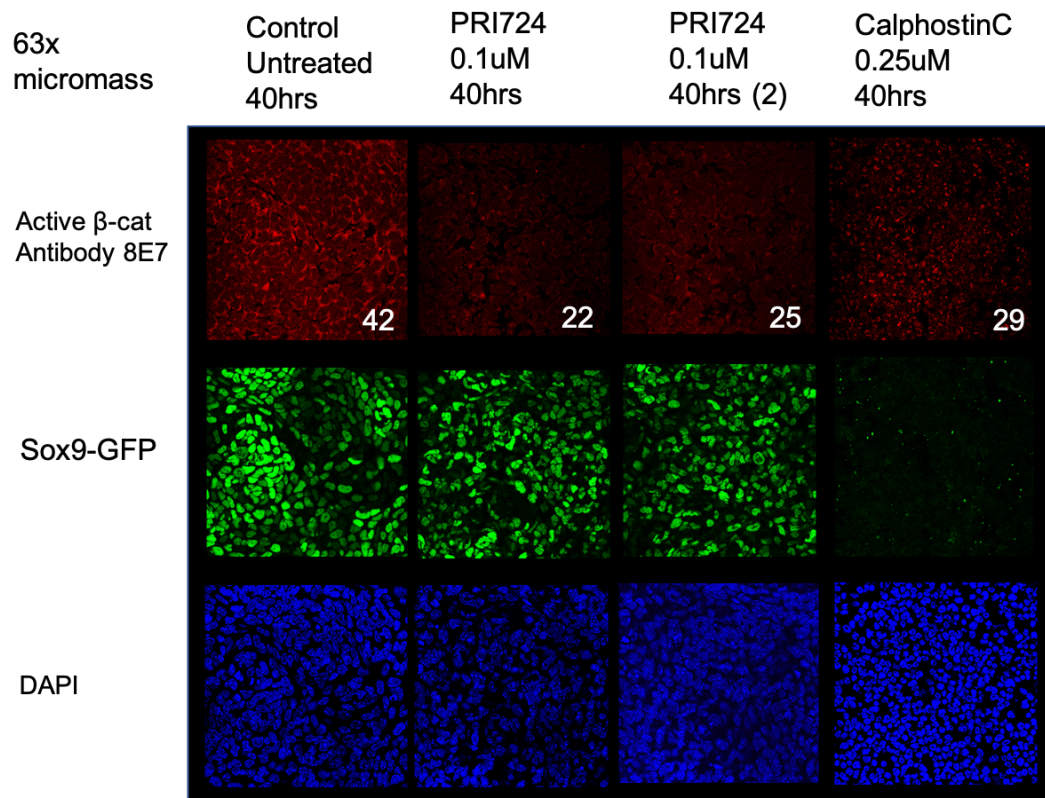
Ligand/ Inhibitor Name	Mechanism	Limb Culture Experiment					Digit Shape changes	Number of Biological Replicates
		Ctl	5µM	25µM	100µM			
iCRT14	TCF4-β-cat binding inhibitor						Digit Sharpening	2-3
PRI724	CBP-β-cat binding inhibitor						Digit Merging 0.5µM : Distal digit widening 10, 100µM : Peripheral digit loss	2-3
Calphostin C	TCF-β-cat binding inhibitor						Digit Merging 0.15µM : Digit period decrease	2



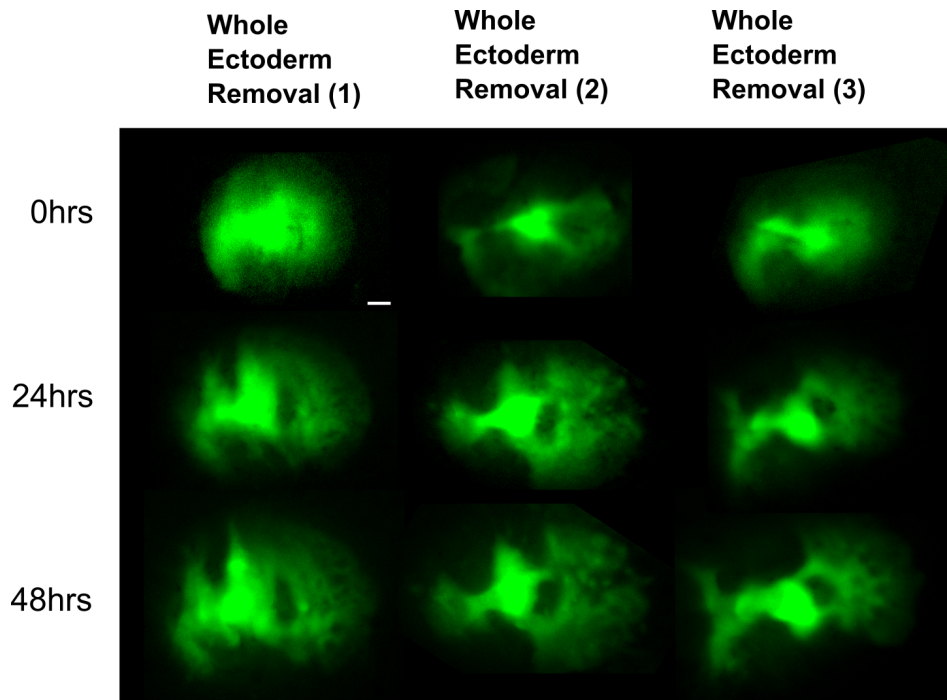
Supplementary Figure 2. Limb culture raw experimental images at various concentrations, and their digit shape phenotypes.

	Cell/limb culture death
Micromass	<p>hsBcl-9</p> <p>Ctl 1μM 5μM 10μM</p> 
Limb culture	<p>Calphostin C</p> <p>Ctl 0.15μM 0.15μM 1μM</p> <p>0hrs</p> <p>24hrs</p> <p>48hrs</p> 

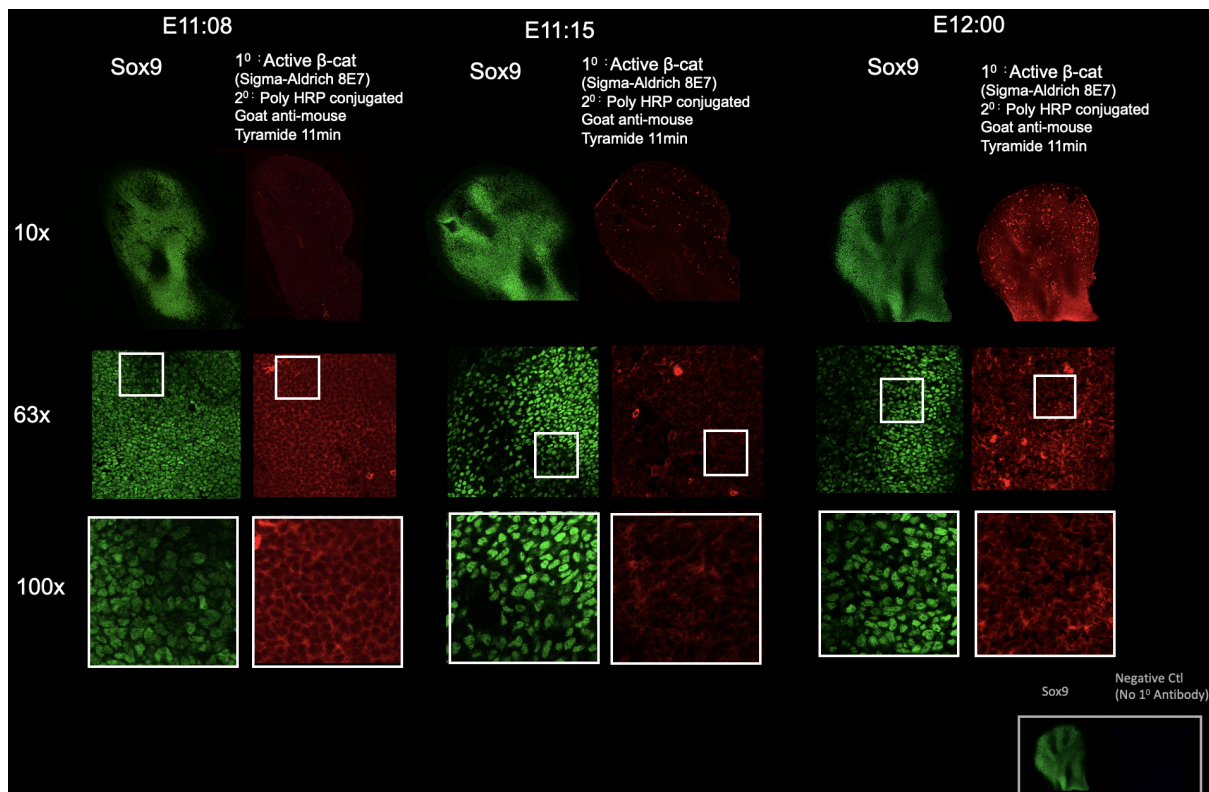
Supplementary Table 2. Examples of dead micromass and limb culture upon high dosage - The micromass culture is dead at 10 μ M for hsBcl-9, and limb culture at 1 μ M for Calphostin C.



Supplementary Figure 3. Magnified micromass stained images following application of PRI724 and CalphostinC. To gauge the strength of overall Wnt signalling, antibody against active β -cat is used, and to verify the result, the identical staining protocol was also tried on the micromass treated with Wnt3a. Magnified micromass images up to 150x are shown compare β -cat expression. In the control, β -cat upregulation on the cell membranes compared to the cytosol is shown, whereas the overall β -cat level, as well as such contrast, is less visible on PRI724 treated cells.



Supplementary Figure 4. Whole ectoderm removal results in spreading out of the limb mesenchymal cells towards the mesh which the limb sits on. It is difficult to analyse the pattern change as the physical movement of mesenchymal cells result in fractal-like branching patterns.



Supplementary Figure 5. High magnification microscopy of active β -catenin on mouse embryonic limb does not differentiate between Sox9+ and Sox9- areas. Active β -Catenin antibody(Sigma Aldrich 8E7) recognizes β -cat with unphosphorylated Ser33, Ser37, and Thr41. The experiment was performed at multiple timepoints of digit patterning(E11:08, E11:15, E12:00).

Bibliography

- [1] D. W. Thompson, *On growth and form*, vol. 2. Cambridge university press, 1942.
- [2] C. Collinet and T. Lecuit, 'Programmed and self-organized flow of information during morphogenesis', *Nat Rev Mol Cell Biol*, vol. 22, no. 4, pp. 245–265, Apr. 2021, doi: 10.1038/s41580-020-00318-6.
- [3] T. Saha and M. Galic, 'Self-organization across scales: from molecules to organisms', *Phil. Trans. R. Soc. B*, vol. 373, no. 1747, p. 20170113, May 2018, doi: 10.1098/rstb.2017.0113.
- [4] J. A. Rego, J. A. A. Harvey, A. L. MacKinnon, and E. Gatdula, 'Asymmetric synthesis of a highly soluble "trimeric" analogue of the chiral nematic liquid crystal twist agent Merck S1011', *Liquid Crystals*, vol. 37, no. 1, pp. 37–43, Dec. 2009, doi: 10.1080/02678290903359291.
- [5] I. D. Couzin and J. Krause, 'Self-Organization and Collective Behavior in Vertebrates', in *Advances in the Study of Behavior*, vol. 32, Elsevier, 2003, pp. 1–75. doi: 10.1016/S0065-3454(03)01001-5.
- [6] S. Wennekamp, S. Mesecke, F. Nédélec, and T. Hiiragi, 'A self-organization framework for symmetry breaking in the mammalian embryo', *Nat Rev Mol Cell Biol*, vol. 14, no. 7, pp. 452–459, Jul. 2013, doi: 10.1038/nrm3602.
- [7] A. M. Turing, 'The Chemical Basis of Morphogenesis', *Philosophical Transactions of the Royal Society of London. Series B, Biological Sciences*, vol. 237, no. 641, pp. 37–72, 1952.
- [8] A. J. Koch and H. Meinhardt, 'Biological pattern formation: from basic mechanisms to complex structures', *Rev. Mod. Phys.*, vol. 66, no. 4, pp. 1481–1507, Oct. 1994, doi: 10.1103/RevModPhys.66.1481.
- [9] L. Wolpert, 'Chapter 6 Positional Information and Pattern Formation', in *Current Topics in Developmental Biology*, vol. 6, Elsevier, 1971, pp. 183–224. doi: 10.1016/S0070-2153(08)60641-9.
- [10] L. Wolpert, 'Positional information and the spatial pattern of cellular differentiation', *J Theor Biol*, vol. 25, no. 1, pp. 1–47, Oct. 1969, doi: 10.1016/s0022-5193(69)80016-0.
- [11] T. H. Morgan, 'Regeneration in *Allolobophora foetida*', *Archiv für Entwicklungsmechanik der Organismen*, vol. 5, no. 3, pp. 570–586, 1897.
- [12] D. Busson, 'Peter A. Lawrence (1992); "The Making of a Fly: The Genetics of Animal Design"', Blackwell Scientific Publications, Oxford, 229 pp. f16.95. ISBN: 0-632-30048-8', *J Evolution Biol*, vol. 6, no. 4, pp. 609–610, Jul. 1993, doi: 10.1046/j.1420-9101.1993.6040609.x.
- [13] W. Driever and C. Nüsslein-Volhard, 'A gradient of bicoid protein in *Drosophila* embryos', *Cell*, vol. 54, no. 1, pp. 83–93, Jul. 1988, doi: 10.1016/0092-8674(88)90182-1.
- [14] C. Tickle, D. Summerbell, and L. Wolpert, 'Positional signalling and specification of digits in chick limb morphogenesis', *Nature*, vol. 254, no. 5497, pp. 199–202, Mar. 1975, doi: 10.1038/254199a0.
- [15] A. Gierer and H. Meinhardt, 'A theory of biological pattern formation', *Kybernetik*, vol. 12, no. 1, pp. 30–39, Dec. 1972, doi: 10.1007/BF00289234.
- [16] A. Nakamasu, G. Takahashi, A. Kanbe, and S. Kondo, 'Interactions between zebrafish pigment cells responsible for the generation of Turing patterns', *Proceedings of the National Academy of Sciences*, vol. 106, no. 21, pp. 8429–8434, May 2009, doi: 10.1073/pnas.0808622106.
- [17] A. D. Economou *et al.*, 'Periodic stripe formation by a Turing mechanism operating at growth zones in the mammalian palate', *Nat Genet*, vol. 44, no. 3, pp. 348–351, Feb. 2012, doi: 10.1038/ng.1090.
- [18] T. Schlake and S. Sick, 'Canonical WNT Signalling Controls Hair Follicle Spacing', *Cell Adhesion & Migration*, vol. 1, no. 3, pp. 149–151, Jul. 2007, doi: 10.4161/cam.1.3.5073.
- [19] P. Martin, 'Tissue patterning in the developing mouse limb', *Int J Dev Biol*, vol. 34, no.

- 3, pp. 323–336, Sep. 1990.
- [20] R. Zeller, J. López-Ríos, and A. Zuniga, ‘Vertebrate limb bud development: moving towards integrative analysis of organogenesis’, *Nat Rev Genet*, vol. 10, no. 12, pp. 845–858, Dec. 2009, doi: 10.1038/nrg2681.
- [21] D. Summerbell, J. H. Lewis, and L. Wolpert, ‘Positional Information in Chick Limb Morphogenesis’, *Nature*, vol. 244, no. 5417, pp. 492–496, Aug. 1973, doi: 10.1038/244492a0.
- [22] M. Musy, K. Flaherty, J. Raspopovic, A. Robert-Moreno, J. T. Richtsmeier, and J. Sharpe, ‘A quantitative method for staging mouse embryos based on limb morphometry’, *Development*, vol. 145, no. 7, Art. no. 7, Apr. 2018, doi: 10.1242/dev.154856.
- [23] H. Akiyama, M.-C. Chaboissier, J. F. Martin, A. Schedl, and B. de Crombrughe, ‘The transcription factor Sox9 has essential roles in successive steps of the chondrocyte differentiation pathway and is required for expression of Sox5 and Sox6’, *Genes Dev.*, vol. 16, no. 21, pp. 2813–2828, Nov. 2002, doi: 10.1101/gad.1017802.
- [24] H. Akiyama *et al.*, ‘Misexpression of Sox9 in mouse limb bud mesenchyme induces polydactyly and rescues hypodactyly mice’, *Matrix Biology*, vol. 26, no. 4, pp. 224–233, May 2007, doi: 10.1016/j.matbio.2006.12.002.
- [25] J. W. Saunders and M. T. Gasseling, *Ectodermal-mesodermal interactions in the origin of limb symmetry*. Williams and Wilkins.
- [26] J. Zhu, R. Patel, A. Trofka, B. D. Harfe, and S. Mackem, ‘Sonic Hedgehog is not a limb morphogen but acts as a trigger to specify all digits’, *Developmental Biology*, preprint, May 2020. doi: 10.1101/2020.05.28.122119.
- [27] P. K. Maini, T. E. Woolley, R. E. Baker, E. A. Gaffney, and S. S. Lee, ‘Turing’s model for biological pattern formation and the robustness problem’, *Interface Focus.*, vol. 2, no. 4, pp. 487–496, Aug. 2012, doi: 10.1098/rsfs.2011.0113.
- [28] J. Raspopovic, L. Marcon, L. Russo, and J. Sharpe, ‘Modeling digits. Digit patterning is controlled by a Bmp-Sox9-Wnt Turing network modulated by morphogen gradients’, *Science*, vol. 345, no. 6196, Art. no. 6196, Aug. 2014, doi: 10.1126/science.1252960.
- [29] A. Bandyopadhyay, K. Tsuji, K. Cox, B. D. Harfe, V. Rosen, and C. J. Tabin, ‘Genetic Analysis of the Roles of BMP2, BMP4, and BMP7 in Limb Patterning and Skeletogenesis’, *PLoS Genet*, vol. 2, no. 12, p. e216, 2006, doi: 10.1371/journal.pgen.0020216.
- [30] D. ten Berge, S. A. Brugmann, J. A. Helms, and R. Nusse, ‘Wnt and FGF signals interact to coordinate growth with cell fate specification during limb development’, *Development*, vol. 135, no. 19, pp. 3247–3257, Oct. 2008, doi: 10.1242/dev.023176.
- [31] C. Parada *et al.*, ‘Mechanical feedback defines organizing centers to drive digit emergence’, *Developmental Cell*, vol. 57, no. 7, pp. 854–866.e6, Apr. 2022, doi: 10.1016/j.devcel.2022.03.004.
- [32] T. W. Hiscock, P. Tschopp, and C. J. Tabin, ‘On the Formation of Digits and Joints during Limb Development’, *Developmental Cell*, vol. 41, no. 5, pp. 459–465, Jun. 2017, doi: 10.1016/j.devcel.2017.04.021.
- [33] H. M. Blau, C.-P. Chiu, and C. Webster, ‘Cytoplasmic activation of human nuclear genes in stable heterocaryons’, *Cell*, vol. 32, no. 4, pp. 1171–1180, Apr. 1983, doi: 10.1016/0092-8674(83)90300-8.
- [34] M. Skipper, U. Weiss, and N. Gray, ‘Plasticity’, *Nature*, vol. 465, no. 7299, Art. no. 7299, Jun. 2010, doi: 10.1038/465703a.
- [35] A. Bjorklund and C. Svendsen, ‘Breaking the brain-blood barrier’, *Nature*, vol. 397, no. 6720, Art. no. 6720, Feb. 1999, doi: 10.1038/17495.
- [36] K. Takahashi and S. Yamanaka, ‘Induction of Pluripotent Stem Cells from Mouse Embryonic and Adult Fibroblast Cultures by Defined Factors’, *Cell*, vol. 126, no. 4, pp. 663–676, Aug. 2006, doi: 10.1016/j.cell.2006.07.024.
- [37] G. E. Solini, C. Dong, and M. Saha, ‘Embryonic transplantation experiments: Past, present, and future’, *Trends Dev Biol*, vol. 10, pp. 13–30, 2017.
- [38] G. Schubiger and M. Schubiger, ‘Distal transformation in Drosophila leg imaginal disc

- fragments', *Developmental Biology*, vol. 67, no. 2, pp. 286–295, Dec. 1978, doi: 10.1016/0012-1606(78)90200-2.
- [39] L. a Wyngaarden and S. Hopyan, 'Plasticity of proximal-distal cell fate in the mammalian limb bud.', *Developmental biology*, vol. 313, no. 1, Art. no. 1, Jan. 2008, doi: 10.1016/j.ydbio.2007.10.039.
- [40] D. T. Grimes, 'Making and breaking symmetry in development, growth and disease', *Development*, vol. 146, no. 16, p. dev170985, Aug. 2019, doi: 10.1242/dev.170985.
- [41] D. A. Fowler and H. C. E. Larsson, 'The tissues and regulatory pattern of limb chondrogenesis', *Developmental Biology*, vol. 463, no. 2, pp. 124–134, Jul. 2020, doi: 10.1016/j.ydbio.2020.04.009.
- [42] G. F. Oster, J. D. Murray, and A. K. Harris, 'Mechanical aspects of mesenchymal morphogenesis', *J Embryol Exp Morphol*, vol. 78, pp. 83–125, Dec. 1983.
- [43] T. Mammoto *et al.*, 'Mechanochemical Control of Mesenchymal Condensation and Embryonic Tooth Organ Formation', *Developmental Cell*, vol. 21, no. 4, pp. 758–769, Oct. 2011, doi: 10.1016/j.devcel.2011.07.006.
- [44] K. Y. Volokh, 'Tissue morphogenesis: a surface buckling mechanism', *Int. J. Dev. Biol.*, vol. 50, no. 2–3, pp. 359–365, 2006, doi: 10.1387/ijdb.052039kv.
- [45] B. Boehm *et al.*, 'The Role of Spatially Controlled Cell Proliferation in Limb Bud Morphogenesis', *PLoS Biol*, vol. 8, no. 7, p. e1000420, Jul. 2010, doi: 10.1371/journal.pbio.1000420.
- [46] H. Hikasa and S. Y. Sokol, 'Wnt signaling in vertebrate axis specification', *Cold Spring Harb Perspect Biol*, vol. 5, no. 1, p. a007955, Jan. 2013, doi: 10.1101/cshperspect.a007955.
- [47] A. C. Hall, F. R. Lucas, and P. C. Salinas, 'Axonal Remodeling and Synaptic Differentiation in the Cerebellum Is Regulated by WNT-7a Signaling', *Cell*, vol. 100, no. 5, pp. 525–535, Mar. 2000, doi: 10.1016/S0092-8674(00)80689-3.
- [48] J. Galceran, S.-C. Hsu, and R. Grosschedl, 'Rescue of a *Wnt* mutation by an activated form of LEF-1: Regulation of maintenance but not initiation of *Brachyury* expression', *Proc. Natl. Acad. Sci. U.S.A.*, vol. 98, no. 15, pp. 8668–8673, Jul. 2001, doi: 10.1073/pnas.151258098.
- [49] Z. Steinhart and S. Angers, 'Wnt signaling in development and tissue homeostasis', *Development*, vol. 145, no. 11, p. dev146589, Jun. 2018, doi: 10.1242/dev.146589.
- [50] C. Niehrs, 'On growth and form: a Cartesian coordinate system of Wnt and BMP signaling specifies bilaterian body axes', *Development*, vol. 137, no. 6, pp. 845–857, Mar. 2010, doi: 10.1242/dev.039651.
- [51] K. Willert *et al.*, 'Wnt proteins are lipid-modified and can act as stem cell growth factors', *Nature*, vol. 423, no. 6938, pp. 448–452, May 2003, doi: 10.1038/nature01611.
- [52] L. Zhai, D. Chaturvedi, and S. Cumberledge, 'Drosophila Wnt-1 Undergoes a Hydrophobic Modification and Is Targeted to Lipid Rafts, a Process That Requires Porcupine', *Journal of Biological Chemistry*, vol. 279, no. 32, pp. 33220–33227, Aug. 2004, doi: 10.1074/jbc.M403407200.
- [53] C. Bänziger, D. Soldini, C. Schütt, P. Zipperlen, G. Hausmann, and K. Basler, 'Wntless, a Conserved Membrane Protein Dedicated to the Secretion of Wnt Proteins from Signaling Cells', *Cell*, vol. 125, no. 3, pp. 509–522, May 2006, doi: 10.1016/j.cell.2006.02.049.
- [54] B. Hoang, M. Moos, S. Vukicevic, and F. P. Luyten, 'Primary Structure and Tissue Distribution of FRZB, a Novel Protein Related to Drosophila Frizzled, Suggest a Role in Skeletal Morphogenesis', *Journal of Biological Chemistry*, vol. 271, no. 42, pp. 26131–26137, Oct. 1996, doi: 10.1074/jbc.271.42.26131.
- [55] D. Wawrzak, M. Métioui, E. Willems, M. Hendrickx, E. de Genst, and L. Leyns, 'Wnt3a binds to several sFRPs in the nanomolar range', *Biochemical and Biophysical Research Communications*, vol. 357, no. 4, pp. 1119–1123, Jun. 2007, doi: 10.1016/j.bbrc.2007.04.069.
- [56] L. M. Galli *et al.*, 'Differential inhibition of Wnt-3a by Sfrp-1, Sfrp-2, and Sfrp-3', *Dev. Dyn.*, vol. 235, no. 3, pp. 681–690, Mar. 2006, doi: 10.1002/dvdy.20681.

- [57] A. Bafico, A. Gazit, T. Pramila, P. W. Finch, A. Yaniv, and S. A. Aaronson, 'Interaction of Frizzled Related Protein (FRP) with Wnt Ligands and the Frizzled Receptor Suggests Alternative Mechanisms for FRP Inhibition of Wnt Signaling', *Journal of Biological Chemistry*, vol. 274, no. 23, pp. 16180–16187, Jun. 1999, doi: 10.1074/jbc.274.23.16180.
- [58] I. Ackers and R. Malgor, 'Interrelationship of canonical and non-canonical Wnt signalling pathways in chronic metabolic diseases', *Diabetes and Vascular Disease Research*, vol. 15, no. 1, pp. 3–13, Jan. 2018, doi: 10.1177/1479164117738442.
- [59] H.-C. Huang and P. S. Klein, 'The Frizzled family: receptors for multiple signal transduction pathways', *Genome Biol*, vol. 5, no. 7, p. 234, 2004, doi: 10.1186/gb-2004-5-7-234.
- [60] K. I. Pinson, J. Brennan, S. Monkley, B. J. Avery, and W. C. Skarnes, 'An LDL-receptor-related protein mediates Wnt signalling in mice', *Nature*, vol. 407, no. 6803, pp. 535–538, Sep. 2000, doi: 10.1038/35035124.
- [61] B. Mao *et al.*, 'Kremen proteins are Dickkopf receptors that regulate Wnt/beta-catenin signalling', *Nature*, vol. 417, no. 6889, pp. 664–667, Jun. 2002, doi: 10.1038/nature756.
- [62] A. Glinka, W. Wu, H. Delius, A. P. Monaghan, C. Blumenstock, and C. Niehrs, 'Dickkopf-1 is a member of a new family of secreted proteins and functions in head induction', *Nature*, vol. 391, no. 6665, pp. 357–362, Jan. 1998, doi: 10.1038/34848.
- [63] D. C. Slusarski, J. Yang-Snyder, W. B. Busa, and R. T. Moon, 'Modulation of Embryonic Intracellular Ca²⁺ Signaling by Wnt-5A', *Developmental Biology*, vol. 182, no. 1, pp. 114–120, Feb. 1997, doi: 10.1006/dbio.1996.8463.
- [64] M. Katoh, 'WNT/PCP signaling pathway and human cancer (review)', *Oncol Rep*, vol. 14, no. 6, pp. 1583–1588, Dec. 2005.
- [65] M. D. Gordon and R. Nusse, 'Wnt Signaling: Multiple Pathways, Multiple Receptors, and Multiple Transcription Factors', *Journal of Biological Chemistry*, vol. 281, no. 32, pp. 22429–22433, Aug. 2006, doi: 10.1074/jbc.R600015200.
- [66] R. van Amerongen, C. Fuerer, M. Mizutani, and R. Nusse, 'Wnt5a can both activate and repress Wnt/ β -catenin signaling during mouse embryonic development', *Developmental Biology*, vol. 369, no. 1, pp. 101–114, Sep. 2012, doi: 10.1016/j.ydbio.2012.06.020.
- [67] A. Kikuchi, H. Yamamoto, A. Sato, and S. Matsumoto, 'Wnt5a: its signalling, functions and implication in diseases: **Wnt5a signalling and cellular functions**', *Acta Physiologica*, vol. 204, no. 1, pp. 17–33, Jan. 2012, doi: 10.1111/j.1748-1716.2011.02294.x.
- [68] T. P. Hill, D. Später, M. M. Taketo, W. Birchmeier, and C. Hartmann, 'Canonical Wnt/ β -Catenin Signaling Prevents Osteoblasts from Differentiating into Chondrocytes', *Developmental Cell*, vol. 8, no. 5, pp. 727–738, May 2005, doi: 10.1016/j.devcel.2005.02.013.
- [69] T. P. Hill, M. M. Taketo, W. Birchmeier, and C. Hartmann, 'Multiple roles of mesenchymal β -catenin during murine limb patterning', *Development*, vol. 133, no. 7, pp. 1219–1229, Apr. 2006, doi: 10.1242/dev.02298.
- [70] C.-M. Cruciat and C. Niehrs, 'Secreted and Transmembrane Wnt Inhibitors and Activators', *Cold Spring Harbor Perspectives in Biology*, vol. 5, no. 3, pp. a015081–a015081, Mar. 2013, doi: 10.1101/cshperspect.a015081.
- [71] R. Morello *et al.*, 'Brachy-syndactyly caused by loss of *Sfrp2* function', *J. Cell. Physiol.*, vol. 217, no. 1, pp. 127–137, Oct. 2008, doi: 10.1002/jcp.21483.
- [72] A. M. DeLise, E. Stringa, W. A. Woodward, M. A. Mello, and R. S. Tuan, 'Embryonic Limb Mesenchyme Micromass Culture as an In Vitro Model for Chondrogenesis and Cartilage Maturation', in *Developmental Biology Protocols*, vol. 137, New Jersey: Humana Press, 2000, pp. 359–375. doi: 10.1385/1-59259-066-7:359.
- [73] K. Daniels, R. Reiter, and M. Solursh, 'Chapter 12 Micromass Cultures of Limb and Other Mesenchyme', in *Methods in Cell Biology*, vol. 51, Elsevier, 1996, pp. 237–247. doi: 10.1016/S0091-679X(08)60631-7.
- [74] V. Lefebvre and B. de Crombrughe, 'Toward understanding SOX9 function in

- chondrocyte differentiation', *Matrix Biology*, vol. 16, no. 9, pp. 529–540, Mar. 1998, doi: 10.1016/S0945-053X(98)90065-8.
- [75] W. J. Moore *et al.*, 'Modulation of Wnt Signaling Through Inhibition of Secreted Frizzled-Related Protein 1 (sFRP-1) with N-Substituted Piperidinyll Diphenylsulfonyl Sulfonamides', *J. Med. Chem.*, vol. 52, no. 1, pp. 105–116, Jan. 2009, doi: 10.1021/jm801144h.
- [76] K. Summerhurst, M. Stark, J. Sharpe, D. Davidson, and P. Murphy, '3D representation of Wnt and Frizzled gene expression patterns in the mouse embryo at embryonic day 11.5 (Ts19)', *Gene Expression Patterns*, vol. 8, no. 5, pp. 331–348, May 2008, doi: 10.1016/j.gep.2008.01.007.
- [77] B. Gao *et al.*, 'Coordinated directional outgrowth and pattern formation by integration of Wnt5a and Fgf signaling in planar cell polarity', *Development*, p. dev.163824, Jan. 2018, doi: 10.1242/dev.163824.
- [78] M. Zhang, K. Li, M. Xie, and S. Ding, 'Chemical Approaches to Controlling Cell Fate', in *Principles of Developmental Genetics*, Elsevier, 2015, pp. 59–76. doi: 10.1016/B978-0-12-405945-0.00004-1.
- [79] U. S. Eggert, 'The why and how of phenotypic small-molecule screens', *Nat Chem Biol*, vol. 9, no. 4, pp. 206–209, Apr. 2013, doi: 10.1038/nchembio.1206.
- [80] A. Amsterdam and N. Hopkins, 'Mutagenesis strategies in zebrafish for identifying genes involved in development and disease', *Trends in Genetics*, vol. 22, no. 9, pp. 473–478, Sep. 2006, doi: 10.1016/j.tig.2006.06.011.
- [81] H. Renner *et al.*, 'A fully automated high-throughput workflow for 3D-based chemical screening in human midbrain organoids', *eLife*, vol. 9, p. e52904, Nov. 2020, doi: 10.7554/eLife.52904.
- [82] F.-H. Paradis, C. Huang, and B. F. Hales, 'The Murine Limb Bud in Culture as an In Vitro Teratogenicity Test System', in *Developmental Toxicology*, vol. 889, C. Harris and J. M. Hansen, Eds. Totowa, NJ: Humana Press, 2012, pp. 197–213. doi: 10.1007/978-1-61779-867-2_12.
- [83] R. H. Mohammed and D. Sweetman, 'Grafting of Beads into Developing Chicken Embryo Limbs to Identify Signal Transduction Pathways Affecting Gene Expression', *J Vis Exp*, no. 107, p. e53342, Jan. 2016, doi: 10.3791/53342.
- [84] M. Uzkudun, L. Marcon, and J. Sharpe, 'Data-driven modelling of a gene regulatory network for cell fate decisions in the growing limb bud', *Mol Syst Biol*, vol. 11, no. 7, Art. no. 7, Jul. 2015, doi: 10.15252/msb.20145882.
- [85] D. Summerbell, 'The effect of local application of retinoic acid to the anterior margin of the developing chick limb', *J Embryol Exp Morphol*, vol. 78, pp. 269–289, Dec. 1983.
- [86] K. Yashiro *et al.*, 'Regulation of retinoic acid distribution is required for proximodistal patterning and outgrowth of the developing mouse limb.', *Developmental cell*, vol. 6, no. 3, Art. no. 3, Mar. 2004.
- [87] S. Probst *et al.*, 'SHH propagates distal limb bud development by enhancing CYP26B1-mediated retinoic acid clearance via AER-FGF signalling.', *Development (Cambridge, England)*, vol. 138, no. 10, Art. no. 10, May 2011, doi: 10.1242/dev.063966.
- [88] D. M. Kochhar, 'Limb development in mouse embryos. I. Analysis of teratogenic effects of retinoic acid', *Teratology*, vol. 7, no. 3, pp. 289–298, Jun. 1973, doi: 10.1002/tera.1420070310.
- [89] C. Tickle, B. Alberts, L. Wolpert, and J. Lee, 'Local application of retinoic acid to the limb bud mimics the action of the polarizing region', *Nature*, vol. 296, no. 5857, pp. 564–566, Apr. 1982, doi: 10.1038/296564a0.
- [90] P. Dollé *et al.*, 'Differential expression of genes encoding α , β and γ retinoic acid receptors and CRABP in the developing limbs of the mouse', *Nature*, vol. 342, no. 6250, pp. 702–705, Dec. 1989, doi: 10.1038/342702a0.
- [91] H. Jiang *et al.*, 'Modulation of limb bud chondrogenesis by retinoic acid and retinoic acid receptors', *Int J Dev Biol*, vol. 39, no. 4, pp. 617–627, Aug. 1995.
- [92] D. E. Cash, C. B. Bock, K. Schughart, E. Linney, and T. M. Underhill, 'Retinoic Acid

- Receptor α Function in Vertebrate Limb Skeletogenesis: a Modulator of Chondrogenesis', *Journal of Cell Biology*, vol. 136, no. 2, pp. 445–457, Jan. 1997, doi: 10.1083/jcb.136.2.445.
- [93] E. Galdones and B. F. Hales, 'Retinoic Acid Receptor Gamma-Induced Misregulation of Chondrogenesis in the Murine Limb Bud In Vitro', *Toxicological Sciences*, vol. 106, no. 1, pp. 223–232, Nov. 2008, doi: 10.1093/toxsci/kfn169.
- [94] H. J. Dranse, A. V. Sampaio, M. Petkovich, and T. M. Underhill, 'Genetic deletion of *Cyp26b1* negatively impacts limb skeletogenesis by inhibiting chondrogenesis', *Journal of Cell Science*, vol. 124, no. 16, pp. 2723–2734, Aug. 2011, doi: 10.1242/jcs.084699.
- [95] M. A. Pignatello, F. C. Kauffman, and A. A. Levin, 'Liarozole Markedly Increases all trans-Retinoic Acid Toxicity in Mouse Limb Bud Cell Cultures: A Model to Explain the Potency of the Aromatic Retinoid (E)-4-[2-(5,6,7,8-Tetrahydro-5,5,8,8-tetramethyl-2-naphthylenyl)-1-propenyl] Benzoic Acid', *Toxicology and Applied Pharmacology*, vol. 178, no. 3, pp. 186–194, Feb. 2002, doi: 10.1006/taap.2001.9340.
- [96] R. Bhat, T. Glimm, M. Linde-Medina, C. Cui, and S. A. Newman, 'Synchronization of Hes1 oscillations coordinates and refines condensation formation and patterning of the avian limb skeleton', *Mechanisms of Development*, vol. 156, pp. 41–54, Apr. 2019, doi: 10.1016/j.mod.2019.03.001.
- [97] Y. Dong *et al.*, 'RBPjk-dependent Notch signaling regulates mesenchymal progenitor cell proliferation and differentiation during skeletal development', *Development*, vol. 137, no. 9, pp. 1461–1471, May 2010, doi: 10.1242/dev.042911.
- [98] R. Jiang *et al.*, 'Defects in limb, craniofacial, and thymic development in Jagged2 mutant mice', *Genes & Development*, vol. 12, no. 7, pp. 1046–1057, Apr. 1998, doi: 10.1101/gad.12.7.1046.
- [99] R. Fujimaki, Y. Toyama, N. Hozumi, and K. Tezuka, 'Involvement of Notch signaling in initiation of prechondrogenic condensation and nodule formation in limb bud micromass cultures', *J Bone Miner Metab*, vol. 24, no. 3, pp. 191–198, Apr. 2006, doi: 10.1007/s00774-005-0671-y.
- [100] M. Barbieri *et al.*, 'Complexity of chromatin folding is captured by the strings and binders switch model', *Proceedings of the National Academy of Sciences*, vol. 109, no. 40, pp. 16173–16178, Oct. 2012, doi: 10.1073/pnas.1204799109.
- [101] S. Stern, T. Dror, E. Stolovicki, N. Brenner, and E. Braun, 'Genome-wide transcriptional plasticity underlies cellular adaptation to novel challenge', *Mol Syst Biol*, vol. 3, no. 1, p. 106, Jan. 2007, doi: 10.1038/msb4100147.
- [102] P. Lee, J. Decker, L. Shea, and D. A. Beard, 'Plasticity of fibroblast transcriptional response to physical and biochemical cues revealed by dynamic network analysis', *Systems Biology*, preprint, Dec. 2020. doi: 10.1101/2020.12.13.422572.
- [103] B. Coban, C. Bergonzini, A. J. M. Zweemer, and E. H. J. Danen, 'Metastasis: crosstalk between tissue mechanics and tumour cell plasticity', *Br J Cancer*, vol. 124, no. 1, pp. 49–57, Jan. 2021, doi: 10.1038/s41416-020-01150-7.
- [104] S. A. Lambert *et al.*, 'The Human Transcription Factors', *Cell*, vol. 172, no. 4, pp. 650–665, Feb. 2018, doi: 10.1016/j.cell.2018.01.029.
- [105] J. Tsalikas and J. Romer-Seibert, 'LIN28: roles and regulation in development and beyond', *Development*, vol. 142, no. 14, pp. 2397–2404, Jul. 2015, doi: 10.1242/dev.117580.
- [106] Y. Buganim *et al.*, 'The Developmental Potential of iPSCs Is Greatly Influenced by Reprogramming Factor Selection', *Cell Stem Cell*, vol. 15, no. 3, pp. 295–309, Sep. 2014, doi: 10.1016/j.stem.2014.07.003.
- [107] J. Zhang *et al.*, 'LIN28 Regulates Stem Cell Metabolism and Conversion to Primed Pluripotency', *Cell Stem Cell*, vol. 19, no. 1, pp. 66–80, Jul. 2016, doi: 10.1016/j.stem.2016.05.009.
- [108] Y. Atsuta *et al.*, 'Direct Reprogramming of Non-limb Fibroblasts to Cells with Properties of Limb Progenitors', *Developmental Biology*, preprint, Oct. 2021. doi: 10.1101/2021.10.01.462632.

- [109] R. Akiyama, H. Kawakami, J. Wong, I. Oishi, R. Nishinakamura, and Y. Kawakami, 'Sall4-Gli3 system in early limb progenitors is essential for the development of limb skeletal elements', *Proc. Natl. Acad. Sci. U.S.A.*, vol. 112, no. 16, pp. 5075–5080, Apr. 2015, doi: 10.1073/pnas.1421949112.
- [110] J. Böhm *et al.*, 'Sall1, Sall2, and Sall4 Are Required for Neural Tube Closure in Mice', *Am J Pathol*, vol. 173, no. 5, pp. 1455–1463, Nov. 2008, doi: 10.2353/ajpath.2008.071039.
- [111] C.-I. Tai and Q.-L. Ying, 'Gbx2, a LIF/Stat3 target, promotes reprogramming to and retention of the pluripotent ground state', *Journal of Cell Science*, vol. 126, no. 5, pp. 1093–1098, Mar. 2013, doi: 10.1242/jcs.118273.
- [112] M. Fernandez-Guerrero, S. Zdral, A. Castilla-Ibeas, L. Lopez-Delisle, D. Duboule, and M. A. Ros, 'Time-sequenced transcriptomes of developing distal mouse limb buds: A comparative tissue layer analysis', *Dev Dyn*, Jul. 2021, doi: 10.1002/dvdy.394.
- [113] C. Melton, R. L. Judson, and R. Blelloch, 'Opposing microRNA families regulate self-renewal in mouse embryonic stem cells', *Nature*, vol. 463, no. 7281, pp. 621–626, Feb. 2010, doi: 10.1038/nature08725.
- [114] M. E. Peter, 'Let-7 and miR-200 microRNAs: Guardians against pluripotency and cancer progression', *Cell Cycle*, vol. 8, no. 6, pp. 843–852, Mar. 2009, doi: 10.4161/cc.8.6.7907.
- [115] J. J. Lancman *et al.*, 'Analysis of the regulation of *lin-41* during chick and mouse limb development', *Dev. Dyn.*, vol. 234, no. 4, pp. 948–960, Dec. 2005, doi: 10.1002/dvdy.20591.
- [116] J. Pickering *et al.*, 'An intrinsic cell cycle timer terminates limb bud outgrowth', *eLife*, vol. 7, p. e37429, Sep. 2018, doi: 10.7554/eLife.37429.
- [117] R.-S. Wang, 'Perturbation', in *Encyclopedia of Systems Biology*, W. Dubitzky, O. Wolkenhauer, K.-H. Cho, and H. Yokota, Eds. New York, NY: Springer New York, 2013, pp. 1680–1681. doi: 10.1007/978-1-4419-9863-7_385.
- [118] B. Mattes *et al.*, 'Wnt3 and Wnt3a are required for induction of the mid-diencephalic organizer in the caudal forebrain', *Neural Dev*, vol. 7, no. 1, p. 12, Dec. 2012, doi: 10.1186/1749-8104-7-12.
- [119] S. Jeensuk, M. S. Ortega, M. Saleem, B. Hawryluk, T. L. Scheffler, and P. J. Hansen, 'Actions of WNT family member 5A to regulate characteristics of development of the bovine preimplantation embryo', *Biology of Reproduction*, p. ioac127, Jun. 2022, doi: 10.1093/biolre/ioac127.
- [120] M. L. King *et al.*, 'WNT7A/ β -catenin signaling induces FGF1 and influences sensitivity to niclosamide in ovarian cancer', *Oncogene*, vol. 34, no. 26, pp. 3452–3462, Jun. 2015, doi: 10.1038/onc.2014.277.
- [121] A. C. Denicol, K. B. Dobbs, K. M. McLean, S. F. Carambula, B. Loureiro, and P. J. Hansen, 'Canonical WNT signaling regulates development of bovine embryos to the blastocyst stage', *Sci Rep*, vol. 3, no. 1, p. 1266, Dec. 2013, doi: 10.1038/srep01266.
- [122] Z. Feng *et al.*, 'In ovo injection of CHIR-99021 promotes feather follicles development via activating Wnt/ β -catenin signaling pathway during chick embryonic period', *Poultry Science*, vol. 101, no. 6, p. 101825, Jun. 2022, doi: 10.1016/j.psj.2022.101825.
- [123] Q. Zhang *et al.*, 'Small-molecule synergist of the Wnt/ β -catenin signaling pathway', *Proc. Natl. Acad. Sci. U.S.A.*, vol. 104, no. 18, pp. 7444–7448, May 2007, doi: 10.1073/pnas.0702136104.
- [124] R. C. Dregalla, J. Zhou, R. R. Idate, C. L. R. Battaglia, H. L. Liber, and S. M. Bailey, 'Regulatory roles of tankyrase 1 at telomeres and in DNA repair: suppression of T-SCE and stabilization of DNA-PKcs', *Aging*, vol. 2, no. 10, pp. 691–708, Oct. 2010, doi: 10.18632/aging.100210.
- [125] M. Feng *et al.*, 'Pharmacological inhibition of β -catenin/BCL9 interaction overcomes resistance to immune checkpoint blockades by modulating T_{reg} cells', *Sci. Adv.*, vol. 5, no. 5, p. eaau5240, May 2019, doi: 10.1126/sciadv.aau5240.
- [126] J. A. Wisniewski, J. Yin, K. B. Teuscher, M. Zhang, and H. Ji, 'Structure-Based Design of 1,4-Dibenzoylpiperazines as β -Catenin/B-Cell Lymphoma 9 Protein–Protein

- Interaction Inhibitors', *ACS Med. Chem. Lett.*, vol. 7, no. 5, pp. 508–513, May 2016, doi: 10.1021/acsmedchemlett.5b00284.
- [127] S. Schmidtova *et al.*, 'Targeting of Deregulated Wnt/ β -Catenin Signaling by PRI-724 and LGK974 Inhibitors in Germ Cell Tumor Cell Lines', *IJMS*, vol. 22, no. 8, p. 4263, Apr. 2021, doi: 10.3390/ijms22084263.
- [128] R.-H. Chen, W. V. Ding, and F. McCormick, 'Wnt Signaling to β -Catenin Involves Two Interactive Components', *Journal of Biological Chemistry*, vol. 275, no. 23, pp. 17894–17899, Jun. 2000, doi: 10.1074/jbc.M905336199.
- [129] E. M. Stein and G. Weiss, *Introduction to Fourier Analysis on Euclidean Spaces*. Princeton University Press.
- [130] E. K. Davis, Y. Zou, and A. Ghosh, 'Wnts acting through canonical and noncanonical signaling pathways exert opposite effects on hippocampal synapse formation', *Neural Dev*, vol. 3, no. 1, p. 32, Dec. 2008, doi: 10.1186/1749-8104-3-32.
- [131] A. Caricasole *et al.*, 'Functional Characterization of WNT7A Signaling in PC12 Cells', *Journal of Biological Chemistry*, vol. 278, no. 39, pp. 37024–37031, Sep. 2003, doi: 10.1074/jbc.M300191200.
- [132] K. Matsumoto, R. Miki, M. Nakayama, N. Tatsumi, and Y. Yokouchi, 'Wnt9a secreted from the walls of hepatic sinusoids is essential for morphogenesis, proliferation, and glycogen accumulation of chick hepatic epithelium', *Developmental Biology*, vol. 319, no. 2, pp. 234–247, Jul. 2008, doi: 10.1016/j.ydbio.2008.04.021.
- [133] E.-M. Brinkmann, 'Secreted frizzled-related protein 2 (sFRP2) redirects non-canonical Wnt signaling from Fz7 to Ror2 during vertebrate gastrulation', 2016, doi: 10.11588/HEIDOK.00020159.
- [134] Q. Ma *et al.*, 'The SFRP₁ Inhibitor WAY -316606 Attenuates Osteoclastogenesis Through Dual Modulation of Canonical Wnt Signaling', *J of Bone & Mineral Res*, vol. 37, no. 1, pp. 152–166, Jan. 2022, doi: 10.1002/jbmr.4435.
- [135] S. L. Lewis *et al.*, '*Dkk1* and *Wnt3* interact to control head morphogenesis in the mouse', *Development*, vol. 135, no. 10, pp. 1791–1801, May 2008, doi: 10.1242/dev.018853.
- [136] S.-M. A. Huang *et al.*, 'Tankyrase inhibition stabilizes axin and antagonizes Wnt signalling', *Nature*, vol. 461, no. 7264, pp. 614–620, Oct. 2009, doi: 10.1038/nature08356.
- [137] J. L. Catrow, Y. Zhang, M. Zhang, and H. Ji, 'Discovery of Selective Small-Molecule Inhibitors for the β -Catenin/T-Cell Factor Protein–Protein Interaction through the Optimization of the Acyl Hydrazone Moiety', *J. Med. Chem.*, vol. 58, no. 11, pp. 4678–4692, Jun. 2015, doi: 10.1021/acs.jmedchem.5b00223.
- [138] H. Okazaki *et al.*, 'The novel inhibitor PRI-724 for Wnt/ β -catenin/CBP signaling ameliorates bleomycin-induced pulmonary fibrosis in mice', *Experimental Lung Research*, vol. 45, no. 7, pp. 188–199, Aug. 2019, doi: 10.1080/01902148.2019.1638466.
- [139] E. Kobayashi, H. Nakano, M. Morimoto, and T. Tamaoki, 'Calphostin C (UCN-1028C), a novel microbial compound, is a highly potent and specific inhibitor of protein kinase C', *Biochemical and Biophysical Research Communications*, vol. 159, no. 2, pp. 548–553, Mar. 1989, doi: 10.1016/0006-291X(89)90028-4.
- [140] L. Marcon, C. G. Arqués, M. S. Torres, and J. Sharpe, 'A computational clonal analysis of the developing mouse limb bud.', *PLoS computational biology*, vol. 7, no. 2, Art. no. 2, Jan. 2011, doi: 10.1371/journal.pcbi.1001071.
- [141] B. A. Parr and A. P. McMahon, 'Dorsalizing signal Wnt-7a required for normal polarity of D–V and A–P axes of mouse limb', *Nature*, vol. 374, no. 6520, pp. 350–353, Mar. 1995, doi: 10.1038/374350a0.
- [142] F. Witte, J. Dokas, F. Neuendorf, S. Mundlos, and S. Stricker, 'Comprehensive expression analysis of all Wnt genes and their major secreted antagonists during mouse limb development and cartilage differentiation', *Gene Expression Patterns*, vol. 9, no. 4, pp. 215–223, Apr. 2009, doi: 10.1016/j.gep.2008.12.009.
- [143] M. Fernandez-Teran, M. A. Ros, and F. V. Mariani, 'Evidence that the limb bud

- ectoderm is required for survival of the underlying mesoderm', *Developmental Biology*, vol. 381, no. 2, pp. 341–352, Sep. 2013, doi: 10.1016/j.ydbio.2013.06.032.
- [144] N. Mercader, E. Leonardo, M. E. Piedra, C. Martínez-A, M. a Ros, and M. Torres, 'Opposing RA and FGF signals control proximodistal vertebrate limb development through regulation of Meis genes.', *Development (Cambridge, England)*, vol. 127, no. 18, Art. no. 18, Sep. 2000.
- [145] C. E. Nelson *et al.*, 'Analysis of Hox gene expression in the chick limb bud.', *Development (Cambridge, England)*, vol. 122, no. 5, Art. no. 5, May 1996.
- [146] M. Beguerisse-Díaz, R. Desikan, and M. Barahona, 'Linear models of activation cascades: analytical solutions and coarse-graining of delayed signal transduction', *Journal of The Royal Society Interface*, vol. 13, no. 121, p. 20160409, Aug. 2016, doi: 10.1098/rsif.2016.0409.
- [147] A. Börsch and J. Schaber, 'How time delay and network design shape response patterns in biochemical negative feedback systems', *BMC Systems Biology*, vol. 10, no. 1, p. 82, Aug. 2016, doi: 10.1186/s12918-016-0325-9.
- [148] A. Kicheva *et al.*, 'Kinetics of Morphogen Gradient Formation', *Science*, vol. 315, no. 5811, pp. 521–525, Jan. 2007, doi: 10.1126/science.1135774.
- [149] H. M. Blau and D. Baltimore, 'Differentiation requires continuous regulation.', *Journal of Cell Biology*, vol. 112, no. 5, pp. 781–783, Mar. 1991, doi: 10.1083/jcb.112.5.781.
- [150] A. Martínez-Arias, J. Nichols, and C. Schröter, 'A molecular basis for developmental plasticity in early mammalian embryos', *Development*, vol. 140, no. 17, pp. 3499–3510, Sep. 2013, doi: 10.1242/dev.091959.
- [151] M. Bienz, 'β-Catenin: A Pivot between Cell Adhesion and Wnt Signalling', *Current Biology*, vol. 15, no. 2, pp. R64–R67, Jan. 2005, doi: 10.1016/j.cub.2004.12.058.
- [152] Y. Kam and V. Quaranta, 'Cadherin-Bound β-Catenin Feeds into the Wnt Pathway upon Adherens Junctions Dissociation: Evidence for an Intersection between β-Catenin Pools', *PLOS ONE*, vol. 4, no. 2, p. e4580, Feb. 2009, doi: 10.1371/journal.pone.0004580.
- [153] B. Sanson, P. White, and J.-P. Vincent, 'Uncoupling cadherin-based adhesion from wingless signalling in *Drosophila*', *Nature*, vol. 383, no. 6601, pp. 627–630, Oct. 1996, doi: 10.1038/383627a0.
- [154] F. Kuphal and J. Behrens, 'E-cadherin modulates Wnt-dependent transcription in colorectal cancer cells but does not alter Wnt-independent gene expression in fibroblasts', *Experimental Cell Research*, vol. 312, no. 4, pp. 457–467, Feb. 2006, doi: 10.1016/j.yexcr.2005.11.007.
- [155] M. Peifer and E. Wieschaus, 'The segment polarity gene *armadillo* encodes a functionally modular protein that is the *Drosophila* homolog of human plakoglobin', *Cell*, vol. 63, no. 6, pp. 1167–1178, Dec. 1990, doi: 10.1016/0092-8674(90)90413-9.
- [156] M. E. Fernández-Sánchez *et al.*, 'Mechanical induction of the tumorigenic β-catenin pathway by tumour growth pressure', *Nature*, vol. 523, no. 7558, pp. 92–95, Jul. 2015, doi: 10.1038/nature14329.
- [157] J.-C. Röper *et al.*, 'The major β-catenin/E-cadherin junctional binding site is a primary molecular mechano-transducer of differentiation in vivo', *eLife*, vol. 7, p. e33381, Jul. 2018, doi: 10.7554/eLife.33381.
- [158] W. Satoh, T. Gotoh, Y. Tsunematsu, S. Aizawa, and A. Shimono, '*Sfrp1* and *Sfrp2* regulate anteroposterior axis elongation and somite segmentation during mouse embryogenesis', *Development*, vol. 133, no. 6, pp. 989–999, Mar. 2006, doi: 10.1242/dev.02274.
- [159] L. Topol, X. Jiang, H. Choi, L. Garrett-Beal, P. J. Carolan, and Y. Yang, 'Wnt-5a inhibits the canonical Wnt pathway by promoting GSK-3-independent β-catenin degradation', *Journal of Cell Biology*, vol. 162, no. 5, pp. 899–908, Sep. 2003, doi: 10.1083/jcb.200303158.
- [160] R. K. Ladher *et al.*, 'Cloning and Expression of the Wnt Antagonists *Sfrp-2* and *Frzb* during Chick Development', *Developmental Biology*, vol. 218, no. 2, pp. 183–198, Feb. 2000, doi: 10.1006/dbio.1999.9586.

- [161] M. D. Phillips, M. Mukhopadhyay, C. Poscablo, and H. Westphal, 'Dkk1 and Dkk2 regulate epicardial specification during mouse heart development', *International Journal of Cardiology*, vol. 150, no. 2, pp. 186–192, Jul. 2011, doi: 10.1016/j.ijcard.2010.04.007.
- [162] O. Aguilera *et al.*, 'Epigenetic inactivation of the Wnt antagonist DICKKOPF-1 (DKK-1) gene in human colorectal cancer', *Oncogene*, vol. 25, no. 29, pp. 4116–4121, Jul. 2006, doi: 10.1038/sj.onc.1209439.
- [163] P. W. Finch *et al.*, 'Purification and molecular cloning of a secreted, Frizzled-related antagonist of Wnt action', *Proc. Natl. Acad. Sci. U.S.A.*, vol. 94, no. 13, pp. 6770–6775, Jun. 1997, doi: 10.1073/pnas.94.13.6770.
- [164] A. Kispert, S. Vainio, L. Shen, D. H. Rowitch, and A. P. McMahon, 'Proteoglycans are required for maintenance of Wnt-11 expression in the ureter tips', *Development*, vol. 122, no. 11, pp. 3627–3637, Nov. 1996, doi: 10.1242/dev.122.11.3627.
- [165] A. Niida *et al.*, 'DKK1, a negative regulator of Wnt signaling, is a target of the β -catenin/TCF pathway', *Oncogene*, vol. 23, no. 52, pp. 8520–8526, Nov. 2004, doi: 10.1038/sj.onc.1207892.
- [166] H. Akiyama *et al.*, 'Interactions between Sox9 and β -catenin control chondrocyte differentiation', *Genes Dev.*, vol. 18, no. 9, pp. 1072–1087, May 2004, doi: 10.1101/gad.1171104.
- [167] M. S. Hu *et al.*, 'Embryonic skin development and repair', *Organogenesis*, vol. 14, no. 1, pp. 46–63, Jan. 2018, doi: 10.1080/15476278.2017.1421882.
- [168] H. A. Kestler and M. Kühl, 'Generating a Wnt switch: it's all about the right dosage', *Journal of Cell Biology*, vol. 193, no. 3, pp. 431–433, May 2011, doi: 10.1083/jcb.201103167.
- [169] G. Nalesso *et al.*, 'WNT-3A modulates articular chondrocyte phenotype by activating both canonical and noncanonical pathways', *J Cell Biol*, vol. 193, no. 3, pp. 551–564, May 2011, doi: 10.1083/jcb.201011051.
- [170] K. A. Mulligan, C. Fuerer, W. Ching, M. Fish, K. Willert, and R. Nusse, 'Secreted Wingless-interacting molecule (Swim) promotes long-range signaling by maintaining Wingless solubility', *Proc. Natl. Acad. Sci. U.S.A.*, vol. 109, no. 2, pp. 370–377, Jan. 2012, doi: 10.1073/pnas.1119197109.
- [171] F. V. Mariani, M. Fernandez-Teran, and M. A. Ros, 'Ectoderm-mesoderm crosstalk in the embryonic limb: The role of fibroblast growth factor signaling: FGF in Limb Development', *Dev. Dyn.*, vol. 246, no. 4, pp. 208–216, Apr. 2017, doi: 10.1002/dvdy.24480.
- [172] B. García-Reyes *et al.*, 'Discovery of Inhibitor of Wnt Production 2 (IWP-2) and Related Compounds As Selective ATP-Competitive Inhibitors of Casein Kinase 1 (CK1) δ/ϵ ', *J. Med. Chem.*, vol. 61, no. 9, pp. 4087–4102, May 2018, doi: 10.1021/acs.jmedchem.8b00095.
- [173] M. Johansson, F. A. Giger, T. Fielding, and C. Houart, 'Dkk1 Controls Cell-Cell Interaction through Regulation of Non-nuclear β -Catenin Pools', *Developmental Cell*, vol. 51, no. 6, pp. 775–786.e3, Dec. 2019, doi: 10.1016/j.devcel.2019.10.026.
- [174] L. A. Kirby *et al.*, 'Glycogen Synthase Kinase 3 (GSK3) Inhibitor, SB-216763, Promotes Pluripotency in Mouse Embryonic Stem Cells', *PLoS ONE*, vol. 7, no. 6, p. e39329, Jun. 2012, doi: 10.1371/journal.pone.0039329.
- [175] L. H. Goodnough, G. J. DiNuoscio, J. W. Ferguson, T. Williams, R. A. Lang, and R. P. Atit, 'Distinct Requirements for Cranial Ectoderm and Mesenchyme-Derived Wnts in Specification and Differentiation of Osteoblast and Dermal Progenitors', *PLoS Genet*, vol. 10, no. 2, p. e1004152, Feb. 2014, doi: 10.1371/journal.pgen.1004152.